STRUCTURAL INTEGRITY MONITORING OF A FIXED-BOTTOM FRAME TOWER

MERVIN ALLAN MARSHALL

CANADIAN THESES ON MICROFICHE

I.S.B.N.

THESES CANADIENNES SUR MICROFICHE

National Library of Canada
Collections Development Branch

Canadian Theses on
Microfiche Service

Ottawa, Canada
K1A 0N4

Bibliothèque nationale du Canada
Direction du développement des collections

Service des thèses canadiennes
sur microfiche

NOTICE

The quality of this microfiche is heavily dependent upon the quality of the original thesis submitted for microfilming. Every effort has been made to ensure the highest quality of reproduction possible.

If pages are missing, contact the university which granted the degree.

Some pages may have indistinct print especially if the original pages were typed with a poor typewriter ribbon or if the university sent us a poor photocopy.

Previously copyrighted materials (journal articles, published tests, etc.) are not filmed.

Reproduction in full or in part of this film is governed by the Canadian Copyright Act, R.S.C. 1970, c. C-30. Please read the authorization forms which accompany this thesis.

THIS DISSERTATION
HAS BEEN MICROFILMED
EXACTLY AS RECEIVED

AVIS

La qualité de cette microfiche dépend grandement de la qualité de la thèse soumise au microfilmage. Nous avons tout fait pour assurer une qualité supérieure de reproduction.

S'il manque des pages, veuillez communiquer avec l'université qui a conféré le grade.

La qualité d'impression de certaines pages peut laisser à désirer, surtout si les pages originales ont été dactylographiées à l'aide d'un ruban usé ou si l'université nous a fait parvenir une photocopie de mauvaise qualité.

Les documents qui font déjà l'objet d'un droit d'auteur (articles de revue, examens publiés, etc.) ne sont pas microfilmés.

La reproduction, même partielle, de ce microfilm est soumise à la Loi canadienne sur le droit d'auteur, SRC 1970, c. C-30. Veuillez prendre connaissance des formules d'autorisation qui accompagnent cette thèse.

LA THÈSE A ÉTÉ
MICROFILMÉE TELLE QUE
NOUS L'AVONS REÇUE

Canada

NL-339 (r. 82/08)

STRUCTURAL INTEGRITY MONITORING OF A FIXED-BOTTOM FRAME TOWER

by

Mervin Allan Marshall, B. Eng.

A Thesis submitted in partial fulfillment
of the requirements for the degree of
Master of Engineering

Faculty of Engineering and Applied Science
Memorial University of Newfoundland

March 1982

St. John's Newfoundland, Canada

To My Grandmother

(Mrs. Evannah Stanley)

ACKNOWLEDGEMENTS

I should like to express sincere gratitude to Dr. Michael Booton (project and thesis supervisor) and to Dr. A. John Christian (Chairman of Civil Engineering and co-supervisor) for their encouragement and guidance throughout my years of study. Their contributions of time and technical expertise have helped immensely.

A special word of thanks is extended to Mr. Gerald Guy for his invaluable assistance throughout the experimental phase of this investigation, and to Mr. Hussein El-Tahan for his many helpful suggestions. Furthermore, thanks are expressed to Mr. Charles Carter and Mr. Stephen K. Foster of Technical Services, Memorial University, for building the experimental model.

The funding for this research by National Research Council of Canada, grant number 85-875, is gratefully acknowledged. Also, I am indebted to Dr. F. A. Aldrich, Dean of Graduate Studies at Memorial University, for the award of a Graduate Fellowship.

Last, but by no means least, I should like to thank the Almighty for making everything possible.

ABSTRACT

As a consequence of the increasing necessity for structural safety of drilling platforms, the need for monitoring techniques capable of detecting early damage of subsurface structural components increases.

The purpose of this study is to provide theoretical and laboratory experimental evidence that a predictable relationship exists between physical damage of certain structural components, and changes in the resonant frequencies of a structure measured at the deck level. To achieve this objective, experiments were carried out on a k-braced model of an offshore tower using random vibration analyses, and the results were compared to those determined from a finite element model of the structure (free vibration STRUDL II analyses).

Natural frequencies were determined for the intact and damaged structure and the results, experimental and analytical, were compared to measure the effects of the damaged member(s) on the resonant frequencies of the structure. By removing an inclined member in a k-braced panel to simulate damage of that member, a 22.75% decrease in the natural frequency of the 2nd sway mode was measured on the transfer function of the experimental model; the theoretical results indicated a 16.02% decrease. Investigations into the effect of a member cracking showed a 9.2% decrease in the excitation frequency of the 2nd sway mode, when a k-brace member was cut halfway across at one joint on the experimental model.

From the results obtained, it was concluded that the changes in

natural frequencies clearly indicated that the structure had, in fact, undergone damage. Moreover, the theoretical results showed that the mode(s) most affected depended on the location of the damaged member(s).

It is recommended that although the technique appears promising, it should not be viewed as a panacea for solving the problem of early detection of subsurface structural damage with great certainty since certainty, in such a complex environment as the ocean, can rarely be assured. Nonetheless, if the structural integrity monitoring technique is applied in conjunction with conventional detection procedures, the effectiveness of early damage detection will be enhanced.

TABLE OF CONTENTS

LIST OF TABLES

LIST OF FIGURES

NOMENCLATURE

A.C.	Alternating current
B	Band width or maximum frequency content of the random signal
D_1	External diameter of tubular member
D_o	Internal diameter of tubular member
det	Determinant
DFT	Discrete Fourier Transform
Δt	Time duration between sample points of Random Sample Record
Δf	Frequency resolution
$(DFT)^{-1}$	Inverse Discrete Fourier Transform
dB (or DB)	Decibels
E	Modulus of Elasticity
f_s	Sample Frequency ($f_s \leq 2B$)
f	Frequency in Hertz
g	Acceleration due to gravity
$\lvert \overline{G}_{yx}(f) \rvert$	Magnitude of Cross Spectrum (Power Spectrum)
$\overline{G}_{xx}(f)$	Input Auto Spectrum
$\overline{G}_{yy}(f)$	Output Auto Spectrum
$\gamma^2_{yx}(f)$	Coherence function for output signal y, and input signal x
H(f)	Transfer Function
I_x	Moment of Inertia about the x-axis
I_y	Moment of Inertia about the y-axis

I_z	Moment of Inertia about the z-axis
j	$(-1)^{\frac{1}{2}}$
J	Polar Moment of Inertia
[K]	Stiffness Matrix
k	1, 2, 3, 4 ....
LIN	Linear scale
L.L.F.	Lower Limit Frequency
M_x	Sway (bending) about the x-axis
M_y	Sway (torsion) about the y-axis
M_z	Sway (bending) about the z-axis
[M]	Mass Matrix
Mem.	Member
Mems.	Members
MAG.	Logarithmic Magnitude
$N\Delta t$	Duration of Sample Record
N	Number of sample values for the chosen Δt
P	Pole (Eigenvalue)
$P_1^2, P_2^2 \ldots\ldots P_N^2$	N roots of the system's matrix
$R(\tau)$	Auto Correlation Function
σ_o	Damping coefficient
S_x	Section Modulus about the x-axis
S_y	Section Modulus about the y-axis
T	Time duration of Random Signal ($N\Delta t$)
T_o	Time duration of Sample Record
t_1	Wall thickness of hollow circular section

$\theta_{yx}(f)$	Phase Angle in degress as a function of frequency
τ	Time Lag
U.L.F.	Upper Limit Frequency
V	Volts
W	$e^{j2\pi/N}$
ω_d	Damped natural frequency in radians per seconds ($2\pi f$)
X(f)	Fourier Transform of input signal
x(t)	Random signal function
Y(f)	Fourier Transform of output response
ζ	Damping ratio (zeta)

1. INTRODUCTION

Increased activity in the exploration and production of offshore oil and gas has resulted in structures being installed in deeper waters. However, as this trend continues, the difficulty of inspection to detect damage of subsurface structural components increases; accordingly, the procedure becomes more expensive and more perilous. This results because inspection carried out by divers is usually thwarted by poor visibility, poor lighting and hazardous conditions; for example, very low water temperatures and large water depths. Furthermore, marine growth and corrosion may conceal structural defects (fractures). The inadequacy of these inspection procedures is exemplified by the reports of total or near-loss of drilling rigs in the Gulf of Mexico and the North Sea.

The accident of the Alexander L. Kielland on March 27, 1980, in the North Sea [24] demonstrated that cyclic loading or an extremely large single load does have the capability of damaging structures by promoting fractures (cracks) in certain load carrying members. Since each member plays a paramount role in the structure's internal damping or stiffness, any change in a member can result in changes in the structural dynamical properties.

The resonant frequencies of any structural system depend, to a great extent, on its stiffness. As a consequence, if the stiffness changes, the structure would respond differently, because its resonant frequencies (i.e., frequencies of vibration at which the structure absorbs maximum energy) may shift in value.

Techniques now exist to measure the dynamical properties of a

structure and to represent its dynamic behavior in terms of its vibrational modes. Identification of these vibration modes within a specified frequency range quantifies the structure over the given frequency spectrum. Associated with every vibration mode is a mode shape and its corresponding frequency and damping.

Therefore, by accurately monitoring the modal parameters and detecting any changes in their magnitudes, then comparing them to some established datum point, it is possible to detect damage in a structure. Figure 1.2 gives a synopsis of the major steps of damage assessment.

The objective of this investigation is to provide evidence--both analytically and experimentally--that a predictable relationship exists between physical damage and changes in the structural modes of vibration.

2. LITERATURE REVIEW

Structural integrity monitoring of offshore oil and gas drilling platforms is not without precedence. Loland and Mackenzie [1] experimented on a k-braced offshore model rig from which natural frequencies were computed for the complete structure, and then with a single k-brace in one face removed. Sudden changes in frequencies were observed, particularly the higher ones. Percentage changes as high as 30% were indicated; the frequency most affected depended on the position at which the brace was removed. Begg et al [2] dealt with the theoretical ideas and assumptions from which structural integrity monitoring, using vibration analysis, had been developed. At a later symposium (1978), Begg and Mackenzie [3] presented a state-of-the-art discussion of the technique as applied to steel structures and indicated possible application to concrete offshore platforms.

Loland and Dodds (1976) in Ref. 4, discussed operating experiences, and presented some of the results obtained from a structural integrity system which had been used for a period of 6-9 months on three platforms in the North Sea. The objective of that experiment was to extend the laboratory and computational studies of Loland et al [5]. Loland, Mackenzie and Begg (Ibid.) carried out laboratory experiments on a k-braced model of an offshore platform. Changes in natural frequencies occurred when members in the k-brace were removed. They concluded that these changes were large enough to be detected reliably, and that the method should give positive indication of structural failure.

Begg [6] presented a state-of-the-art discussion of the technique and indicated possible limitations in an offshore environment.

For example, he showed that the higher frequencies involved only a small component; so modes involving underwater members cannot be measured, much less identified, from positions above the water line. Begg and Mackenzie [7] showed that under normal circumstances, vibration monitoring provides a back-up assurance of the ability of the platform to withstand major wave loading. As a result, to obtain an assurance of the maximum possible degree of accuracy, it is of paramount necessity that the dynamical characteristics of the platform be completely understood, so that a good reference point is obtained for later comparisons. Hence, it is necessary to calculate the sensitivity of the platform at various locations in order to provide a basis for identifying the damage from changes in the vibration spectra.

Lock and Jones [8] carried out a short feasibility study in the use of vibration monitoring for assessing the structural integrity (stiffness) of oil production platforms, especially those constructed of steel. To achieve this objective, experimental work was done on a space frame model constructed from 3.8 m and 1.9 cm 16 gauge steel tubes. The model was 3.8 m long with 0.9 m wide sides and weighed 46.0 kgf. Based on the results attained, they suggested that monitoring the vibration of an oil production platform would certainly provide information as to its condition. Notwithstanding, the major stumbling block to the success of the method would be estimating the degree of change in the natural frequency of any particular mode, since mode identification, in these structures, would be difficult (ibid.).

Wooton et al [9] discussed the developments that have taken place in the use of vibration analysis to discern structural failure,

and demonstrated the way in which these techniques could be applied more widely. Brown et al [10] reviewed the various schemes, and outlined the results of recent work in the North Sea. The scope of the work included a theoretical dynamic analysis of the structure, the design, installation and performance of a vibration monitoring system, and the computer analysis of measured vibration spectra, for the purpose of monitoring the integrity of the installation. Vandiver et al [11] presented a detailed study of an offshore pile-supported tower. The tower consisted of a welded steel space frame with four primary legs braced with horizontal and diagonal members. It was fixed to driven steel piles and stood 45.72 m above the mudline in 21.34 m of water, and weighed 2,978.4 kN. Statistical energy analysis was introduced as a method for producing the dynamic response of a wide variety of fixed and floating platforms to random waves. It should be noted that statistical energy analysis provides a means for estimating the maximum energy that a resonant structural mode may have, independent of the structural geometry, and dependent only on the wave height spectrum as well as frequency (ibid.).

In Ref. 12, a study of vibration and damping in offshore structures is involved, which includes laboratory measurements made on a model platform (in and out of water), and a full scale platform in the North Sea. The results were used to assist in designing vibration analysis monitoring systems.

Rubin [13] experimented on an operating eight-leg 115 m tall platform in the Gulf of Mexico. This was the first part of a pilot study to examine the feasibility of ambient vibration monitoring, so

that periodic assessment, from a structural integrity viewpoint, could be performed. The modes detected from the data recorded (lateral, vertical, and angular senses) from force transducers at 17 locations above water on the structure were used to provide a basis for a future analytical phase.

Vandiver and Campbell [14] introduced the Maximum Entropy Method (MEM) of spectral analysis as a powerful technique for estimating the dynamic response properties of offshore platforms. This method was presented in the context of making estimates of natural frequencies and damping ratios for three similar U.S. navy air combat maneuvering range platforms near Cape Hatteras, North Carolina. It should be mentioned that MEM has demonstrated the capability of producing smooth high resolution response spectra from short time histories of deck acceleration. Also, this capability to utilize short record lengths substantially decreases inherent errors arising from the necessary assumption of stationary wave excitation forces (ibid.).

3. THEORY FORMULATIONS

This section is composed of two subsections. The first discusses the techniques and formulations used to analyze the structure using the ICES STRUDL II computer program [34]. The second deals with the formulations used to analyze the experimental results via the Hewlett Packard 5451B Fourier Analyzer.

3.1 The Computer Analysis

The mathematical model for the structure was represented by discretized lumped masses at N nodal points. Such a N degree of freedom system is formulated in matrix form as:

$$[M][\ddot{x}(t)] + [C][\dot{x}(t)] + [K][x(t)] = [F(t)] \qquad (1.0)$$

where:

$[M]$, $[C]$, $[K]$ = mass, damping and stiffness matrices respectively

$[x(t)]$, $[\dot{x}(t)]$, $[\ddot{x}(t)]$ = time dependent displacement, velocity and acceleration vectors respectively

$[F(t)]$ = forcing function vector

There are two ways in which these equations of motion, either generated by STRUDL from the structural data, or input directly in matrix form, can be solved:

(i) Normal mode analysis

(ii) Physical analysis

3.1.1. Normal Mode Analysis

In this method, equation (1.0) is transformed to a new coordinate system to yield uncoupled linear equations. This technique is very

efficient when the response of a multidegree of freedom system is required. However, since only the mode shape and resonant frequencies were needed for the dynamic analysis, the method was not used; so the physical analysis was applied.

3.1.2. The Physical Analysis

This analysis incorporates the physical coordinates of the structure and can be formulated as follows:

A free vibration analysis ($F(t) = 0$) was performed; hence, equation (1.0) reduces to:*

$$[M][\ddot{x}(t)] + [K][x(t)] = [0] \tag{1.1}$$

The response $[x(t)]$ can be assumed to be of the form:

$$[x(t)] = [V]e^{pt} \tag{1.2}$$

where p represents a pole** and [V], the mode shape vector. This expression is substituted in equation (1.1) to result in:

$$[P^2[M] + [K][V]]\ [V]e^{pt} = [0] \tag{1.3}$$

The exponential component never equals zero; so, with the application of Cramer's rule, equation (1.3) reduced to:

$$[V] = \frac{[0]}{\det([P^2[M] + [K]])} \tag{1.4}$$

where:

$\det([P^2[M] + [K]])$ = determinant of the matrix of the system

*Note that the damping component is ignored for simplicity. Nonetheless, in the computer analysis, it is considered.

**$P = \sigma_o + j\omega_o$, where: σ_o = damping coefficient

ω_o = damped natural frequency

$j = (-1)^{\frac{1}{2}}$

A non-trivial solution is possible when the denominator determinant is equated to zero:

$$\det([P^2[M] + [K]]) = [0] \qquad (1.5)$$

When expanded, the result is a polynomial of the N-th degree in terms of the eigenvalues P^2 for the N degree of freedom system. These N roots ($P_1^2, P_2^2 \ldots P_N^2$) are computer generated, and they represent the N resonant frequencies of the structural model.

The mode shapes are then computed when these eigenvalues are substituted in equation (1.3). A unique mode shape (eigenvector) results for every distinct eigenvalue.

3.2 The Experimental Analysis

In the experimental phase of this investigation, the structure was excited with an input force generated from a random signal noise generator (more details will be presented in the section on Experimental Procedure). The input force, as well as the output acceleration and displacement were recorded, and the analyses performed with the Fourier analyzer. Formulations for the frequency domain analyses are given as follows:

If a sample record of a random signal having N discrete samples x(t) with known maximum frequency is available (i.e., $x(n\Delta t)$ is known when $N\Delta t = T$), the signal can be converted into frequency components by taking the Discrete Fourier Transform (DFT) of the signal given by:

$$X(m\Delta f) = \frac{\Delta t}{T} \sum_{n=0}^{N-1} x(n\Delta t)\, e^{-\frac{j2\pi nm}{N}} \qquad (1.6)$$

or,

$$X(m\Delta f) = \frac{\Delta t}{N\Delta t} \sum_{n=0}^{N-1} x(n\Delta t)\, W^{-nm} \qquad (1.7)$$

or,

$$X(m\Delta f) = \frac{1}{N} \sum_{n=0}^{N-1} x(n\Delta t)\, W^{-nm} \qquad (1.8)$$

The inverse DFT $(DFT)^{-1}$ is:

$$x(n\Delta t) = \sum_{m=0}^{N-1} X(m\Delta f)\, W^{nm} \qquad (1.9)$$

where:

Δt = time increment between samples (1/fs)

Δf = frequency resolution

T = duration of the signal to be investigated

f_s = sample frequency ($f_s \leq 2B$)

B = band width or maximum frequency content of the signal

N = number of samples

$W = e^{j2\pi/N}$

Note that the DFT and the $(DFT)^{-1}$ are computed using the efficient, so called, Fast Fourier Transform algorithm (FFT). The nature of this algorithm requires N to be in the form 2^k, k = 1, 2, 3.... That is, N = 32, 64, 128, 512....

The DFT values of $x(m\Delta f)$ are periodic functions of $m\Delta f$ with period $(N\Delta f)^{-1} = (f_s)^{-1}$. Because of this, the Fourier Analyzer displays N/2 sample values plus a DC (direct current) term $x(0\Delta f)$; that is, the value of the signal at zero frequency.

To obtain the undistorted spectrum (Fourier coefficients) related to the aperiodic signal x(t) with maximum frequency content BHz, and duration T seconds, the following method is used:

(i) a sample frequency $f_s \leq 2B$ is selected ($\Delta t = 1/f_s$)

(ii) a proper data block length is selected such that:

$$T = N \times \Delta t$$

$$= N \times \frac{1}{f_s} > T$$

$$\Delta f = 1/T$$

$$= 1/N\Delta t$$

$$= f_s/N$$

The acquired spectrum can be modified in the frequency domain by multiplying by another spectrum. This operation is equivalent to signal filtering.

To determine the relationship between the input and output signal to and from the structure, the transfer function, coherence function and phase function are required.

Transfer Function:

This function represents a mathematical description of the system and is used to measure the relationship between two signals. It is defined as:

$$\text{Transfer function} = \frac{\text{Fourier Transform of Output}}{\text{Fourier Transform of Input}} \qquad (1.10)$$

or,

$$H(f) = Y(f)/X(f) \qquad (1.11)$$

where:

$H(f)$ = Transfer function

$Y(f)$ = Fourier transform of output response

$X(f)$ = Fourier transform of input signal

Coherence Function:

A coherence function measures the degree of causality between any two signals. It can, therefore, be used to check the validity of the transfer function. When a transfer function is computed, extraneous inputs or whether or not the system is linear may not be too evident. Both these factors would introduce error in the computed transfer function. The coherence function ranges between 0 and 1. Zero means no coherence between the input and output signal or, in other words, extraneous inputs and/or the system is non-linear. One means a complete coherence between input and output or, in other words, only one input and a linear system. The mathematical relationship used to calculate the coherence function is expressed as:

$$\gamma^2_{yx}(f) = \frac{|\overline{G}_{yx}(f)|^2}{\overline{G}_{xx}(f)\,\overline{G}_{yy}(f)} \qquad (1.12)$$

where:

$|\overline{G}_{yx}(f)|^2$ = square of the magnitude of the cross spectrum (power spectrum)

$\overline{G}_{xx}(f)$ = input auto spectrum (power spectrum)

$\overline{G}_{yy}(f)$ = output auto spectrum (power spectrum)

The Fourier Transform relationship between the auto correlation function $R(\tau)$ and the power spectrum $G(f)$ is given by:

$$G(f) = \int_{-\infty}^{\infty} R(\tau)\, e^{-j2\pi f\tau} \qquad (1.13)$$

where:

$$R(\tau) = \lim_{T\to\infty} \frac{1}{T} \int_{-T/2}^{T/2} x(t)x(t+\tau)\,dt \qquad (1.14)$$

where:

τ = time lag between sample values

Nevertheless, for numerical purposes, the auto-correlation function can be estimated at discrete lags; $R(\tau = m\Delta t)$ is given by:

$$R(\tau=m\Delta t) = \frac{1}{N} \sum_{m=-\infty}^{\infty} x(t)\, x(t+m\Delta t) \qquad (1.15)$$

or,

$$R(k) = \frac{1}{N} \sum_{m=-\infty}^{\infty} x(t)\, x(t+k) \qquad (1.16)$$

where:

$k = m\Delta t$ (i.e., time lag between sample values)

$$x(t) = \begin{cases} x(t) & 0<t\leq N-1 \\ 0 & t>N-1 \end{cases}$$

then, the spectral density (power spectrum) is estimated for the first L lags as:

$$G(f) = \Delta t \sum_{m=-\infty}^{\infty} R(\tau=m\Delta t)\, e^{-j2\pi f m\Delta t} \qquad (1.17)$$

or,

$$G(f) = \Delta t \sum_{m=-\infty}^{\infty} R(k)\, e^{-j2\pi f k} \qquad (1.18)$$

where:

$|f| \leq \frac{1}{2}\Delta t$

$$R(k) = \begin{cases} R(k) & \text{for } |k| \leq L \\ 0 & \text{for } |k| > L \end{cases}$$

Phase Shift:

The phase shift or phase angle between an input and an output signal at a particular frequency is given as:

$$\Theta_{yx}(f) = \frac{C_{yx}(f)}{|G_x(f)|} \qquad (1.19)$$

where:

$\Theta_{yx}(f)$ = phase angle in degrees

Like the functions described previously, this mathematical relationship can be used to indicate frequencies at which non-linearity occurs in the system.

4. ANALYTICAL STUDY

4.1. Structure to be Analyzed

The structure analyzed was a space frame model of an offshore tower which had the dimensions depicted in Figure 1.0. The following are the structural data:

Material	Polyvinyl Chloride (P.V.C.)
Modulus of Elasticity (E)	2.413×10^6 KN/m^2
Individual member cross section	Hollow circular section
Thickness (t_i)	0.399 cm
External diameter (D_i)	2.1636 cm
Internal diameter (D_o)	1.3360 cm
Area	2.1737 cm^2
Moment of Inertia about the local y-axis (I_y)	0.8607 cm^4
Moment of Inertia about the local z-axis (I_z)	0.8607 cm^4
Polar moment of inertia (J)	172.14 cm^4
Section modulus about the local y-axis (S_y)	0.8195 cm^3
Section modulus about the local z-axis (S_z)	0.8195 cm^3
Effective damping percent (ζ)	3.0%

For the purpose of the analyses, certain assumptions were made:

- Connections at joints are rigid
- Masses are lumped at the nodal points
- Rigid deck
- Member properties prismatic.

4.2. Analytical Procedure

The analyses of the structure were obtained using the three dimensional frame analysis computer program ICES STRUDL II. Figure 1.1 shows a flow diagram of the analyses. To simulate a rigid deck, the properties (A_x, I_y, I_z, I_x) of the deck members (61 to 64) were adjusted. It was felt that it would not have been possible to excite the higher modes (e.g., 2nd sway) to any noticeable magnitudes throughout the experimental phase of this investigation. As a result, lumped masses were placed at the eight nodal points two levels from the deck level (1.826 kg per node) in order to decrease the vibration frequencies at which these modes could be excited.*** This was achieved in the computer analyses by increasing the specific densities of member 83, 86, 89 and 92 (Figure 1.2) proportional to the added masses at both ends of each of these members. Since the addition of lumped masses would decrease the higher frequencies, 14.60 kg of mass were added at the deck level to decrease the fundamental frequency in order to facilitate the recognition of the various modes in the experimental phase. This was achieved in the computer analyses by increasing the specific densities of the deck members (45 to 60) proportional to the weight of the lumped mass.

In order to simulate structural damage or failure, the member(s) under consideration was/were removed in the computer analyses. This was accomplished by removing these member(s) as well as the properties of the member(s) from the computations.

***The advantage of this procedure will be discussed in more detail in the section on "Comparison of Results."

4.3. Mathematical Model of Structure

A finite element model was used to perform the analyses. The method is summarized as follows:

- Discretize the structure (i.e., subdivide the structure into components)
- Select an interpolation function which represents the assumed number of degrees of freedom
- Select the element properties
- Assemble the element properties to obtain system properties
- Solve the system equations
- Interpret the results by making additional calculations if necessary.

As a consequence, the structural model was discretized as shown in Figure 1.3. At each node six degrees of freedom were assumed; that is, three translational and three rotational degrees of freedom. Thus, for each structural member, a total of twelve degrees of freedom were established as shown in Figure 1.4.

The equations of motion for each element plus all the boundary points at connecting nodes between each element were computer generated from the geometrical and physical properties of the input data for each element or member as indicated in Figure 1.5. Finally, the equations of motion were assembled by the computer into one equation representing the structure, and the analyses were performed. Two sample computer programs used to carry out the analyses are shown in Appendix A1.

It should be emphasized that since it would be difficult and extremely time consuming to obtain exact analytical solutions for the structure considered, numerical analyses of the physical model, based on certain approximations, are incorporated in the computer approach.

5. EXPERIMENTAL STUDY

The dynamic testing of the experimental model is discussed in this section. Dynamic testing is extremely advantageous because it can be used to:

(i) verify the analytical dynamic model

(ii) diagnose (trouble shoot) the vibration problem

(iii) assess design changes to the structure

(iv) devise a dynamic model for parts of the structure too difficult to model analytically.

For all these cases, the purpose of the dynamic testing procedure was to excite and identify the modes of vibration of the structure. In both the analytical and experimental phases of this study, the common entity was the set of modal parameters. The relationship is summarized diagramatically in Figure 1.6.

5.1. Description of Model

The offshore tower model was a k-braced frame manufactured from polyvinyl chloride (P.V.C.) material (the properties of which were presented in section 4.1) and had the dimensions exhibited in Figure 1.0. It was bolted to a circular plywood base 152.4 cm in diameter and 2.54 cm thick (see Figure 1.7 and Figure 1.8). To represent a rigid fixed foundation, 200 kg of steel weights were used and arranged as shown in Figure 1.9. The deck was constructed of a 66.04 cm x 66.04 cm, 1.27 cm thick plywood plate which was connected to the tower in a similar manner as the base (see Figure 1.10 and Figure 1.11).

To simulate a rigid connection at the structural joints, the individual structural components (members) were connected to each other

at the nodes with a P.V.C. weld. A photograph of the entire arrangement is presented in Figure 1.12.

5.2. Equipment Installation

Excitation Circuit:

Random noise was generated from a digital noise generator which produced a low pass filtered noise having a Gaussian amplitude distribution with a selected maximum frequency content. The signal was passed through a power amplifier which amplified the input noise and supplied the power to the vibration exciter—an electro-mechanical device for physically shaking the tower.

Force and Acceleration Circuit:

The shaker was suspended from a steel beam with ropes. It was connected to an impedance head which was attached to the deck of the tower as demonstrated in Figure 1.11. This impedance head is a force gauge and accelerometer. Therefore, it measured the input force and output acceleration at the point of application of the input random noise.

These signals from the impedance head (i.e., force and acceleration) were passed through conditioning amplifiers where they were amplified and calibrated. From these devices, the signals were passed through a Krohm-Hite filter used as a low pass filter, and then to a 4-channel F.M. tape recorder.

Displacement Circuit:

The displacement of the tower at the deck level was measured

independently with a proximity transducer. This is a non-contacting device which measures the change in capacitance between the electrode, and a metal plate attached to the tower at the point where the displacement is required (Figures 1.13 and 1.14).

From the transducer, the signal was passed through a reactance converter. This instrument detects changes in capacitance and outputs the information as a voltage.

From the reactance converter, the signal was passed through a Rockland filter which was used as a low-pass filter; and, consequently, to the 4-channel F.M. tape recorder. For diagrams of the entire equipment installation, refer to Figures 1.15(A) and 1.15(B).

5.3 Experimental Procedure

The experiments were conducted in two stages. In the initial stage, the model was excited without the lumped masses at the nodal points and deck. This was done to ascertain whether the dynamic behavior of the experimental and theoretical model corresponded reasonably, without the lumped masses. It was only necessary, at this stage, to measure the input force and the output acceleration.

In the second stage, the lumped masses were added as previously described in section 4.2 (see Figure 1.16). These added masses were implemented because the higher resonant frequencies of the structure were never apparent to any reasonable amplitude on the transfer function for the experimental results in the first stage (i.e., without the added masses). For the second condition, the input force, output acceleration and displacement signals were recorded.

To arrive at the best possible position of the transducers, experiments were conducted with different combinations of the locations of the input force, and the output displacement. For reference purposes, the four corners of the deck of the model were denoted A, B, C, and D. For instance, one arrangement was the shaker at location A and the displacement measured at location D in a direction parallel or perpendicular to the line of action of the applied force from the shaker. These different configurations were carried out, so that the oscillation frequencies of the experimental model conformed closely with those from the computer analyses. The best configuration occurred with the shaker applying a force in the z-direction midway between A and B, and the displacement measured at C in the direction perpendicular to the line of action of the applied force (see Figure 1.17).

With the proper position of the transducers determined, the member under consideration (member 91) was severed in three stages. Initially, an incision was made halfway through the member at node 23. (see Figure 1.3) to establish if there would be any obvious change in the transfer function. Secondly, the member was cut all the way through at that same joint. In so doing, the stiffness of the structure was reduced appreciably, but the mass remained unchanged. Ultimately, the member was severed completely at the other node (node 13). At each of these failure stages, the input force, output acceleration and displacement were recorded. It should be acknowledged that in the final stage, the member was removed. Thus, the mass of the structure was reduced by the mass of the severed member (see Figure 1.18).

When the first member was removed, a similar member positioned in the plane parallel to the previous severed member was removed (member 84) in an analogous manner as the first member, and the essential measurements repeated.

5.4 Analyses via Fourier Analyzer

Having stored the pertinent information, the analyses were performed by transferring the stored experimental signals mentioned previously from the F.M. tape recorder to the Fourier analyzer (see Figure 1.19). The signals were then passed through an analog to digital converter. This component converted the analog signals into a sequence of numbers (digits) and then stored them on digital tape. These stored signals were then "dumped" into the memory of the computer. From then onwards, the Fourier analyses were performed to determine the modal parameters.

Digital signals are stored in the memory of the computer in blocks of data (sample records). The number of sample records required to represent a particular signal depends on the size of the data block selected. Once the sample records have been selected, the Fourier analyzer treats each record as periodic signals. However, to reduce the leakage between two harmonic signals, a Hann window is used. By using the F.F.T. algorithm, the computer calculates the Fourier coefficients separately by making the resolution $\Delta f = 1/T_o$ in the frequency domain.[+] At each resolution, the Fourier coefficients are computed. Note that each coefficient behaves as a random variable. For instance,

[+] T_o represents the duration of the sample signals.

if the power spectrum of the random signal x(t) is required, the magnitude (absolute value) of each Fourier coefficient computed at corresponding frequency resolution in each sample record are added. The final spectrum is attained by taking the average at each corresponding resolution per sample record. The process is depicted in Figures 1.22 and 1.23. Note that since the Fourier analyzer treats the sample records as if they were periodic, the power spectrum is composed of an amplitude component at a specific frequency (discrete spectra), as opposed to a continuous plot of amplitude versus frequency. Nonetheless, for display purposes, the spectrum appears as a continuous plot because the graphic capability of the computer allows the user to join neighbouring points. This, therefore, exemplifies the concept that the smaller the size of the frequency resolution chosen, the more accurate will be the frequency domain analyses. A synopsis in flow chart form of the entire experimental procedure is shown in Figure 1.20.

6. RESULTS

In this section, the theoretical (computer analyses) and experimental results are presented. It should be remembered that in the experimental analyses, only two members were cut off to represent damage of these members because once a member was severed it could not be easily replaced.

However, in the computer analyses, many members were removed to simulate damage of those members. This was executed in order to indicate the most suitable member(s) to be severed in the experimental investigation, so that the effect of the structural integrity technique could be maximized.

6.1. Theoretical Results

Calculated natural frequencies for the intact and damage structure are presented in Table 1.0. Only eight natural frequencies were computed, because it was felt that it would have been very unlikely to excite more resonant frequencies experimentally.

For simplicity, only the frequencies of the damage structure with member 91, and members 91 and 84 are given. This was done, so that the comparison between experiment and theory could be easily demonstrated.

The type of mode was determined from the eigenvalues for each mode from the computer program results. With each mode angular rotation about the x, y, and z axes corresponding to the nodes of the structure were computed. By comparing the angular rotations of the nodal points along the four vertical edges of the structure about the x, y, and z

axes, the predominant sway or twist about a particular axis was verified. Having established the direction, the type of sway (i.e., 1st, 2nd, etc.) was defined from the eigenvector information from the computer results. These eigenvectors provided information of the normalized displacements in the x, y, and z directions. Therefore, with the predominant direction of sway and the elements of the eigenvectors available, the mode shapes were plotted for the nodes located along the four vertical edges of the structure. Table 1.1 shows the elements of the eigenvector for mode 8, as well as the angular rotations associated with each nodal point. The mode shape along the four vertical edges of the structure for mode 8 are depicted in Figures 2.1(A) to 2.1(D). Also, the mode shapes for mode 4 before and after damage are shown in Figures 2.2(A), (B), (C), (D) to 2.8 (A), (B), (C), (D). Note that these curves were plotted using a cubic spline interpolation and polynomial approximation with the necessary boundary conditions; for instance, at the base of the structure the slope of the polynomial, in addition to the displacement function represented by the polynomial, were set equal to zero to simulate a fixed foundation. The data were plotted via a Fortran program using the various plotting subroutines on a P.D.P. 1160 computer.

This technique for mode shape detection was repeated for the various failure conditions of interest. In other words, for each member(s) severed analytically, the type of sway or torsional mode was determined. With the oscillation frequencies of the undamaged structure as a base line (reference point), the percentage changes in natural frequencies due to the effect of the damaged (cut-off) member(s) were computed for each mode, and the results tabulated in Table 1.2.

6.2. Experimental Results

Graphical outputs of the experimental results are presented for:

- the input force and the output acceleration at the point of application of the input random force (i.e., located midway between points A and B at the deck)
- the output displacement from the reactance converter (i.e., the non-contacting device) located at point D at the deck.

Acceleration Signals:

The results consist of the frequency domain analyses of the input and output, transfer functions, coherence functions and phase functions (see Figures 3.0 to 3.13).

For the purpose of easy comparison, plots of the transfer functions for the intact and damaged structure are presented in the manner shown in Figures 3.9 to 3.13 in order that the percentage shift of the resonant frequencies, resulting from the effects of the severed member(s), could be easily recognized.

Note that the impedance head (i.e., the force gauge and accelerometer) is limited for frequencies less than or equal to 1.5 Hz. Hence the signals within that range on the plotted results are meaningless.++ Moreover, it will be noticed that in the acceleration results, the graphs for the undamaged structure extends farther in the frequency spectrum than those of the damaged structure. This occurs because the experiments on the intact structure were done at a much earlier date

---

++A sine sweep test was performed with the impedance head attached to the shaker. The input force and the output acceleration were examined on an oscilloscope. At frequencies from 0 to 1.5 Hz, there was distortion--non-linearity due to noise.

than those for the damaged structure; and, when the Fourier analyses were performed, a slightly larger frequency resolution (Δf) was chosen. In all cases, however, the data block sizes are the same.

Displacement Signals:

The displacement results from the reactance converter are presented in an analogous manner as the acceleration results in Figures 4.0 to 4.10. It should be realized that, for reasons mentioned in section 5.3, the analyses of the structure without lumped masses were not performed. Furthermore, since the transfer function, in this case, is a relationship between the input force and the output displacement, the signals from 0 to 1.5 Hz inclusive are meaningless, as a consequence of the limitations of the impedance head.

7. DISCUSSION OF RESULTS

7.1. Theoretical Results

An examination of the results tabulated in Table 1.0 indicates that, as was to be expected, the addition of lumped masses to the structure did decrease the resonant frequencies. For instance, mode 1 changed from 6.67 Hz to 2.77 Hz. Also, mode 4 changed from 16.97 Hz to 11.92 Hz.

The percentage changes in natural frequencies due to damage, as shown in Table 1.2, reveals that the mode most affected was the 2nd sway mode (M_x). When member 91, or member 84, was severed independently, a decrease of 16.02% resulted; that is, a change from 11.92 Hz to 10.01 Hz. Furthermore, when two members were severed, the mode most affected was, again, the 2nd sway mode (M_x). For example, the elimination of members 79 and 76 caused a reduction in the resonant frequency of 58.13%. Besides, the removal of members 91 and 84 caused a decrease of 50.60%. For all the simulated damaged conditions chosen, the mode least affected was the 1st sway mode (M_z). The 1st torsional mode (M_y), as well as the 1st sway mode (M_z), were least affected when only one member was eliminated from the computer analyses. Note that the decrease of 15.16% in the 1st sway mode (M_x), resulting from the removal of members 91 and 84, may have occurred because these members were located in a vertical surface along the direction of bending for that mode.

The motion of the intact and damaged structure during its 2nd sway mode (M_x) are represented by the plotted mode shapes (eigenvectors) in Figures 2.2(A), (B), (C), (D) to 2.3(A), (B), (C), (D). Note that when member 91 is removed, the displacement in the z-direction of the vertical surface, where the member was located, is large compared to

the opposite and parallel surface (Figures 2.4(A), (B) and 2.4(C), (D)). This resulted because the removal of member 91 caused a change in the structural symmetry as far as stiffness and mass are concerned. This statement may be supported by the fact that before member 91 was severed, the displacement of the structure as shown in Figures 2.3(A), (B), (C), (D) were unidirectional along the x-axis. On the other hand, with the elimination of member 91, the same vertical surfaces moved along opposite senses in the x-direction (Figures 2.5(A), (B), (C), (D)). When member 91 and 84 were severed, the z-direction displacements are large for the two parallel vertical surfaces where these members were located (Figures 2.6(A), (B), (C), (D)). This, therefore, suggested that the symmetry of the structure was restored. In other words, though the stiffness and mass were decreased, these parameters were more evenly distributed than in the case where member 91 was removed. Figures 2.8(A), (B), (C), (D) indicate that when member 84 is severed, the displacement of the vertical surface containing nodes 5 and 11 is in the positive x-direction. On the other hand, on the vertical surface opposite and parallel (i.e., containing nodes 7 and 9), the displacement is in the negative x-direction. These configurations are opposite to those when member 91 is severed. Therefore, the net result, when both members (91 and 84) are removed is a cancellation effect. This explains why the displacement in the x-direction is extremely small, when members 91 and 84 were severed (Figures 2.7(A), (B), (C), (D)).

The above observations suggest that member 91 and 84 contributed to the stiffness for the 2nd sway mode (M_x). As a result, when the stiffness of the structure was reduced by the removal of these members,

the frequency at which this mode could be excited was reduced.

This reduction in stiffness could be explained as follows: The deformation of the structure during bending results from shear displacement in the panels (i.e., the regions containing the diagonal members). As a consequence, when member 91 or 84 is severed, the neighbouring k-braced member cannot transmit direct load without the horizontal member, to which it is attached, undergoing primary bending. This implies that the companion brace is virtually inactive; so the shear stiffness of the panel is greatly reduced.

It should be mentioned that the frequency reductions were mainly due to a reduction in stiffness rather than a reduction in mass, because the mass of the individual structural members is small (e.g., member 91 = 0.26 kg). Thus, the effect from a reduction in mass would be minimal.

7.2. Experimental Results

The results for the experimental study are summarized in Tables 1.3(A) and 1.3(B). In all cases, the percentage shift in resonant frequencies for the damaged structure are calculated with respect to the intact structure.

7.2.1. Acceleration Results

As mentioned earlier, the higher modes were not excited to any reasonable amplitude on the transfer function for the experiment without lumped masses (Figure 3.2). By adding the lumped masses in the manner described in section 4.2, the resonant frequencies decreased. Also, the amplitudes of the peaks--particularly at the higher frequencies--

increased to more recognizable magnitudes. The decrease in frequencies occurred because of the added masses. Frequency is inversely proportional to mass; therefore, by adding masses, the vibration frequencies were reduced. Further, the increase in the amplitudes of the peaks resulted because the addition of masses caused an induced strain in the individual members. This made the structure more susceptible to the applied random force. That is, the mechanical mobility of the structure was improved.

Member 91 Severed:

For the intact structure three points of resonance are apparent. The first occurs at approximately 2.9 Hz, the second at about 4.2 Hz and the third at about 9.8 Hz (Figure 3.3). It can be recalled that it was verified, based on the computer analyses, that the mode most affected, after the structure underwent damage, was the 2nd sway mode (M_x). From this verification, it seems palpable to assume that if this trend were repeated on the transfer functions in the experimental results for a particular resonant peak, the frequency at that point, before any shift occurred, would be the 2nd sway mode (M_x). In the experimental analyses, the frequency most affected by the removal of member 91 occurs at 9.8 Hz. This means that the 2nd sway mode (M_x) of the structure is excited at that frequency (9.8 Hz). Accordingly, it can be inferred that the resonant peak at 2.88 Hz corresponds to the 1st sway mode (M_x), and the resonant peak at 4.2 Hz is comparable to the 1st torsional mode (M_y).

When an incision was made halfway through member 91 at node 23,

the 2nd sway mode (M_x) shifted from 9.8 Hz to 8.9 Hz, a 9.2% decrease. This resulted because the crack had a significant effect on the bending and axial stiffness of the member. No appreciable shifts occurred in the other resonant frequencies because the stiffness of the panel containing member 91 was only slightly reduced. By cutting off member 91 at node 23, the 2nd sway mode shifted to about 7.8 Hz, a decrease of 20.41% (Figure 3.10). This results because, at this failure stage, the shear stiffness of the panel was reduced appreciably, while the mass of the structure remained virtually unchanged. After member 91 was removed, the 2nd sway mode (M_x) shifted to about 7.57 Hz, a decrease of 22.76% (Figure 3.11). This further reduction was possibly due to the removal of a damping effect which was produced by member 91 vibrating unattached at node 23, while being fixed at the other node. This assumption may be supported by observing that the peak of the 2nd sway mode is sharper when the member is removed than when it was severed only at node 23 (Figures 3.10 and 3.11).

The 8.3% shift (2.88 Hz to 2.64 Hz) in the 1st sway mode (M_x) was due to a reduction in shear stiffness caused by the removal of member 91. Computations carried out by Loland et al [5] have indicated that the relative shear stiffness between levels immediately above and below a damaged panel is reduced by more than one-half. Since the top panel does not have large inclined members, its shear stiffness is much less than that of the other panels. Besides, the mass of the deck is large compared to the rest of the structure; so the reduction in resonant frequency of the 1st sway mode (M_x) is smaller than that of the 2nd sway mode (M_x).

By cutting off member 91 at node 23, the 1st torsional mode (M_y) decreased by 4% (Figure 3.10). At that frequency, the amplitude of the peak on the transfer function is reduced. When the member is removed, the amplitude of the peak disappears.

The reduction in frequency is due to a reduction in shear stiffness. For bending in one plane, only two panels contribute to the shear stiffness. On the other hand, in torsion, all four panels contribute to the shear stiffness. The low amplitude results, because the impedance head measures only the z-direction acceleration component of the 1st torsional mode (M_y). Furthermore, because of the location of the impedance head (between location A and B on the deck), the measured acceleration at that position would be smaller than that measured at the corners of the deck. This statement will be exemplified when the displacement results at the corner of the deck are discussed.

Members 91 and 84 Severed:

When members 91 and 84 are severed, the excitation frequency of the 1st sway mode (M_x) decreased by 31% (2.88 Hz − 2.0 Hz). This large change could have resulted because the panel above these damaged members may have lost much more shear stiffness for reasons discussed previously.+++ Member 84 contributed to the shear stiffness for bending in the y-z plane. For this reason, by removing it, a reduction in the shear stiffness occurred. This contributed to the decrease of the excitation frequency of the 2nd sway mode (M_x) to 7 Hz, a 29% decrease

+++At this stage, the effect of the lumped mass at the deck has a greater influence on the mechanical mobility of the structure at the top panel.

(Figure 3.13), and explains why the new resonant peak at approximately 8 Hz appears. Based on the computer analyses, that resonant peak is comparable to the 3rd sway mode (M_x). The peak of the 1st torsional mode (M_y) is apparent at about 3.25 Hz, when member 84 is severed at node 31. Though the case may be such, for reasons presented earlier, the peak of the 1st torsional mode disappears after the member was removed (Figure 3.13).

7.2.2. Displacement Results

It should be stated that, as a consequence of the complexity of the structure with respect to stiffness, the resonant frequency for a particular mode is coupled; that is, the horizontal motion of the structure is a combination of a z-direction component (i.e., in the direction of the applied force) which is measured with the impedance head, and a x-direction component measured with the reactance converter. Since the structure may not be perfectly symmetrical, both frequency components may not, necessarily, be equal. Thus, it should be understood in this discussion that frequency, unless otherwise stated, refers to the x-direction component of the particular mode being considered. So the percentage changes in natural frequencies, due to the effect of the damaged members, can be attributed to a reduction in shear stiffness as discussed previously.

The displacement results were measured in the manner indicated in order to check the validity of the acceleration results and to give further indication of the location and types of resonant peaks involved. This was, particularly, effective in the detection of the 1st sway

mode (M_y).

An examination of the summarized results--Table 1.4(A) and 1.4(B)--as well as the actual results for the displacement signals (Figures 4.0 to 4.10) indicates similar trends as those from the acceleration results. For instance, three distinct peaks are apparent on the transfer function for the intact structure. It can be observed that the amplitude of the 1st torsional mode (M_y) is very noticeable on the transfer function (Figure 4.0), a result of the location of the reactance converter. This supports the statement made earlier (acceleration results discussion) that the x-direction horizontal component at the corner of the deck, during torsion, is larger in magnitude than the z-direction horizontal component measured with the impedance head between the locations designated A and B.

When member 91 was cut half-way at node 23, the 1st torsional mode (M_y) shifted from 4.0 Hz to 3.73 Hz, a 6.75% decrease (Figure 4.6). There is no appreciable change in the 1st sway mode (M_x), but a 1.5% decrease (9.32 Hz - 9.11 Hz) occurred in the 2nd sway mode (M_x). For the remaining failure stages, the regions on the transfer functions where the 1st torsional mode would possibly be located appear very distorted--non-linear motion. Furthermore, the coherences in these regions are almost zero (Figures 4.2 to 4.5). This illustrates that the measured response power was not caused by the input power. That is, the measured response power is greater than the measured input power, because some extraneous noise source is contributing to the output power. Thus, the coherence functions are less than one (yet slightly greater than zero), for frequencies where the noise source contributes

power. For this reason, the values tabulated in Table 1.4(A) for the 1st torsional mode where specified were obtained from the output displacement spectra, and do not, necessarily, indicate the excitation frequencies of the 1st torsional mode at those failure stages.

A 17.40% decrease resulted in the 2nd sway mode (M_x) when member 91 was removed (Figure 4.8). Also, by removing members 91 and 84, the 2nd sway mode (M_x) shifted to 7.20 Hz, a 22.75% decrease (Figure 4.10). There is no apparent shift in the frequency of the 1st sway mode (M_x). Further, another mode appears at about 8.4 Hz. This trend is also comparable to the acceleration results and is, therefore, associated to 3rd sway mode (M_x).

At many instances on the plotted experimental results, spurious peaks or "split" peaks (two close peaks stemming from a single mode) are present. A possible explanation is a non-linear interaction as a result of the indeterminate connection between the plywood deck and the P.V.C. space frame (refer to Figure 1.11).

Finally, it should be mentioned that the input-spectra (Figure 3.0) are not flat, although the shaker was excited with a signal having a flat input spectrum, except for the filter roll-off. Actually, the structure is excited (as seen in the diagrams referred to before) with a different spectrum, because of the impedance mismatch between the structure and the shaker head.

7.3. Comparison Between Experimental and Theoretical Results

For the purpose of this comparison, only the acceleration results are used, because the displacement results were only carried

out to check the validity of the acceleration results.

There are similar trends between theory (STRUDL computer analyses) and the experimental study. For instance, the theoretical dynamic analysis of the structure without added lumped masses indicates a fundamental mode of approximately 6.67 Hz, which is identical with the experimental results. However, when lumped masses were applied, discrepancies resulted as shown in the following results:

Mode Number	Theoretical Results		Experimental Results	
	No Added Masses	Added Masses	No Added Masses	Added Masses
1st mode (M_x)	6.67 Hz	2.77 Hz	6.67 Hz	2.9 Hz
1st torsional mode (M_y)	8.06 Hz	3.67 Hz	Not excited	4.2 Hz
2nd sway mode (M_x)	16.97 Hz	11.92 Hz	Not excited	9.8 Hz

These discrepancies could have resulted because in the computer analyses it was assumed that the structure is ideal. This is certainly not the case; for example:

(i) The connections at the joints were assumed to have identical rigidity. In the experimental model, this condition may not have been so.

(ii) The mass of the individual structural members was assumed to be concentrated at the joints. This is not the case in the experimental model (reasons will be given later).

(iii) The computer model for the rigid deck may not have been consistent with the actual model.

(iv) The assumption of prismatic member properties in the computer model could have been incorrect as far as the actual model was concerned.

The invalidity of the lumped-mass idealization of the structure could be explained as follows: For any dynamic system, the analysis is greatly complicated by the fact that the inertia forces results from structural displacements which, in turn, are affected by the magnitudes of the inertia forces. This close cycle of cause and effect can be approached directly only by formulating the problem in terms of differential equations. Yet, because the mass of each structural member is distributed continuously along its length, the displacements and accelerations must be defined for each point along the axis of the member, if the inertia forces are to be completely understood. In such a situation, the analysis must be formulated in terms of partial differential equations, because the position along the span of each member, in addition to the time, must be taken as independent variables.

On the contrary, when a lumped-mass idealization is used (as is the case of the STRUDL analysis), the very complicated motion of the structure is greatly reduced, since the inertia forces can only be developed at the nodal points of the structure.

In both the theoretical and experimental results, the mode most affected when a k-brace member was severed (member 91) was the 2nd sway mode (M_x). A 16.02% shift in resonant frequency for the 2nd sway mode (M_x) was calculated from the theoretical results, while, on the other hand, a 22.75% resulted in the experimental results. However, when two members were removed (members 91 and 84), a 29% decrease was observed in the experimental for the 2nd sway mode, compared to a 50.60% for the same mode in the theoretical results. In addition, a 31.0% shift occurred in the 1st sway mode in the experimental analyses compared to

a 15.16% shift in the theoretical results. Again, the modes most affected in both experiment and theory, when two k-brace members are severed, were the 1st sway mode (M_x) and the 2nd sway mode (M_x).

These larger discrepancies could have resulted because, at this failure stage, the affect of the invalidity of the assumptions made in the STRUDL computer analyses could have been more pronounced.

8. CONCLUDING REMARKS

Based on this investigation, it can be concluded that the "structural integrity monitoring technique" certainly demonstrates that a predictable relationship exists between physical damage and the changes in the modes of vibration of the structure. However, as illustrated in the theoretical results (Table 1.2), the effectiveness of the technique depends, to a major extent, on the position or location of the damaged member(s). This observation could not be verified experimentally since once a member was removed it could not be easily replaced.

At each resonant frequency, the structure deformed in a different manner. Hence, the relative magnitudes between the various resonant frequencies should provide an indication of the general location at which the structure had been weakened. The main benefit of such a system is that any damage which has a large influence on the stiffness of a particular vibration mode of the structure will, obviously, result in an analogous large change in the excitation frequency of that mode. For this reason, it is imperative that the stiffness characteristics of the structure be completely understood, so that any large change in the resonant frequency of a specific mode may be localized.

Since this study considers an out-of-water investigation, many factors which may come into play in an aquatic environment, even under laboratory conditions (e.g., a wave tank), which were not considered, could greatly affect the results; for instance, the added mass affect of the water, vortex shedding, and a host of other complex parameters.

Furthermore, if this technique were applied in an ocean environment on an actual operating platform, other complexities such as marine

growth could cause shifts in certain resonant frequencies. It is for this reason why the integrity method using vibration analyses should be carried out on a constant basis in conjunction with conventional detection procedures, if its effectiveness is to be maximized.

9. RECOMMENDATIONS

It should be clearly understood that this technique should not be conceptualized as a panacea for solving the problem of early detection of damage of subsurface structural components with great certainty since certainty, in such a complex environment as the ocean, can rarely be assured. However, if applied in conjunction with conventional detection procedures on a constant basis, the effectiveness of the structural integrity monitoring technique should be enhanced.

From the experience gained in this study, the following recommendations are made:

(i) More time be spent, if future experiments of this type are carried out, to ascertain that the structure is not redundant as far as stiffness is concerned. In so doing, it is believed that more resonant frequencies would be excited experimentally, so that a better comparison could be made between experiment and theory.

(ii) The background noise levels and signal to noise ratios should be fairly well understood.

(iii) Some assessment of the mode shapes of the structure should be obtained in order that a comparison with the theoretical eigenvectors can be made. Therefore, it would, perhaps, be advantageous if a number of sensors were located at nodes along the structure where the mode shapes are required. There is certainly a need for more laboratory work (in and out of water) in this area of study, in addition to more experiments on actual operating platforms in the ocean.

Consequently, it should be mentioned that at the time of writing this thesis, plans are being made to carry out tests on a more refined model in the wave tank facilities at Memorial University. It is hoped, however, that the experience gained from this investigation will be very useful in that study.

REFERENCES

[1] Loland, O., Mackenzie, A.C. On the Natural Frequencies of Damped Offshore Platforms. Mech. Res. Comm., Volume 1, 353-354, Pergamon Press, Department of Mechanical Engineering, University of Glasgow G12 899, Scotland (1974).

[2] Begg, R.D., Mackenzie, A.C., Dodda, C.J., Loland, O. Structural Integrity Monitoring Using Digital Processing of Vibration Signals. 8th Annual Offshore Technology Conference, Houston, Paper No. 2549 (May 3-6, 1976), pp. 305-310.

[3] Begg, R.D., Mackenzie, A.C. Monitoring Offshore Structures Using Vibration Analysis. Proceedings of the IES Symposium, Integrity of Offshore Structures, Glasgow, Scotland (April, 1978).

[4] Loland, O., Dodds, C.J. Experiences in Developing and Operating Integrity Monitoring Systems in the North Sea, OTC. 8th Annual Conference, Paper Number 2551 (May 3-6, 1976), pp. 313-317.

[5] Loland, O., Mackenzie, A.C., Begg, R.D. Integrity Monitoring of Fixed, Steel Offshore Oil Platforms, Department of Mechanical Engineering, University of Glasgow, Scotland, pp. 1-4.

[6] Begg, R.D. Analysis for Deep North Sea Installations, Petroleum Engineer (October, 1977), pp. 108-116.

[7] Begg, R.D., Mackenzie, A.C. Monitoring of Offshore Structures Using Vibration Analysis, Structural Monitoring Seminar on "Structural Integrity Monitoring of Offshore Structures" (April, 1978), pp. 1-7.

[8] Lock, G.P.D., Jones, A.W. The Detection of Failures in Offshore Structures by Vibration Analysis. A Feasibility Study, Interpretation of Complex Signals from Mechanical Systems. Symposium, London (1976), pp. 31-35.

[9] Wooton, L.R. Use of Vibration Monitoring on Offshore Structures. Institution of Civil Engineers, London. Proceedings of Conference, Paper Number 9 (July, 1977), pp. 95-102.

[10] Brown, D.R. Monitoring and Structural Response of Steel Offshore Structures. European Offshore Petroleum Conference, and Exhibition, London (October 24-27, 1978), p. 169.

[11] Vandiver, J.K. Detection of Structural Failure on Fixed Platforms by Measurement of Dynamic Response. Seventh Annual Offshore Technology Conference, Houston, Texas, Paper Number 2267 (May 5-8, 1975), pp. 243-251.

[12] Busby, R.F. Underwater Inspection/Testing/Monitoring of Offshore Structures. Ocean Engineering, Volume 6, pp. 355-491, Pergamon Press Ltd., Britain (1979), pp. 456-471.

[13] Rubin, S. Mode Extraction from Ambient Vibrations of an Offshore Platform. ASCE Spring Convention and Exhibit, Boston (April 2-6, 1979).

[14] Vandiver, J.K., Campbell, R.B. Estimation of Natural Frequencies and Damping Ratios of Three Similar Offshore Platforms Using Maximum Entropy Spectral Analysis. ASCE Spring Convention and Exhibit, Boston, Mass. (April 6, 1979).

[15] Bendat, J.S., Piersol, A.G. Random Data Analysis and Measurements, John Wiley and Sons (1971).

[16] Franks, L.E. Signal Theory. Prentice Hall, Inc. (1969).

[17] Koopmans, L.H. The Spectral Analysis of Time Series. Academic Press (1974).

[18] Miller, S.K. Complex Stochastic Processes. Addison-Wesley Publishing Company, Inc. (1974).

[19] Appenheim, A.V. Applications of Digital Signal Processing. Prentice Hall, Inc. (1978).

[20] Richardson, M. Identification of the Modal Properties of an Elastic Structure from Measured Transfer Function Data. 20th I.S.A., International Symposium, Albuquerque, N.M. (May, 1974).

[21] Richardson, M. Modal Analysis Using Digital Test Systems. Seminar on Understanding Digital Control and Analysis in Vibration Test Systems. Shock and Vibration Information Center Publication, Naval Research Lab., Washington D.C. (May, 1975).

[22] Richardson, M., Kniskern, J. Identifying Modes of Large Structures from Multiple Input and Response Measurements. SAE Aerospace Engineering and Manufacturing Meeting Proceedings, San Diego (1976).

[23] Ramsey, K.A. Effective Measurements for Structural Dynamics Testing. Sound and Vibration Magazine, Part I (November, 1975), pp. 24-35; Part II (April, 1976), pp. 18-31.

[24] Edward, H. Death in the North Sea. Readers' Digest, Montreal (November, 1980), pp. 75-79.

[25] McKinney, W. Band Selectable Fourier Analysis. Hewlett-Packard Journal (April, 1975), pp. 20-24.

[26] Broch, J.T. Mechanical Vibration and Shock Measurements. Brüel and Kjaer (June, 1973).

[27] Richardson, M.H. Detection of Damage in Structures from Changes in their Dynamic (Modal) Properties--A Survey. Structural Measurements, Inc. (1980).

[28] Crandall, S.H., Mark, W.D. Random Vibration in Mechanical Systems. Academic Press (1963).

[29] Malen, D.E., Vaughan, E.A. Digital Filtering for Analysis of Structural Vibration. SAE Paper Number 730503 (May, 1973).

[30] Lang, F.F. Understanding Vibration Measurements. Nicolet Scientific Corp., Apple. Note 9 (June, 1975).

[31] Roth, P. Effective Measurements Using Digital Signal Analysis. IEEE Spectrum (April, 1971), pp. 62-70.

[32] Tretter, S.A. Introduction to Discrete-Time Signal Processing. John Wiley and Sons, Inc. (1976).

[33] Thomas, J.B. An Introduction to Applied Probability and Random Processing. John Wiley and Sons, Inc. (1971).

[34] Logcher, D.R., Connor, J.J., Nelson, M.F. ICES STRUDL II, M.I.T., Second Edition (June, 1971).

[35] Stanley, W.D. Digital Processing of Signals. Reston Publishing Company, Inc. (1975).

[36] Clough, R.W., Penzien, J. Dynamics of Structures. McGraw-Hill Book Company (1975).

TABLES

Table 1.0 Calculated Natural Frequencies for the Intact and Damaged Structure

MODE NUMBER	NO LUMPED MASSES		WITH ADDED LUMPED MASSES		
	Frequency Hz (undamaged structure)	Frequency Hz (undamaged structure)	Frequency Hz (member 91 severed)	Frequency Hz (member 84 severed)	Frequency Hz (members 91 & 84 severed)
MODE 1 (1st sway - M_x)	6.67	2.77	2.69	2.71	2.35
MODE 2 (1st sway - M_z)	6.67	2.81	2.79	2.80	2.80
MODE 3 (1st torsion - M_y)	8.06	3.67	3.58	3.62	3.57
MODE 4 (2nd sway - M_x)	16.97	11.92	10.01	10.01	5.89
MODE 5 (2nd sway - M_z)	20.82	11.95	11.72	11.72	11.61
MODE 6 (3rd sway - M_x)	23.02	12.29	11.92	11.82	11.73
MODE 7 (3rd sway - M_z)	22.73	12.17	12.03	12.10	11.66
MODE 8 (4th sway - M_x)	24.33	12.24	12.20	12.15	11.97

TABLE 1.1 SAMPLE EIGENVECTOR FOR MODE 8 (DISPLACEMENTS AND ROTATIONS AT ALL THE NODAL POINTS FOR THE UNDAMAGED STRUCTURE).

MODE 8 JOINT	DISPLACEMENT		
	X DISP.	Y DISP.	Z DISP.
1	0.0	0.0	0.0
2	0.0	0.0	0.0
3	0.0	0.0	0.0
4	0.0	0.0	0.0
5	0.0	0.0	0.0
6	0.0	0.0	0.0
7	0.0	0.0	0.0
8	0.0	0.0	0.0
9	0.0	0.0	0.0
10	0.0	0.0	0.0
11	0.0	0.0	0.0
12	0.0	0.0	0.0
13	0.0189643	0.0108509	0.0107254
14	-0.8935064	-0.1015154	0.0065610
15	-0.0253073	-0.0013905	0.0127902
16	-0.0204100	0.0010068	-0.0010653
17	-0.0287409	0.0131834	-0.0020855
18	0.8812165	-0.0810300	0.0022656
19	0.0157807	-0.0343927	-0.0047754
20	0.0105874	0.1170980	0.0039552
21	-0.0186787	-0.0113171	-0.0130122
22	0.1635888	0.4086318	-0.0039126
23	0.3354703	0.0522551	0.0005840
24	0.1044054	0.0551969	-0.0005141
25	-0.0268771	0.0387164	-0.0013979
26	-0.0348144	-0.3531880	0.1857318
27	-0.0382276	-0.0457026	0.3944393
28	-0.0370644	-0.0762699	0.2811487
29	-0.0368977	-0.0136886	0.0712134
30	-0.2047905	0.3369696	0.0634304
31	-0.3938865	0.0304171	0.0594587
32	-0.2687541	-0.0709267	0.0610840
33	-0.0363884	0.0416481	0.0655341
34	-0.0251897	-0.5186383	-0.1140131
35	-0.0201859	-0.0743603	-0.3346118
36	-0.0206967	-0.2024303	-0.2348442
37	-0.2578400	-0.0095221	0.5100598
38	-0.5178867	0.0401709	-0.0186782
39	0.0421359	-0.0123298	-0.3653842
40	0.6663386	0.0449425	-0.0008265
41	-0.3415522	-0.0044208	0.1561968
42	-0.3827168	0.0409318	-0.0007234
43	0.2484472	-0.0072985	-0.1632484

44	0.4199798	0.0480889	0.0044370
45	-0.0008165	-0.0053214	-0.0024966
46	0.0052371	-0.1329829	-0.0019400
47	0.0101575	-0.1238389	-0.0027122
48	0.0078054	-0.0339640	-0.0026191
49	-0.0018136	0.8410696	-0.0027656
50	-0.0019611	0.2000219	0.0056378
51	-0.0014027	0.4180030	0.0083000
52	-0.0018467	0.2040867	0.0035819
53	-0.0014270	-0.0071022	-0.0055235
54	-0.0079019	-0.0176380	-0.0044664
55	-0.0121691	0.0495467	-0.0029774
56	-0.0074857	0.0440702	-0.0022461
57	0.0001401	0.0487763	-0.0023439
58	0.0001469	0.3971123	-0.0136729
59	-0.0005257	0.5634990	-0.0140584
60	-0.0003849	0.2021712	-0.0148124

MODE 8 CONTINUED :

JOINT	ROTATION		
	X ROT.	Y ROT.	Z ROT
1	0.0	0.0	0.0
2	0.0	0.0	0.0
3	0.0	0.0	0.0
4	0.0	0.0	0.0
5	0.0	0.0	0.0
6	0.0	0.0	0.0
7	0.0	0.0	0.0
8	0.0	0.0	0.0
9	0.0	0.0	0.0
10	0.0	0.0	0.0
11	0.0	0.0	0.0
12	0.0	0.0	0.0
13	-0.0434206	0.1626339	-0.0038158
14	0.1948710	-0.0056287	-0.0709550
15	-0.1395046	-0.1232218	-0.7510875
16	0.0350081	0.0014852	0.1668182
17	0.7637176	0.1264129	-0.1323223
18	-0.1952618	0.0001697	0.0731065
19	0.3909776	-0.1282728	0.0000899
20	-0.0346083	-0.0020149	-0.1696896
21	0.2119564	-0.0374189	0.0727590
22	0.0098564	-0.0328817	0.0542622
23	0.0132998	-0.0157425	0.0703191
24	-0.0053136	0.0410008	0.1117756
25	0.0040408	0.0398115	0.1677877
26	-0.0007165	0.0345317	0.0124453
27	-0.0311641	0.0249850	0.0126289
28	-0.0063917	-0.0409170	-0.0086643
29	-0.0359732	-0.0359732	-0.0107468
30	-0.0065547	-0.0289244	-0.0238916
31	-0.0073349	-0.0272139	-0.0752298

32	-0.0010513	0.0446524	-0.1537383
33	-0.0065517	0.0092086	-0.2851573
34	-0.0279439	0.0324585	-0.0194151
35	0.0253700	0.0338141	-0.0094250
36	0.1134797	-0.0434794	0.0191453
37	0.0599865	-0.0385453	0.0355169
38	-0.0051834	0.0367547	0.0000369
39	-0.0525564	-0.0929300	-0.0187329
40	-0.0171084	0.0372949	-0.0078821
41	-0.0317860	-0.0043226	-0.0504523
42	0.0117424	0.0044075	-0.0506212
43	0.0936161	-0.0025600	0.0330759
44	0.0007367	0.0047482	0.0702508
45	-0.0270605	-0.0022587	-0.0585804
46	-0.0172084	-0.0015189	-0.0500559
47	0.0055760	-0.0000983	-0.0475596
48	0.0158171	0.0013243	-0.0494593
49	0.0154014	0.0022566	-0.0515521
50	0.0102664	0.0011721	-0.0433267
51	0.0232941	-0.0000250	0.0036340
52	0.0209998	-0.0015838	0.0437211
53	0.0127703	-0.0013287	0.0438363
54	-0.0062878	-0.0011239	0.0398894
55	-0.0079001	-0.0000508	0.0338822
56	0.0009677	0.0018867	0.0033553
57	-0.0023853	0.0023397	0.0715077
58	-0.0072282	0.0007724	0.0012993
59	-0.0356401	0.0000963	-0.0128123
60	-0.0269390	-0.0000231	-0.0573577

Table 1.2 Percentage Changes in Natural Frequencies when Certain Members are Severed

Modes of Vibration \ Member(s) Removed	79	80	21	41	91	79 & 69	79 & 76	79 & 70	91 & 90	91 & 83	91 & 82	91 & 84
Sway 1, M_x	-0.72	-6.13	-12.16	-0.36	-2.88	-11.55	-14.07	-13.71	-3.61	-11.19	-12.27	-15.16
Sway 1, M_z	0.0	-1.06	+0.71	-0.71	-0.71	0.0	-1.06	+0.35	0.0	-2.13	-1.07	-0.36
Torsion 1, M_y	-0.54	0.0	+1.63	-0.54	-2.45	-12.76	-12.80	-13.25	-2.99	-14.61	-8.99	-2.45
Sway 2, M_x	-5.78	-10.57	-0.25	-0.25	-16.02	-57.55	-58.30	-58.13	-15.27	-43.20	-44.04	-50.60
Sway 2, M_z	-0.92	-4.93	-0.41	-12.25	-1.92	-0.33	-0.75	-0.33	-16.32	-8.20	-5.61	-2.93
Sway 3, M_x	-2.44	-2.44	-1.46	-3.01	-3.01	-3.42	-2.77	-3.33	-4.96	-8.14	-4.88	-4.64
Sway 3, M_z	+0.33	-1.89	+0.82	+0.49	-1.07	+0.74	-0.16	-0.16	-3.28	-2.21	-2.47	-4.10
Sway 4, M_x	-0.25	-0.08	-0.08	-0.57	-0.33	-0.82	+0.90	-0.08	-2.61	-2.53	-2.12	-2.20

Table 1.3(A) Measured Resonant Frequencies for the Intact and Damaged Structure (Acceleration)

MODE NUMBER	FREQUENCY IN HERTZ					
	Intact	Slightly damaged at node 23	(node 23 cut off)	Damaged (mem. 91 removed)	Damaged (mem. 91 removed, & 84 cut off at node 31)	Damaged (mems. 91 & 84 removed)
MODE 1 (1st sway M_x)	2.88	2.88	2.88	2.64	2.0	2.0
MODE 1 (1st torsion M_y)	4.2	4.03	4.0	peak disappears	3.25	3.25
MODE 3 (2nd sway M_x)	9.8	8.9	7.8	7.57	7.0	7.0

Table 1.3(B) Percentage Changes in Natural Frequencies for the Damaged Structure (Acceleration)

Modes of Vibration	Member(s) Damaged	Mem. 91 slightly damaged at node 23	Mem. 91 cut off at node 23	Mem. 91 removed	Mem. 91 removed & 84 cut half-way at node 31	Mems. 91 & 84 removed
MODE 1 (1st sway M_x)		0%	0%	8.3%	31.0%	31.0%
MODE 2 (1st torsion M_y)		4.05%	4.76%	—	22.62%	22.62%
MODE 3 (2nd sway M_x)		9.2%	20.41%	22.75%	29.0%	29.0%

Table 1.4(A) Measured Resonant Frequencies for the Intact and Damaged Structure (Displacement)

MODE NUMBER	FREQUENCY IN HERTZ					
	Intact	Slightly damaged at node 23	Damaged (node 23 cut off)	Damaged (mem. 91 removed)	Damaged (mems. 91 & 84 cut off at node 31)	Damaged (mems. 91 & 84 removed)
MODE 1 (1st sway M_x)	2.2	2.2	2.2	2.2	2.2	2.2
MODE 2 (1st torsion M_y)	4.0	3.73	3.0 (displacement spectrum)	3.25 (displacement spectrum)	3.51 (displacement spectrum)	3.56 (displacement spectrum)
MODE 3 (2nd sway M_x)	9.32	9.18	7.9	7.7	7.11	7.2

Table 1.4(B) Percentage Change in Natural Frequencies for the Damaged Structure (Displacement)

Modes of Vibration	Member(s) Damaged	Mem. 91 slightly damaged at node 23	Mem. 91 cut off at node 23	Mem. 91 removed	Mem. 91 removed & 84 cut half-way at node 31	Mems. 91 & 84 removed
MODE 1 (1st sway M_x)		0.0%	0.0%	0.0%	0.0%	0.0%
MODE 2 (1st torsion M_y)		6.75%	--	--	--	--
MODE 3 (2nd sway M_x)		1.5%	15.24%	17.40%	23.71%	22.75%

FIGURES

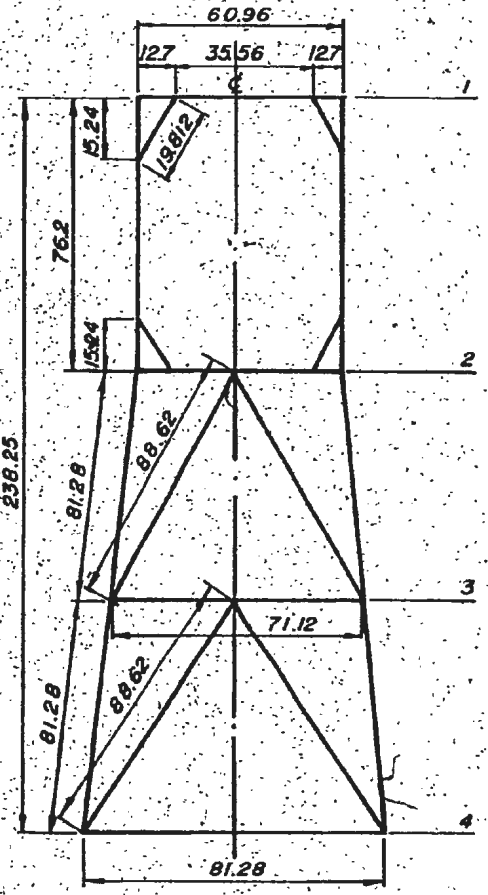

ELEVATION

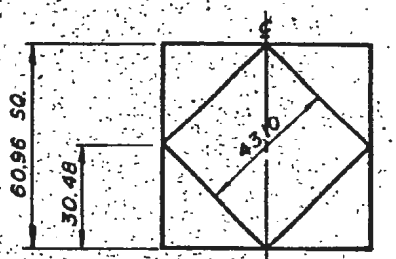

PLAN AT LEVEL 182

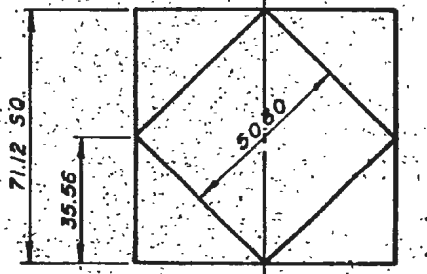

PLAN AT LEVEL 3

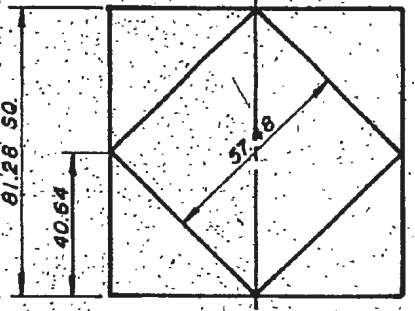

PLAN AT LEVEL 4

FIG. 1.0 MODEL DIMENSIONS

ALL DIMENSION IN Cm.

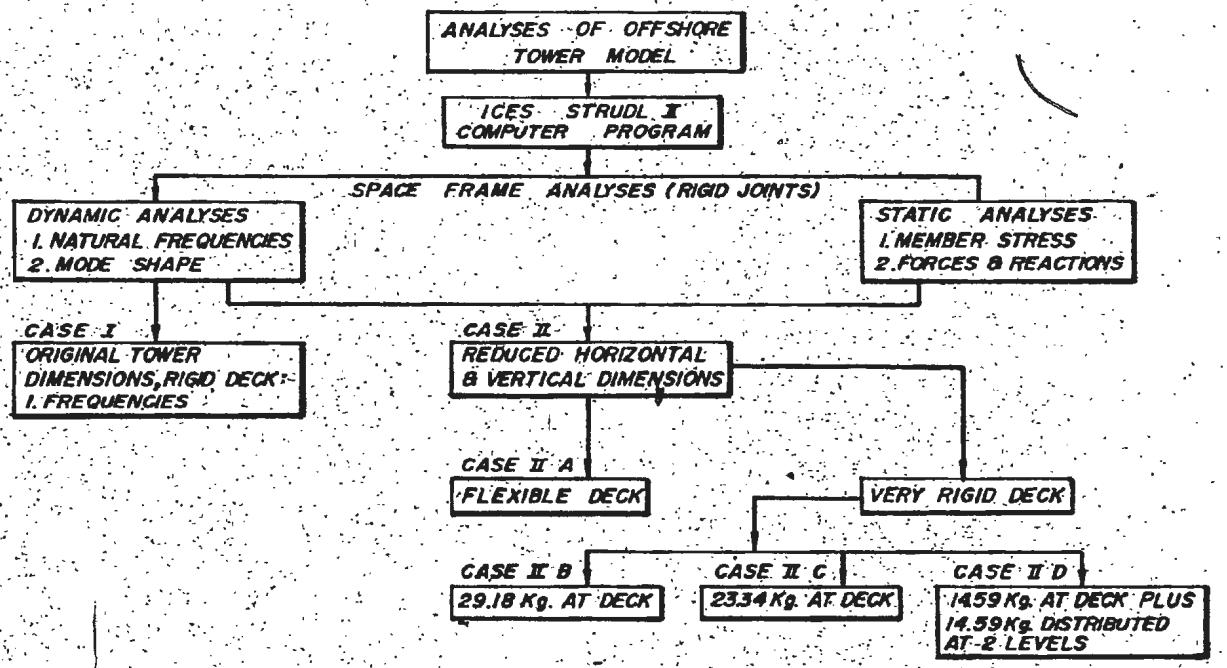

FIG. 1.1 FLOW CHART OF COMPUTER ANALYSES

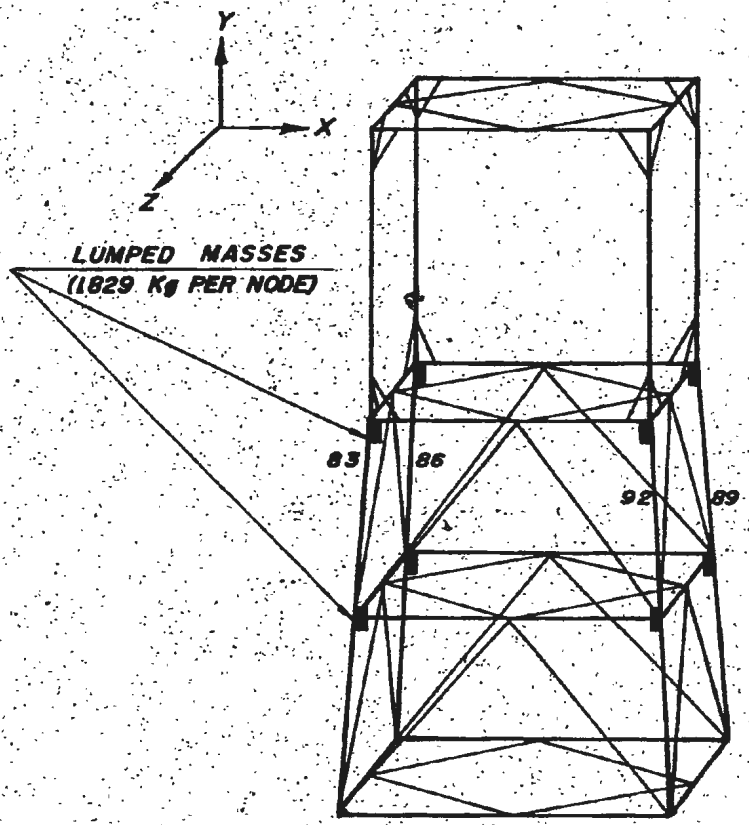

B- MEMBERS HAVING INCREASED SPECIFIC DENSITY

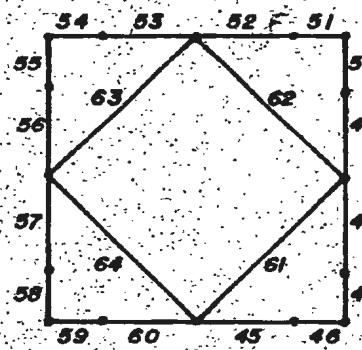

PLAN VIEW OF DECK MEMBERS
A-DECK MEMBERS WITH ADJUSTED PROPERTIES (61-64)

FIG. 1.2 ADJUSTED MEMBERS

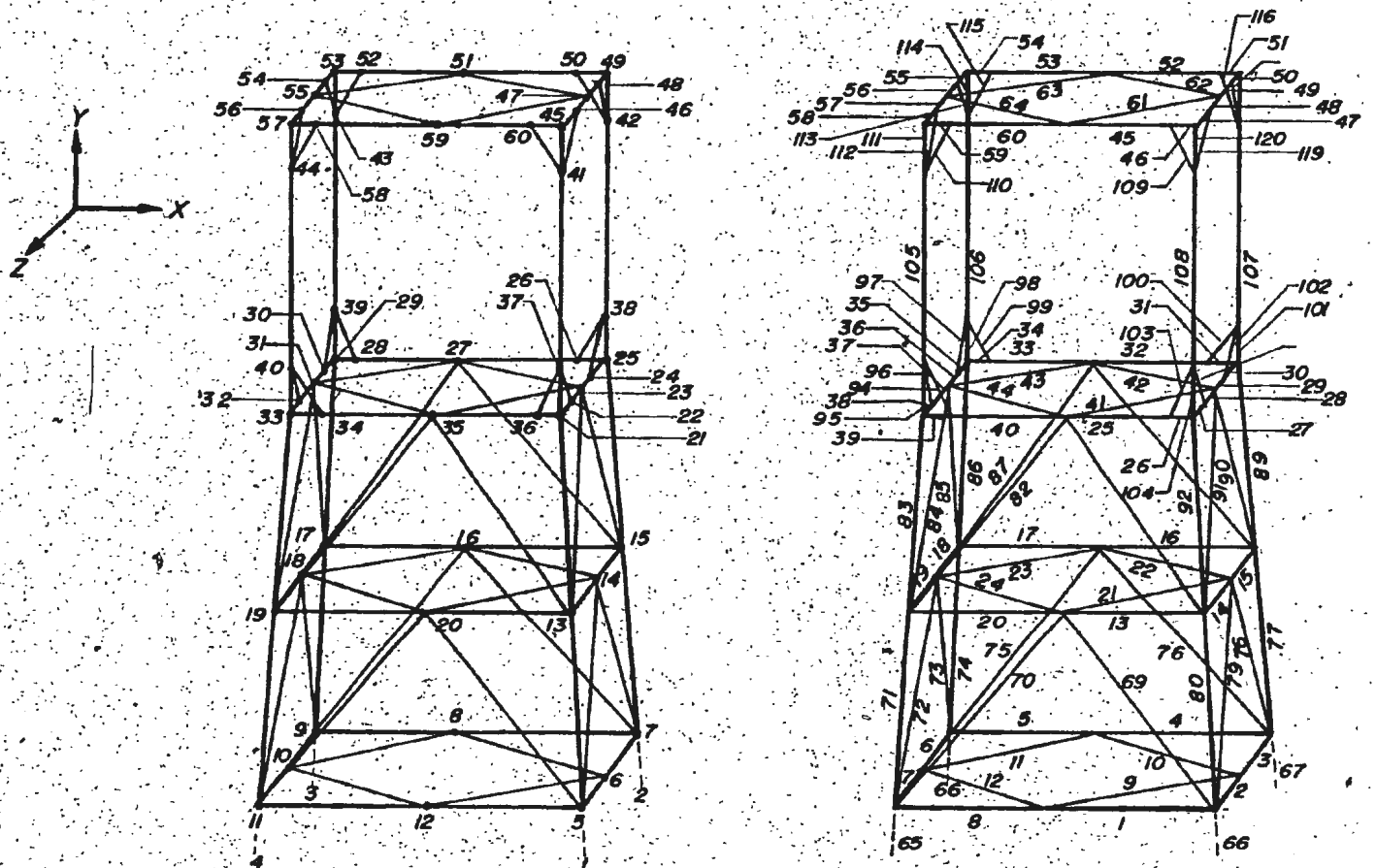

A - NAMING OF STRUCTUTURAL JOINTS B-NAMING OF STRUCTURAL MEMBERS

FIG. 1.3 DISCRETIZATION OF STRUCTURE

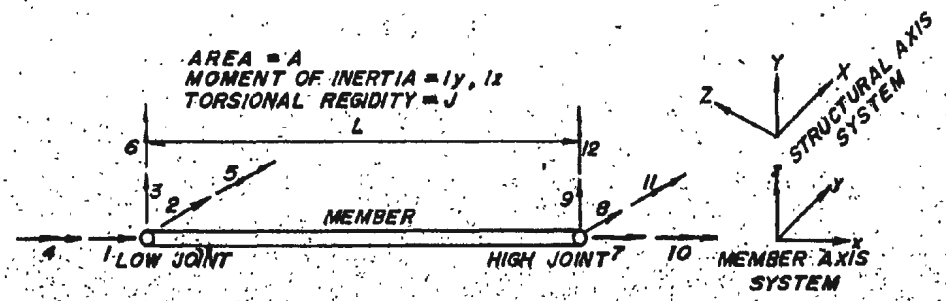

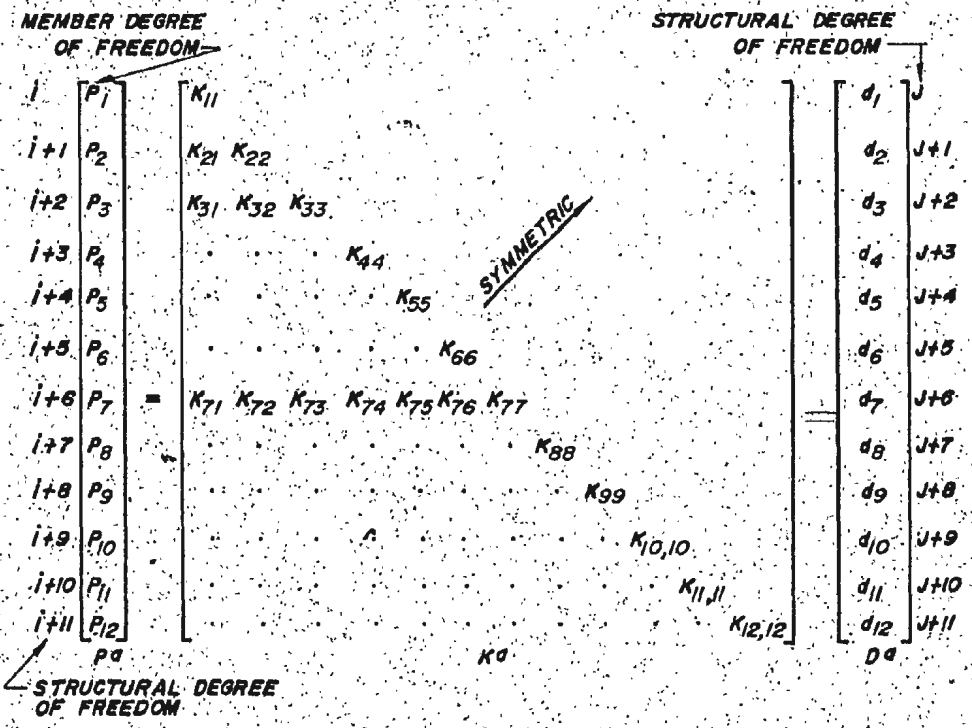

FIG. 14 - STIFFNESS MATRIX OF A MEMBER

1. STRUCTURE IS REPRESENTED BY A COMBINATION OF SMALL ELEMENTS :

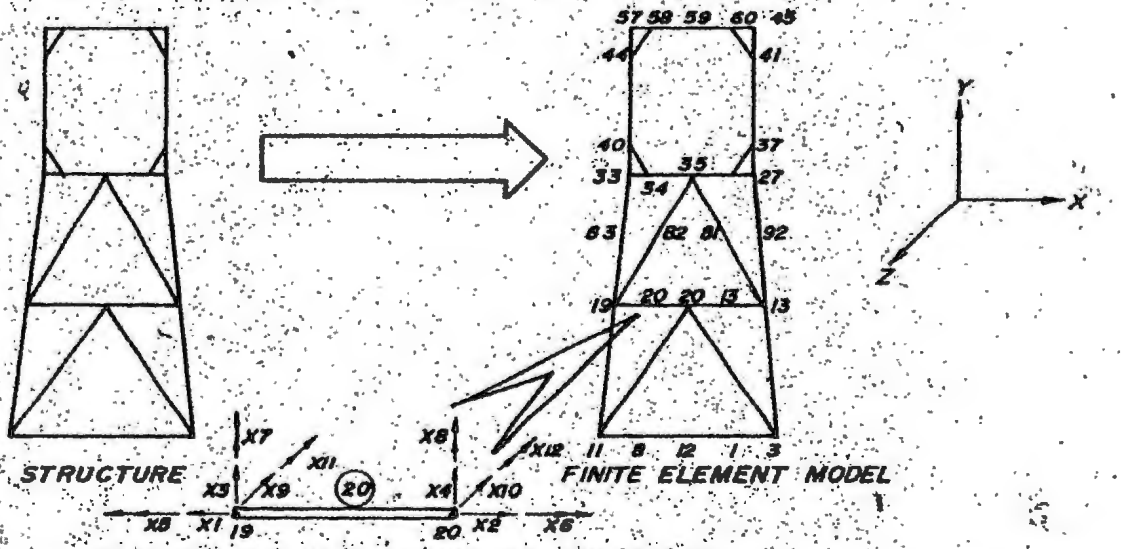

BEAM ELEMENT NO. 20 (12 DEGREES OF FREEDOM)

2. EQUATIONS OF MOTION ARE COMPUTER GENERATED FROM PHYSICAL PROPERTIES OF STRUCTURE:

$$\begin{bmatrix} m_{11} & m_{12} & \cdots \\ m_{21} & & \\ \vdots & & \end{bmatrix} \begin{bmatrix} \ddot{x}_{1(t)} \\ \ddot{x}_{2(t)} \\ \vdots \end{bmatrix} + \begin{bmatrix} c_{11} & c_{12} & \cdots \\ c_{21} & c & \\ \vdots & & \end{bmatrix} \begin{bmatrix} \dot{x}_{1(t)} \\ \dot{x}_{2(t)} \\ \vdots \end{bmatrix} + \begin{bmatrix} k_{11} & k_{12} & \cdots \\ k_{21} & k & \\ \vdots & & \end{bmatrix} \begin{bmatrix} x_{1(t)} \\ x_{2(t)} \\ \vdots \end{bmatrix} = \begin{bmatrix} p_{1(t)} \\ p_{2(t)} \\ \vdots \end{bmatrix}$$

MASS MATRIX — INERTIAL FORCES

DAMPING MATRIX — DISSIPATIVE FORCES

STIFFNESS MATRIX — RESTORING FORCES

EXTERNAL FORCES = 0 (FREE VIBRATION)

FIG. 1.5 COMPUTER GENERATED FINITE ELEMENT METHOD

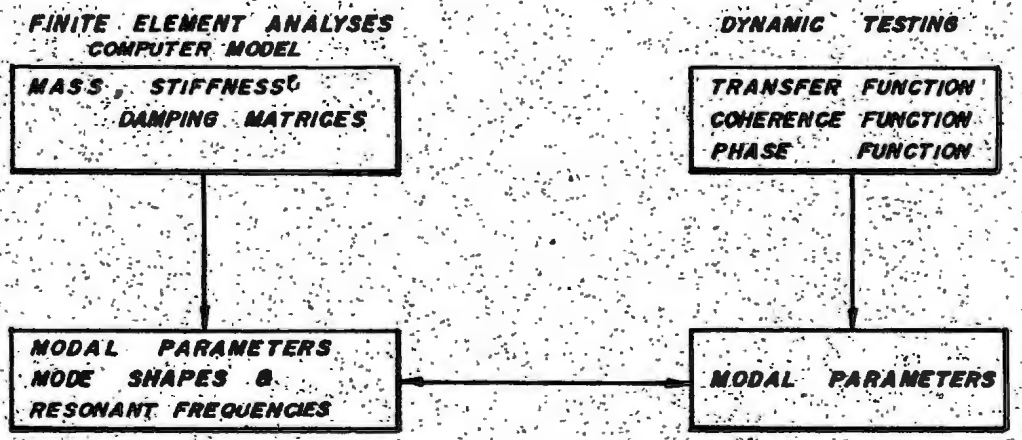

FIG 1.6 COMMON ELEMENTS OF THE ANALYTICAL AND EXPERIMENTAL INVESTIGATIONS

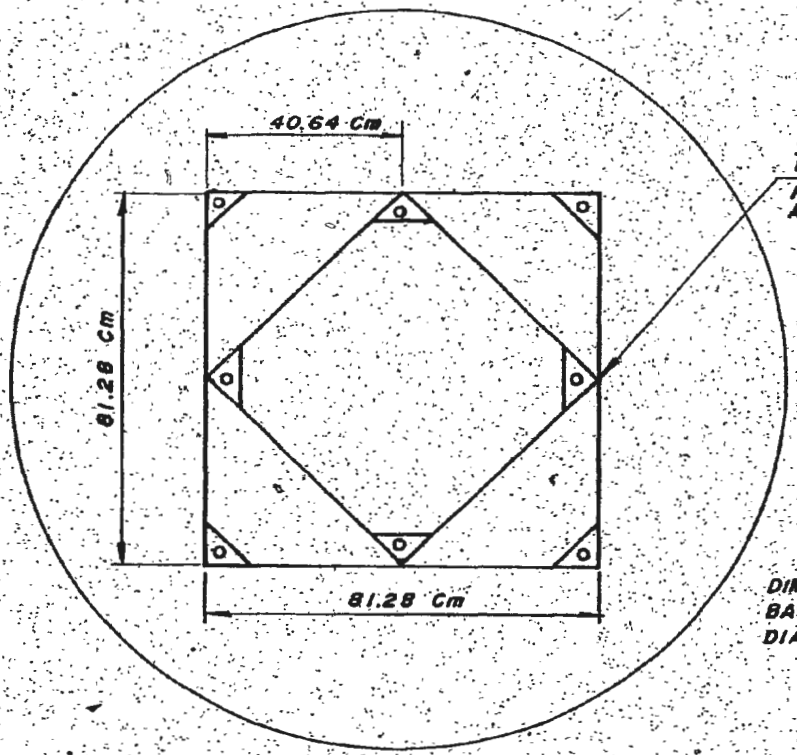

FIG. 17 PLAN VIEW OF FOUNDATION BASE

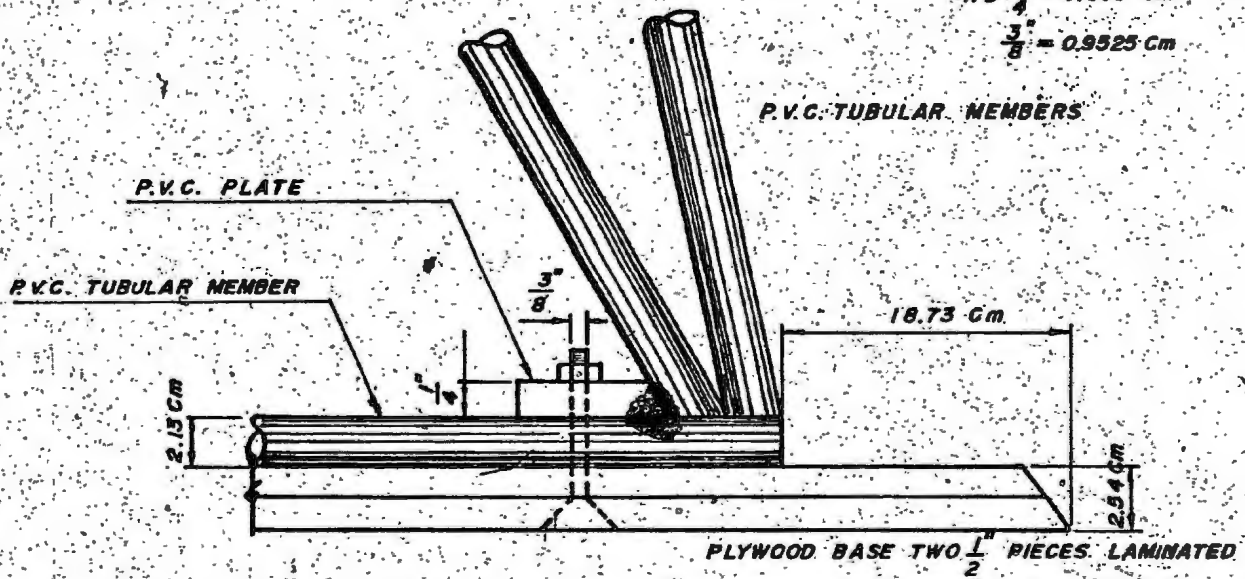

F.I.G.1.8 PROFILE VIEW OF BASE CONNECTION

FIG. 1.9 WEIGHT ARRANGEMENT AT BASE

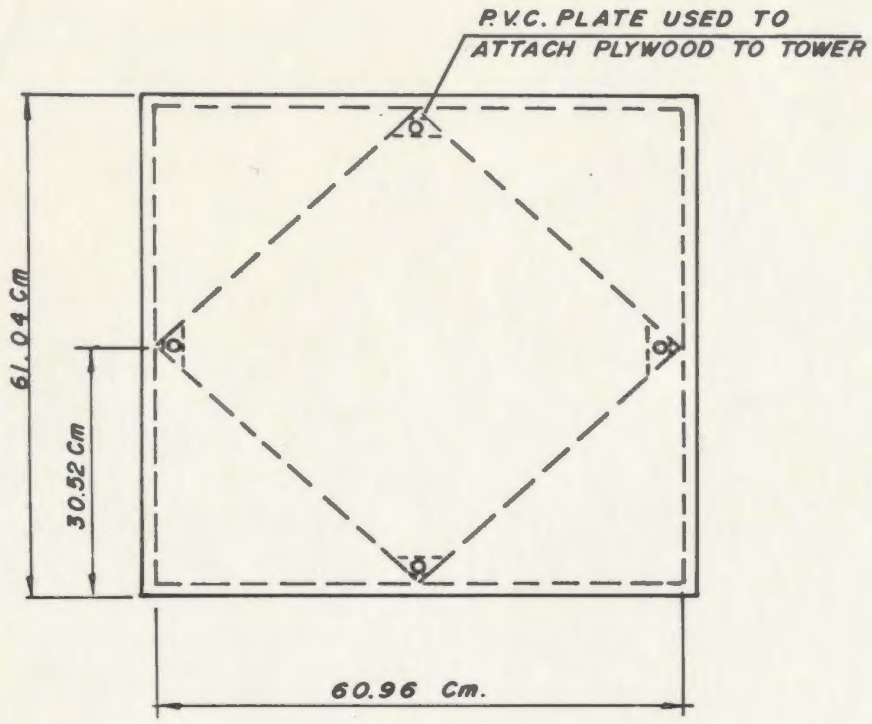

FIG. I.IO PLAN VIEW OF STRUCTURE DECK
NOT TO SCALE

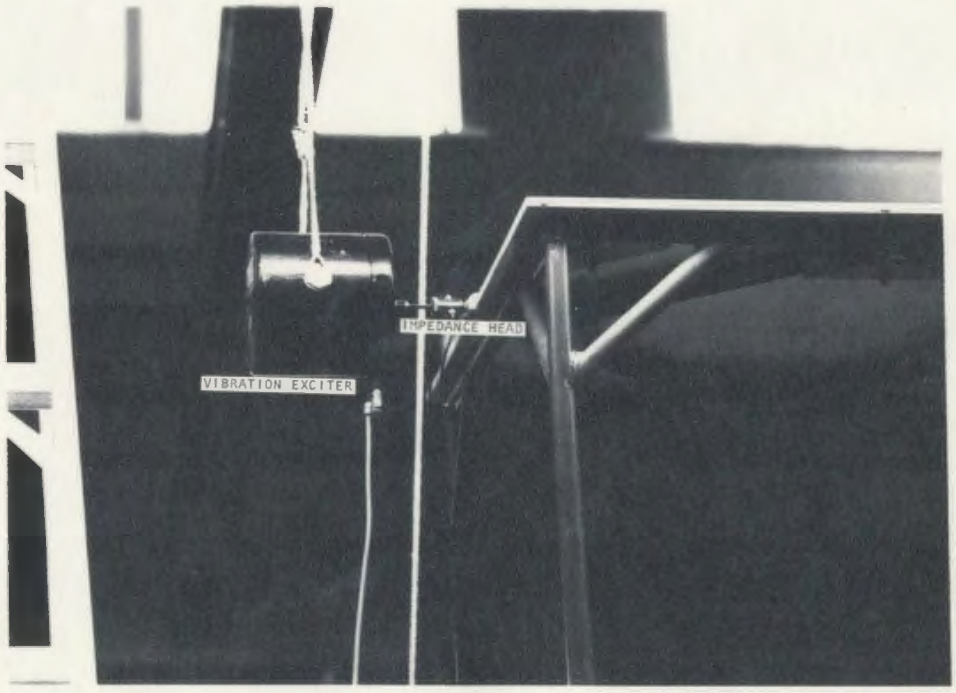

FIG. 1.11 DECK ARRANGEMENT

FIG. 1.12 ARRANGEMENT OF STRUCTURE

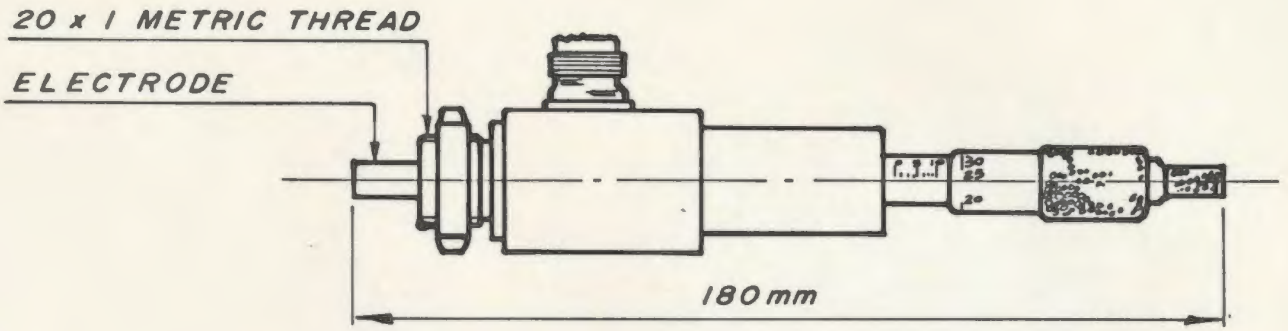

FIG. 1.13 PROXIMITY TRANSDUCER

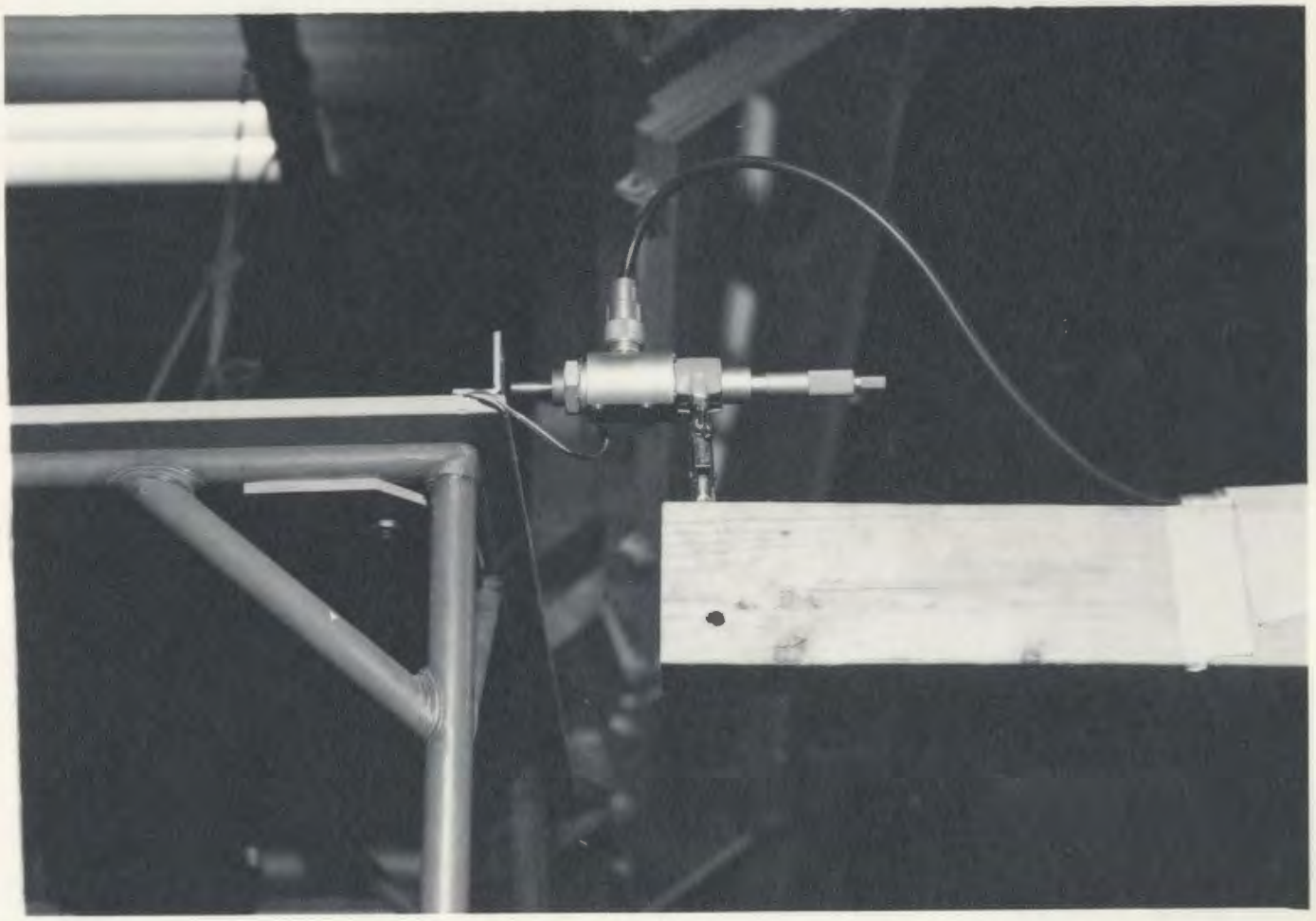

FIG. 1.14 PROXIMITY TRANSDUCER ARRANGEMENT
(See Appendix A2 For Calibrations)

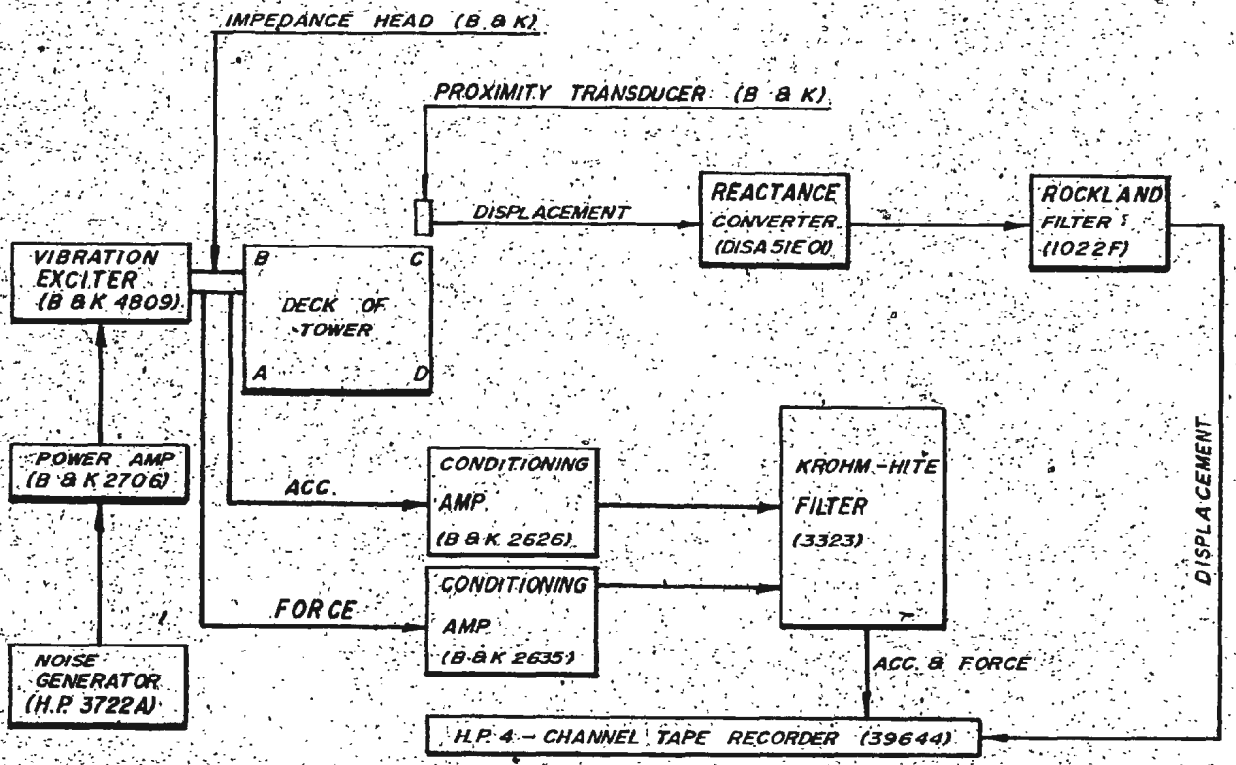

FIG. I.15A EXPERIMENTAL CIRCUIT

SEE APPENDIX A2 FOR INSTRUMENTATION SETTING

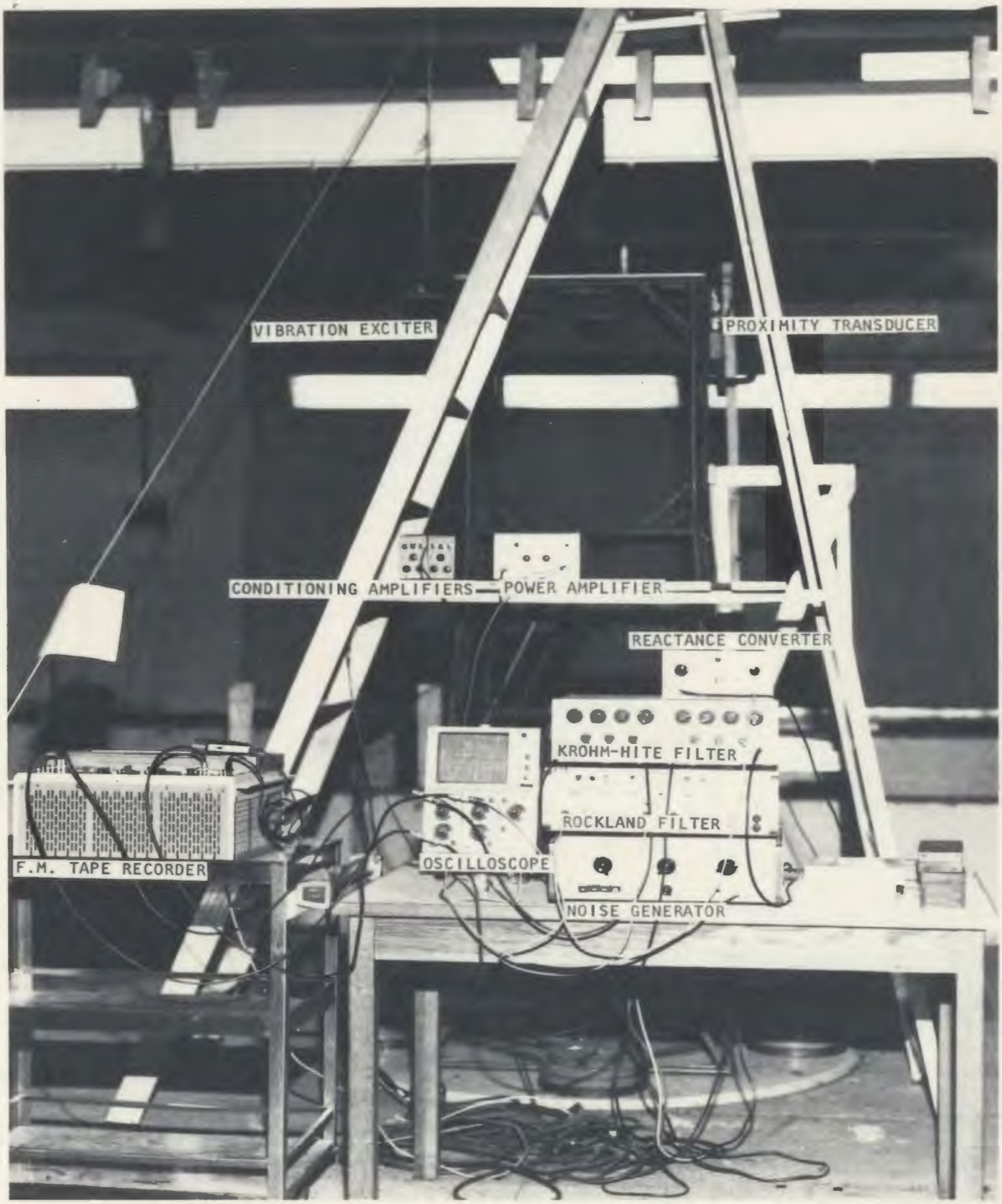

FIG. 1.15(B) TEST APPARATUS

A. Lumped Mass At Deck

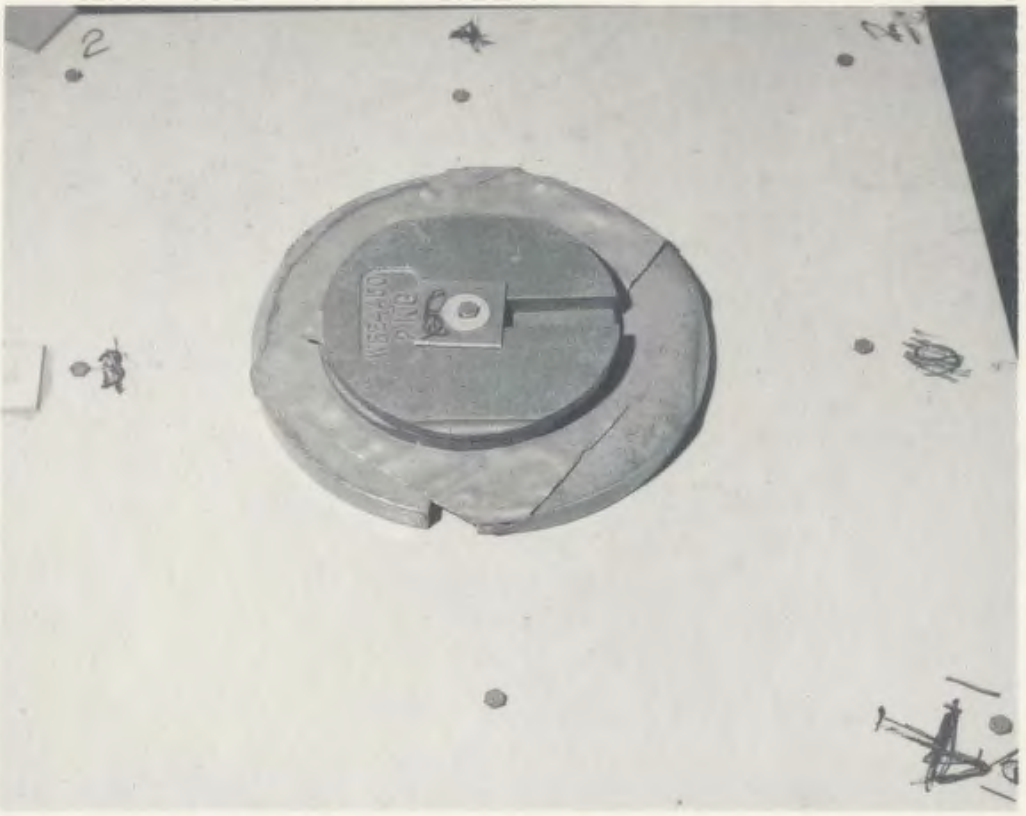

B. Lumped Masses At Nodes

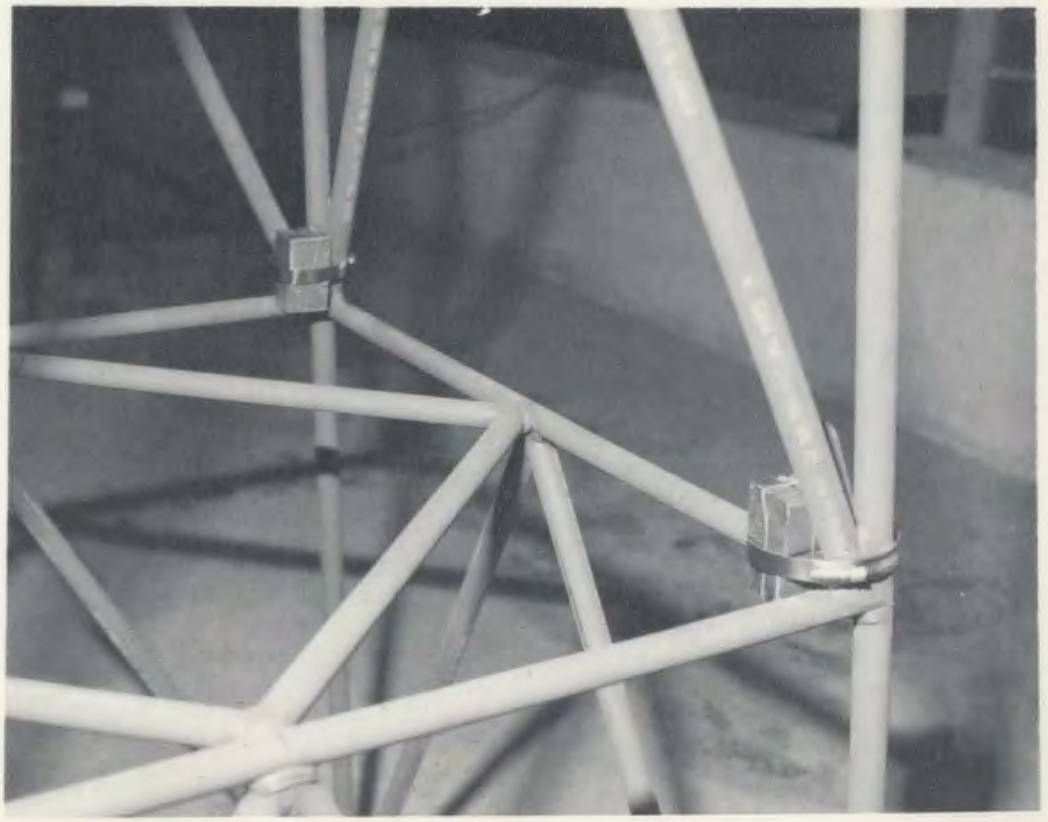

FIG. 1.16 ARRANGEMENT OF MASSES

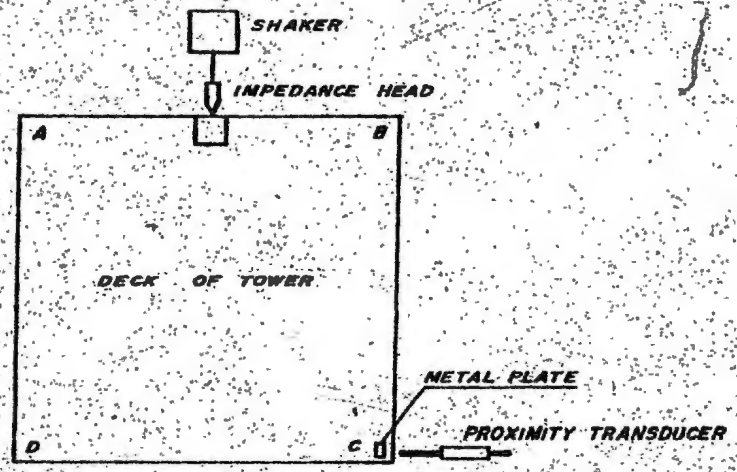

FIG. 17 CHOSEN CONFIGURATION OF TRANSDUCERS

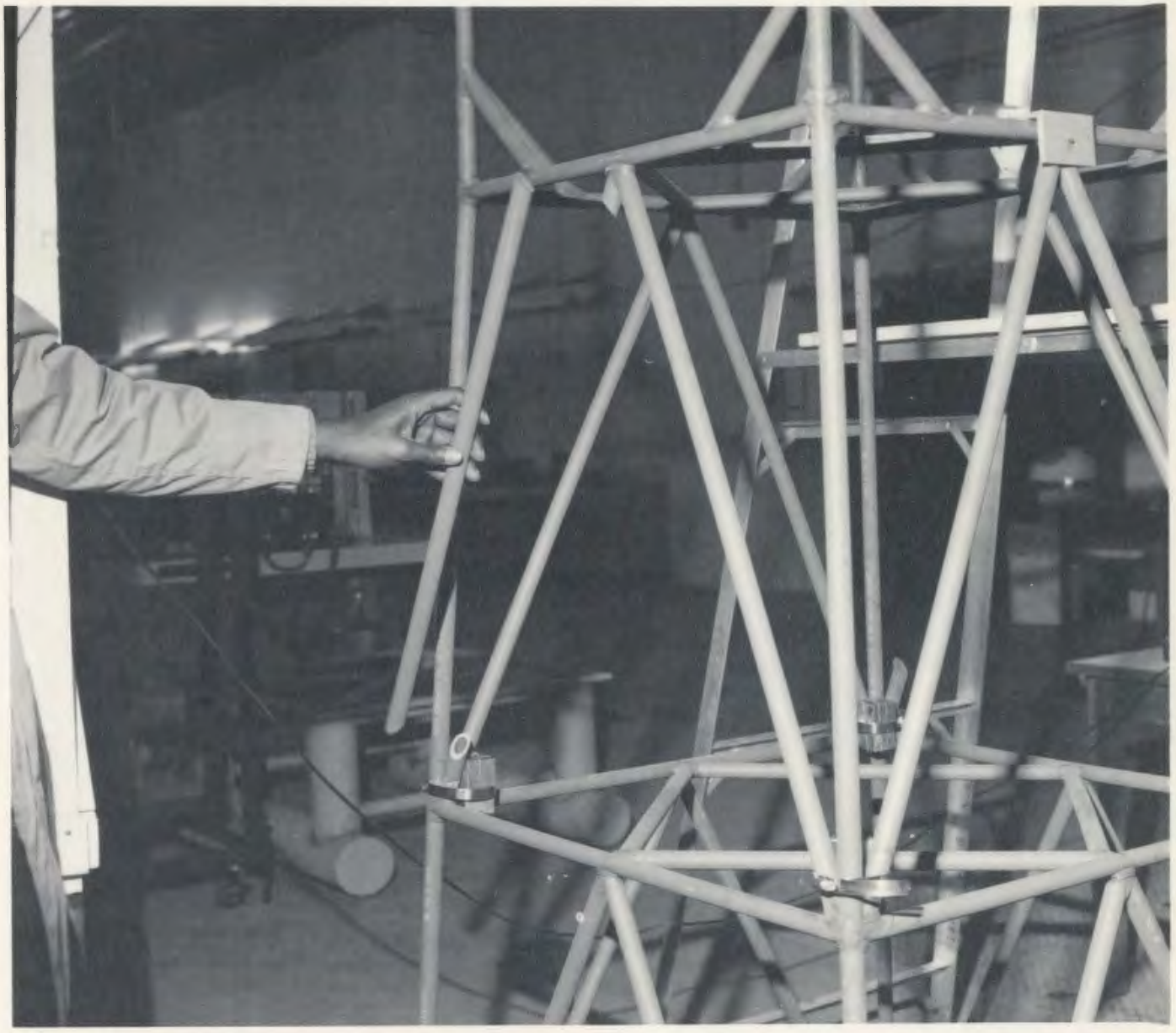

FIG. 1.18 SEVERED MEMBER

FIG. 1.19 THE FOURIER ANALYZER

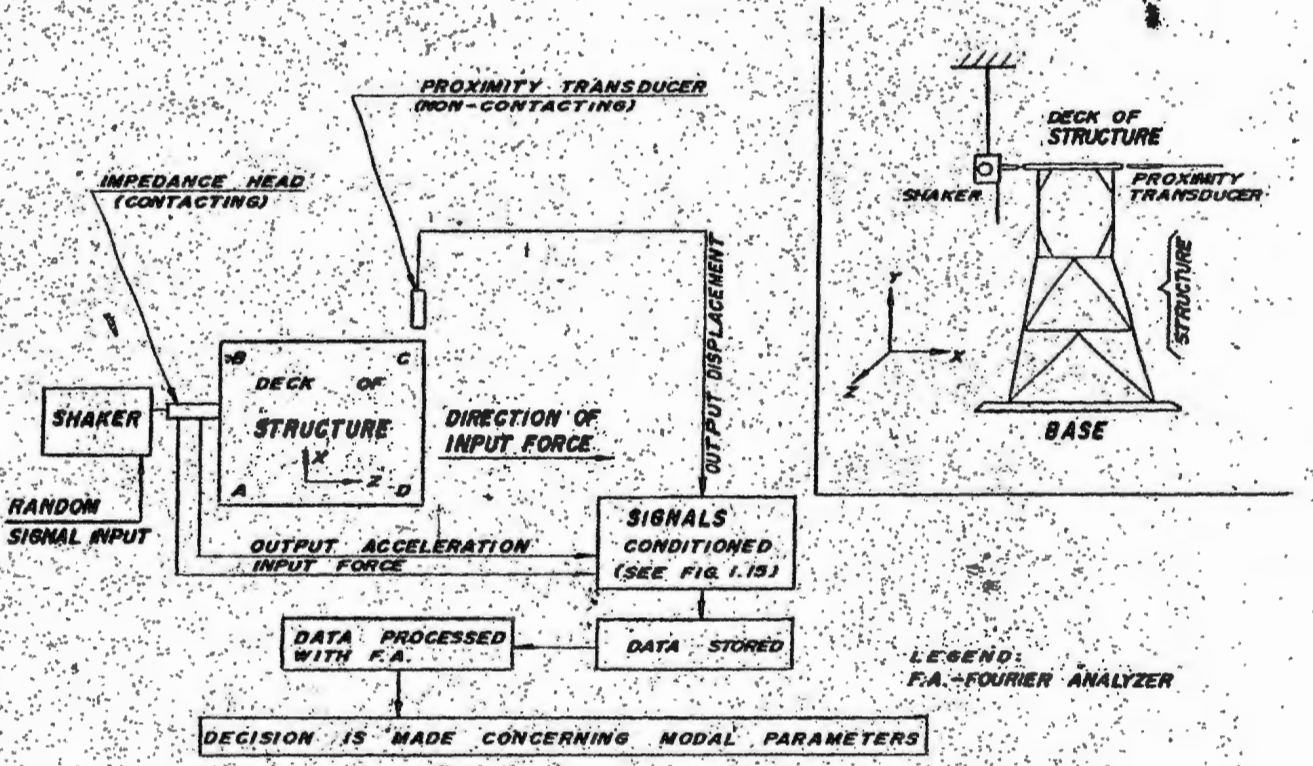

FIG. 1.20 FLOW DIAGRAM OF EXPERIMENTAL PROCEDURE

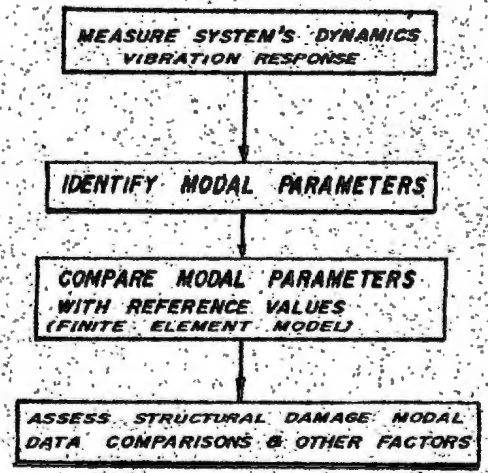

FIG. 1.21 IMPORTANT STEPS FOR INTEGRITY MONITORING

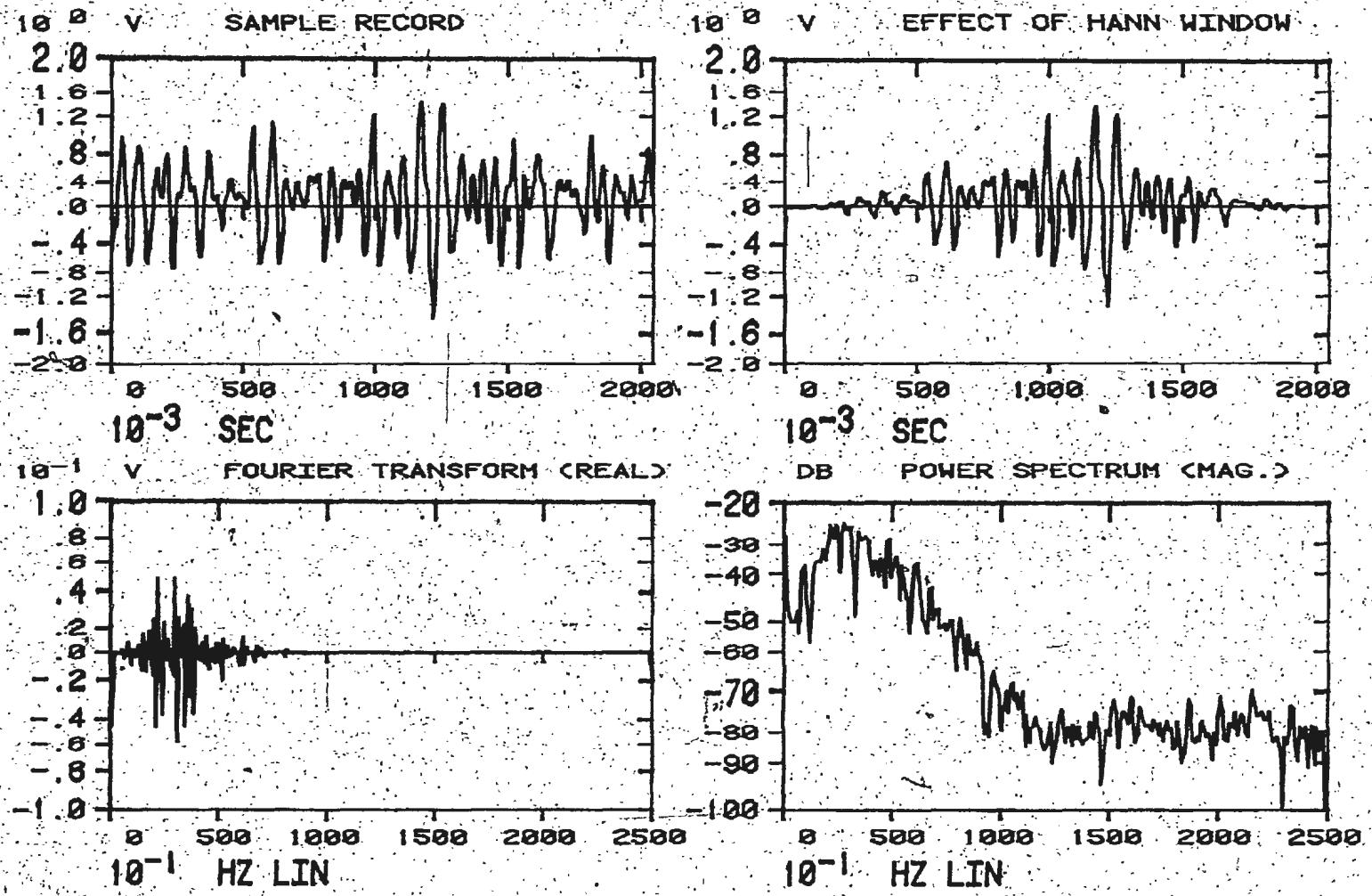

FIG. 1.22 DETERMINATION OF POWER SPECTRUM FOR 1 SAMPLE RECORD
(NB: POWER SPECTRUN IS UNFILTERED)

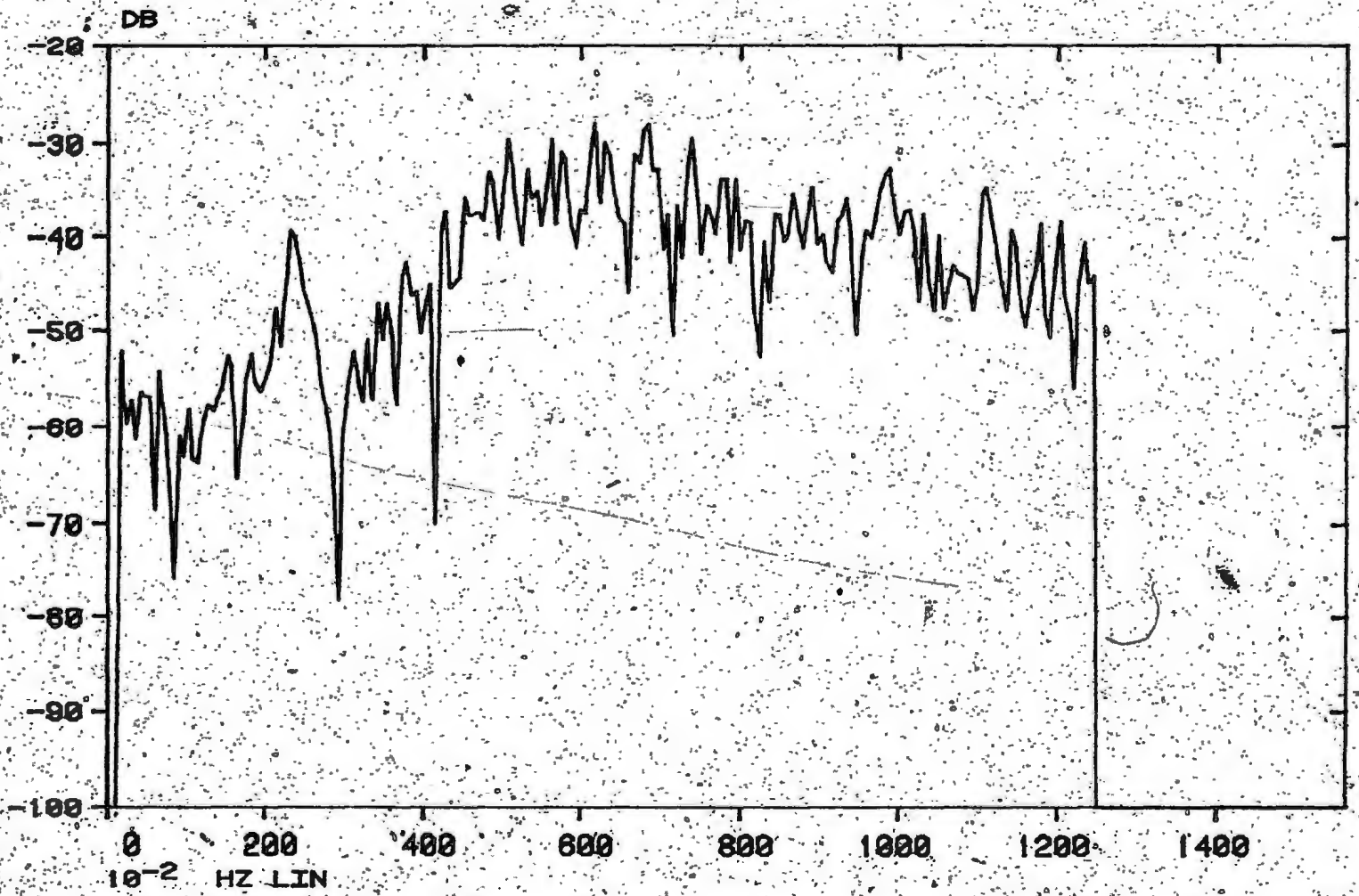

FIG. 1.23 FILTERED POWER SPECTRUM (MAG.) FOR 1 SAMPLE RECORD

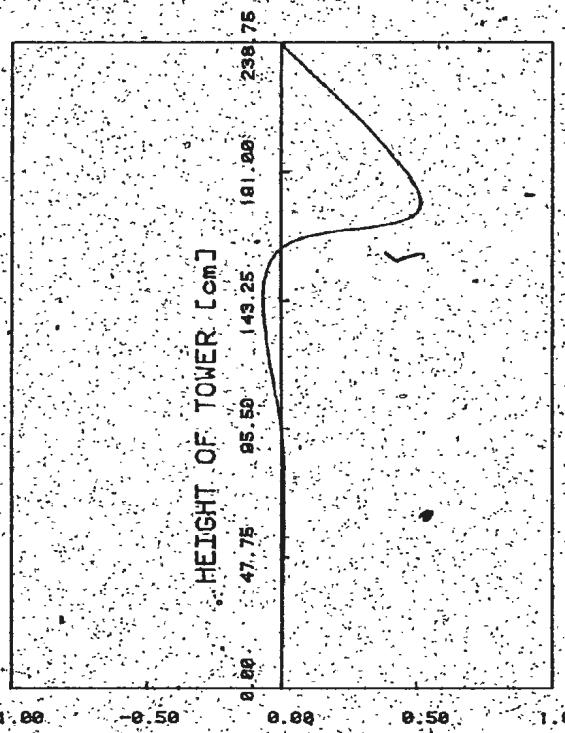

Z AXIS HORIZONTAL DISPLACEMENT

FIG. 2.1(A) MODE 8 (UNDAMAGED)
AT NODES 5,13,21,37,41,45
(VIBRATION FREQUENCY = 12.24 Hz)

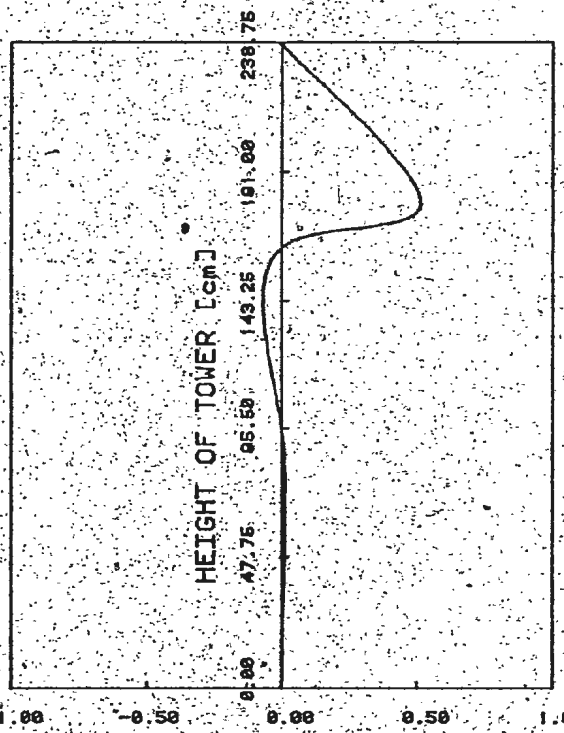

Z AXIS HORIZONTAL DISPLACEMENT

FIG. 2.1(B) MODE 8 (UNDAMAGED)
AT NODES 7,15,25,38,42,49
(VIBRATION FREQUENCY = 12.24 Hz)

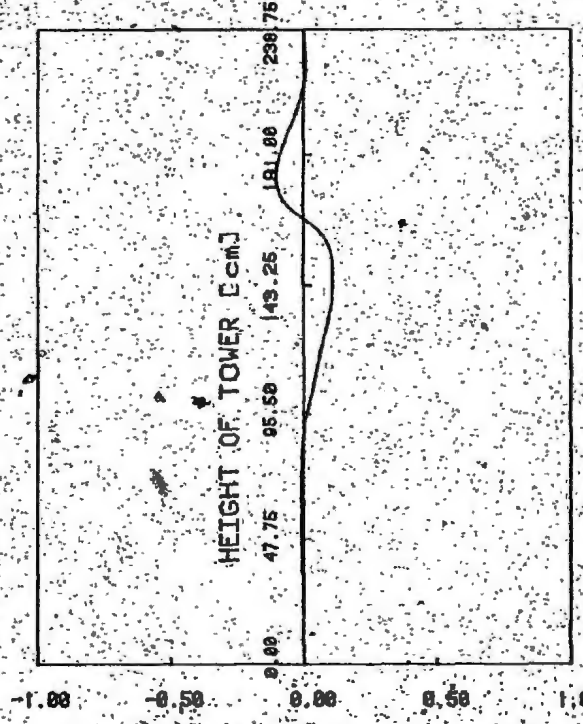

FIG. 2.1(C) MODE 8 (UNDAMAGED)
AT NODES: 11, 19, 33, 40, 44, 57
(VIBRATION FREQUENCY = 12.24 Hz)

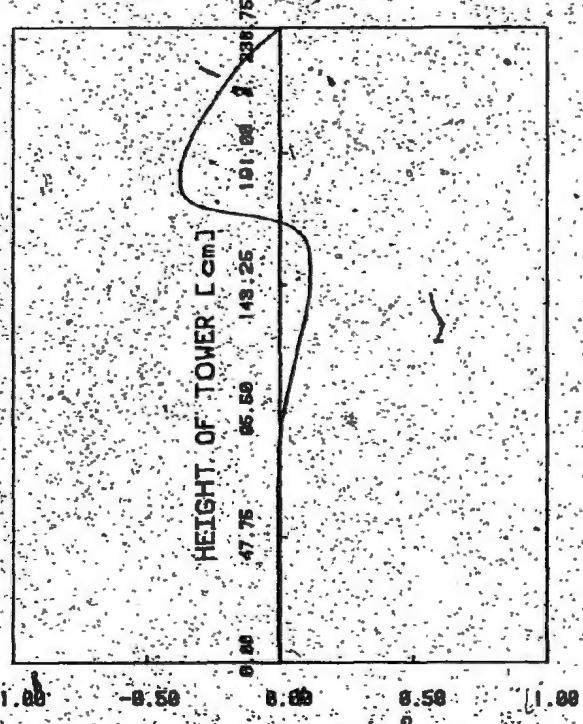

FIG. 2.1(D) MODE 8 (UNDAMAGED)
AT NODES 9, 17, 29, 39, 43, 53
(VIBRATION FREQUENCY = 12.24 Hz)

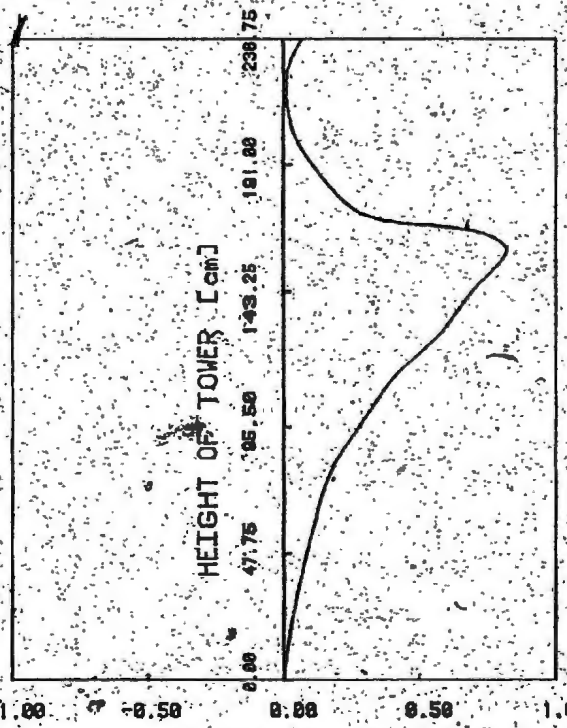

Z AXIS HORIZONTAL DISPLACEMENT

FIG. 2.2(A) MODE 4 (UNDAMAGED)
AT NODES 5,13,21,37,41,45
(VIBRATION FREQUENCY = 11.92 Hz)

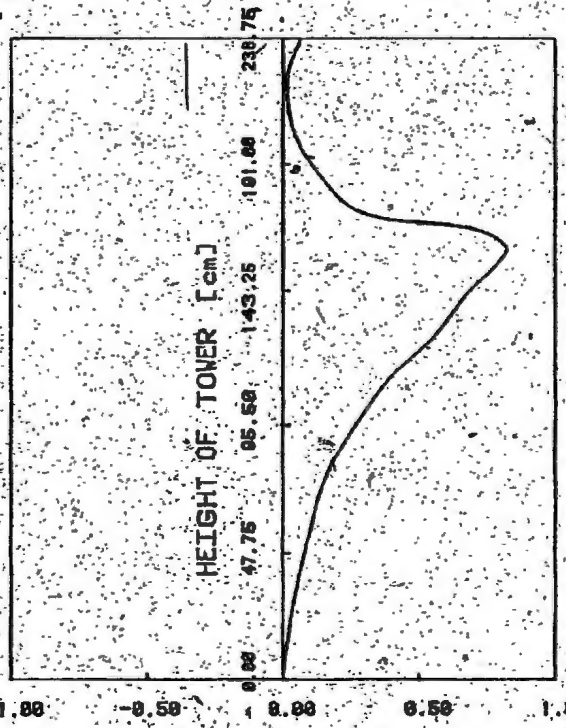

Z AXIS HORIZONTAL DISPLACEMENT

FIG. 2.2(B) MODE 4 (UNDAMAGED)
AT NODES 7,15,25,38,42,49
(VIBRATION FREQUENCY = 11.92 Hz)

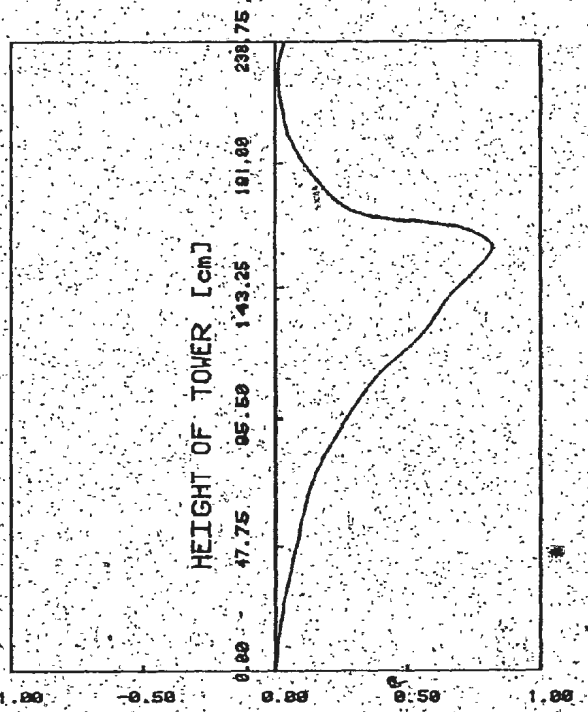

Z AXIS HORIZONTAL DISPLACEMENT

FIG. 2.2(C) MODE 4 (UNDAMAGED)
AT NODES 1,1,19,33,40,44,57
(VIBRATION FREQUENCY = 10.01 Hz)

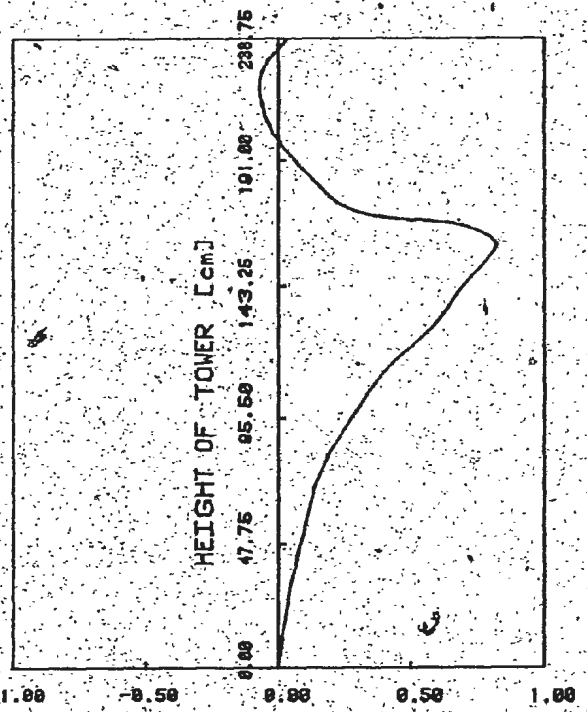

Z AXIS HORIZONTAL DISPLACEMENT

FIG. 2.2(D) MODE 4 (UNDAMAGED)
AT NODES 9,17,29,39,43,53
(VIBRATION FREQUENCY = 10.01 Hz)

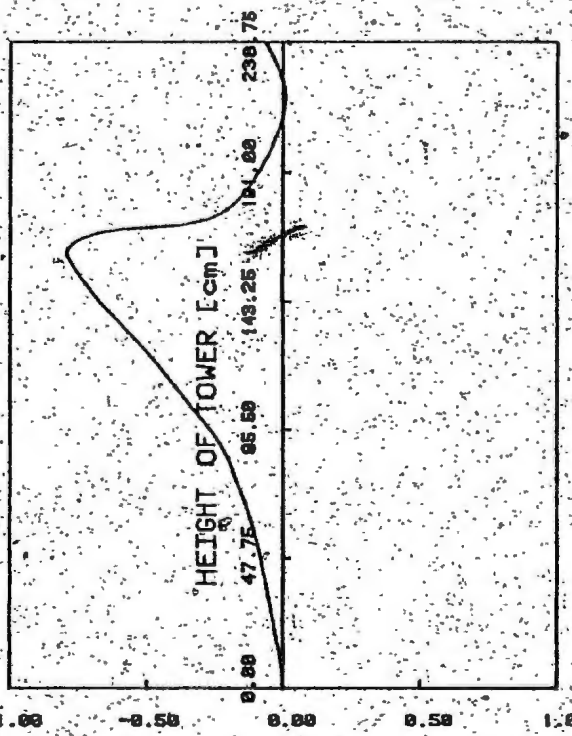

X AXIS HORIZONTAL DISPLACEMENT

FIG. 2.3(A) MODE 4 (UNDAMAGED)
AT NODES 5, 13, 21, 37, 41, 45
(VIBRATION FREQUENCY = 11.92 Hz)

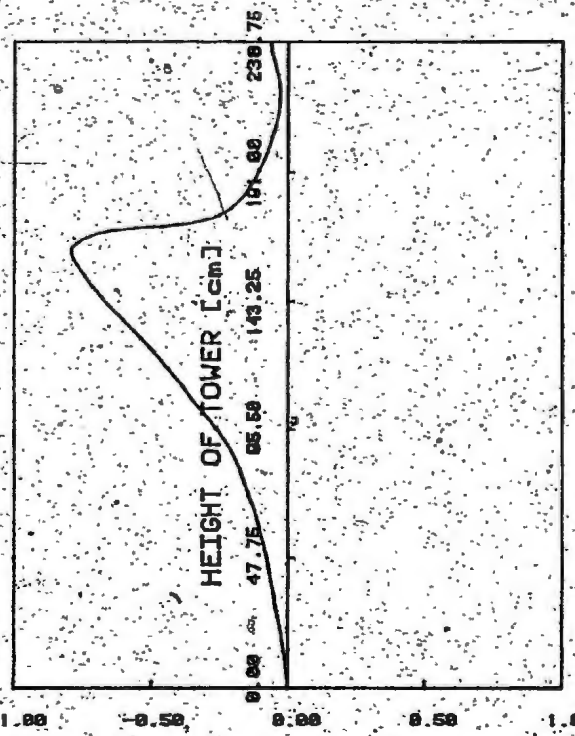

X AXIS HORIZONTAL DISPLACEMENT

FIG. 2.3(B) MODE 4 (UNDAMAGED)
AT NODES 11, 19, 33, 40, 44, 57
(VIBRATION FREQUENCY = 11.92 Hz)

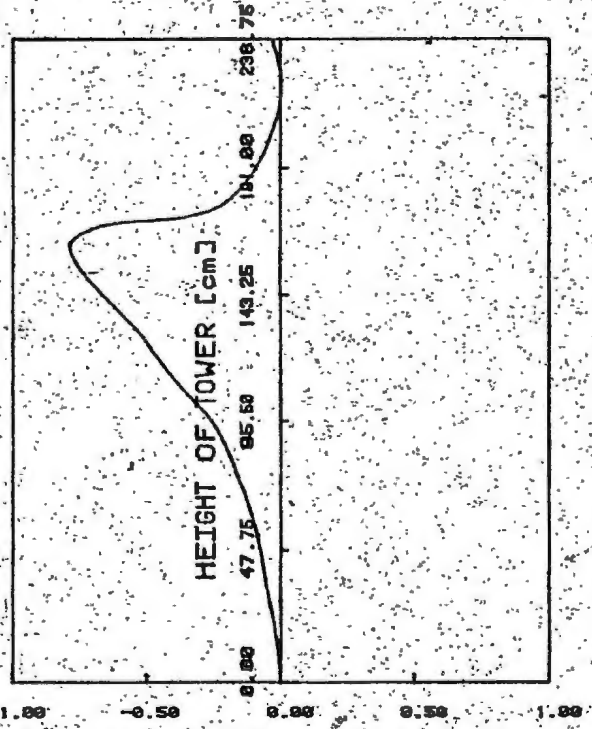

FIG. 2.3(C) MODE 4 (UNDAMAGED)
AT NODES 7,15,25,38,42,49
(VIBRATION FREQUENCY = 11.92 Hz)

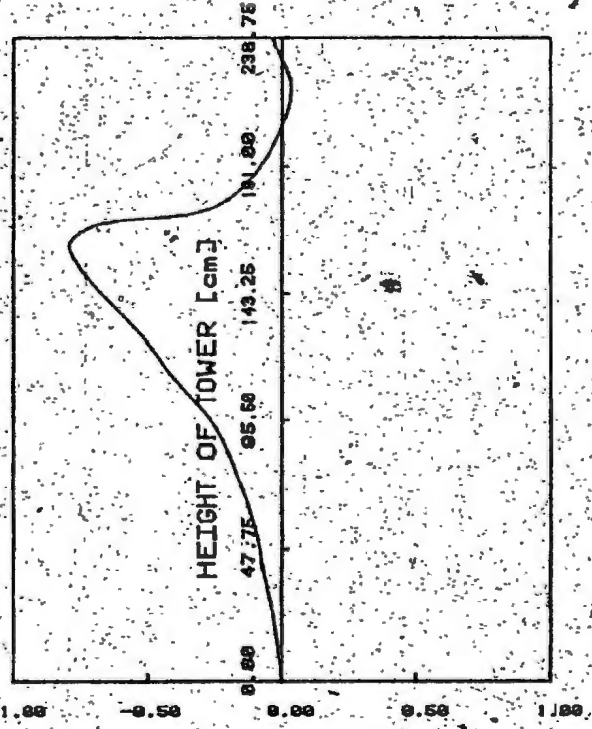

FIG. 2.3(D) MODE 4 (UNDAMAGED)
AT NODES 9,17,29,39,43,53
(VIBRATION FREQUENCY = 11.92 Hz)

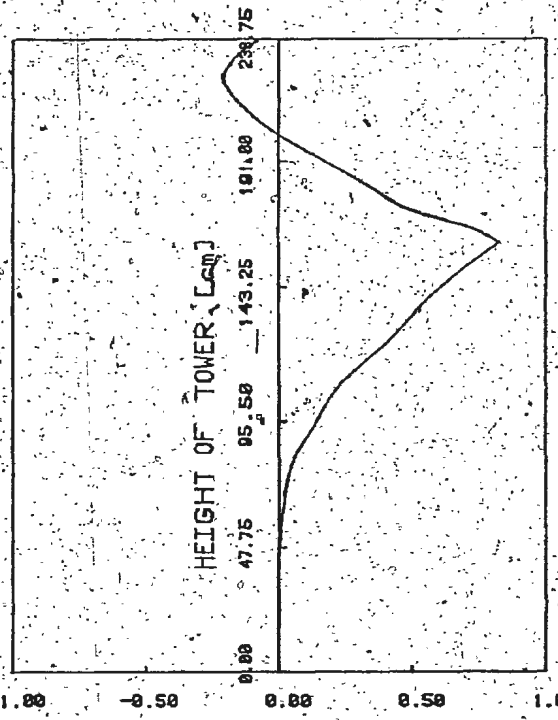

Z AXIS HORIZONTAL DISPLACEMENT

FIG. 2.4(A) MODE 4 (MEMBER 91 SEVERED)
AT NODES 5,13,21,37,41,45
(VIBRATION FREQUENCY = 10.01 Hz)

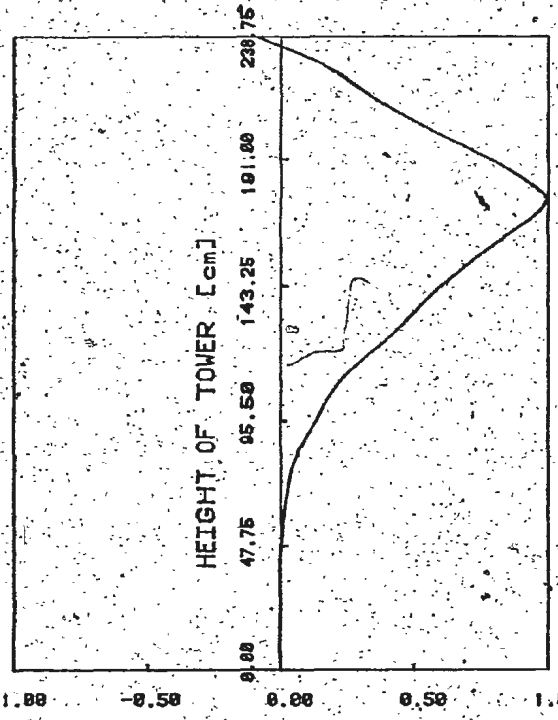

Z AXIS HORIZONTAL DISPLACEMENT

FIG. 2.4(B) MODE 4 (MEMBER 91 SEVERED)
AT NODES 7,15,25,38,42,49
(VIBRATION FREQUENCY = 10.01 Hz)

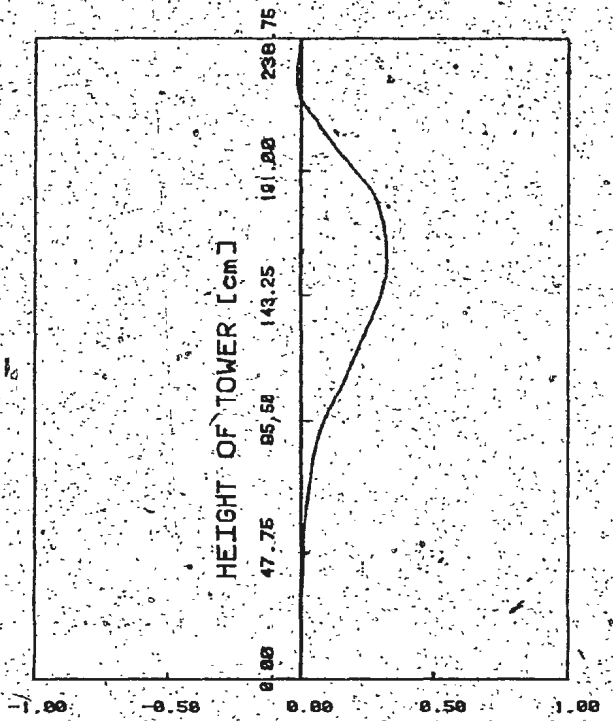

Z AXIS HORIZONTAL DISPLACEMENT

FIG. 2.4(C) MODE 4 (MEMBER 91 SEVERED)
AT NODES 11,19,33,40,44,57
(VIBRATION FREQUENCY = 10.01 Hz)

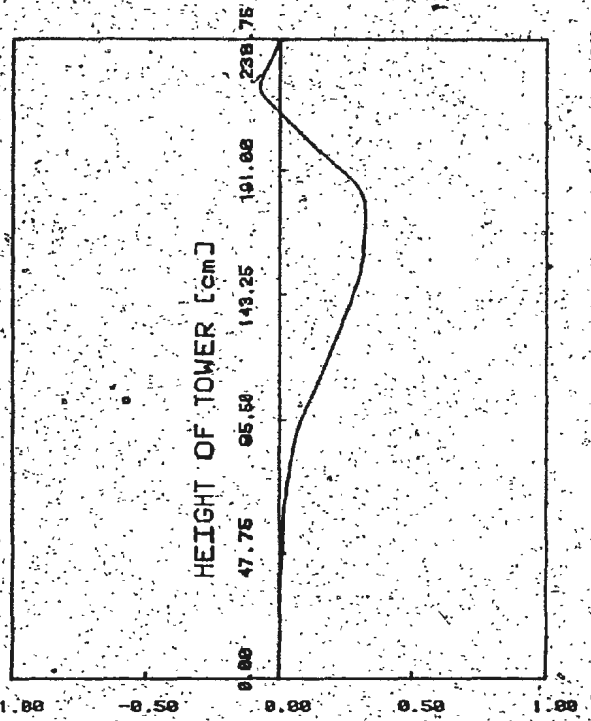

Z AXIS HORIZONTAL DISPLACEMENT

FIG. 2.4(D) MODE 4 (MEMBER 91 SEVERED)
AT NODES 9,17,29,39,43,53
(VIBRATION FREQUENCY = 10.01 Hz)

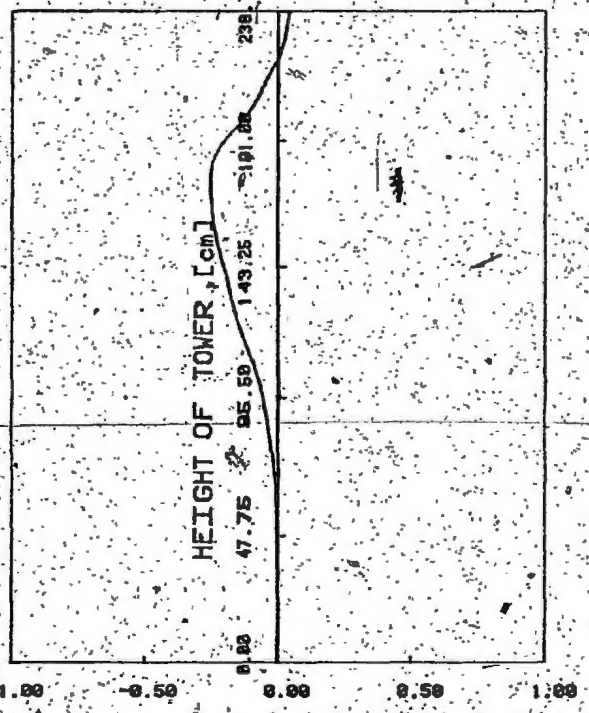

FIG. 2.5(A) MODE 4 (MEMBER 91 SEVERED)
AT NODES 5,13,21,37,41,45
(VIBRATION FREQUENCY = 10.01 Hz)

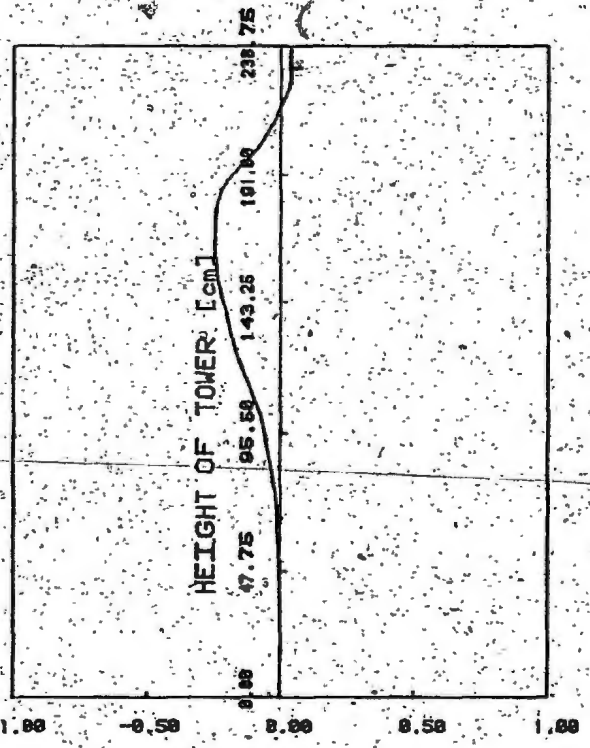

FIG. 2.5(B) MODE 4 (MEMBER 91 SEVERED)
AT NODES 11,19,33,40,44,57
(VIBRATION FREQUENCY = 10.01 Hz)

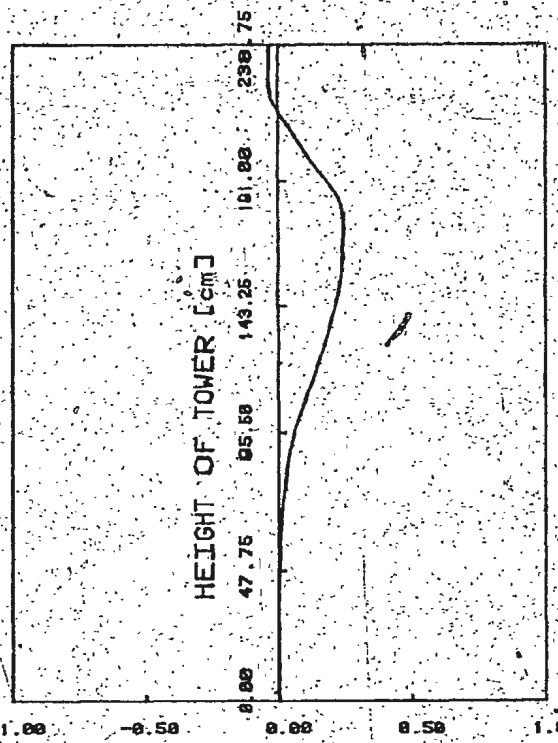

FIG. 2.5(C) MODE 4 (MEMBER 91 SEVERED)
AT NODES 7,15,25,38,42,49
(VIBRATION FREQUENCY = 10.01 Hz)

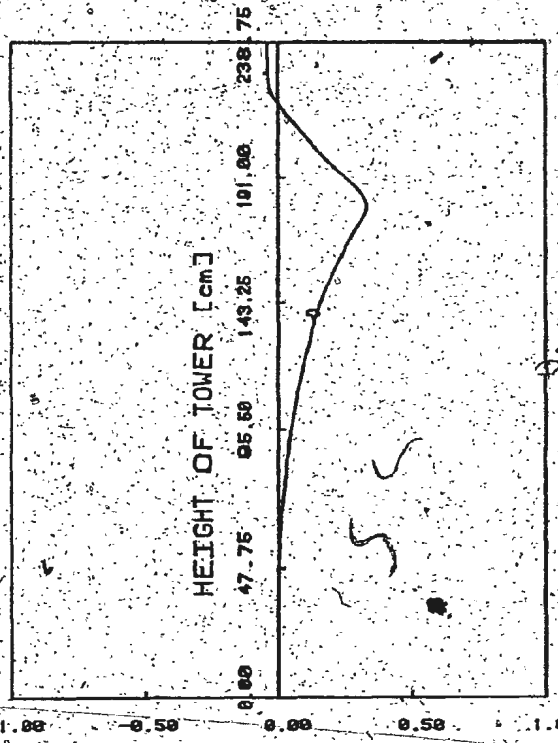

FIG. 2.5(D) MODE 4 (MEMBER 91 SEVERED)
AT NODES 9,17,29,39,43,53
(VIBRATION FREQUENCY = 10.01 Hz)

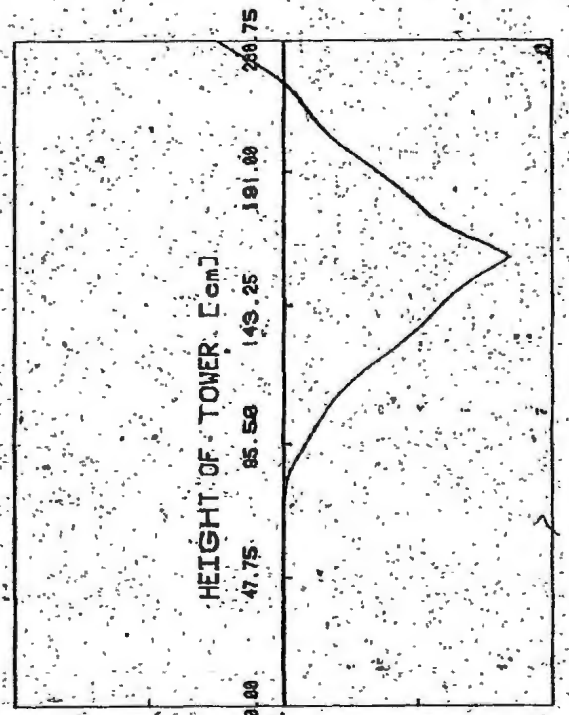

FIG. 2.6(A) MODE 4 (MEMS. 91 & 84 SEVERED)
AT NODES 5,13,21,37,41,45
(VIBRATION FREQUENCY = 5.89 Hz)

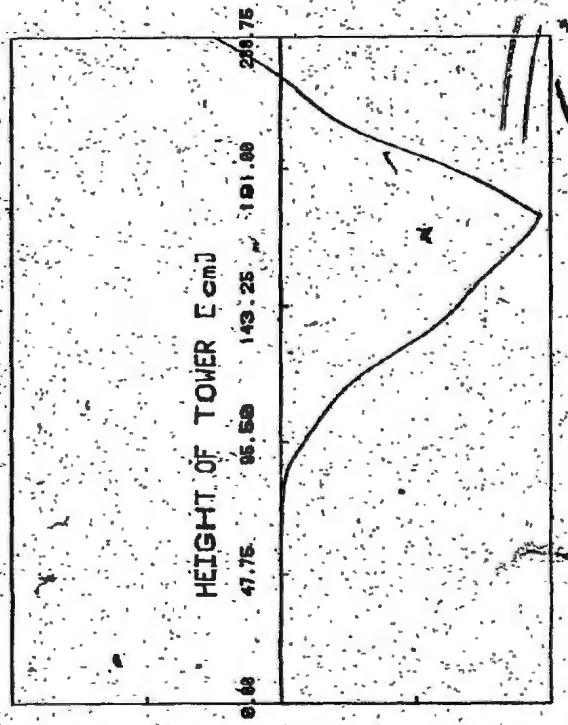

FIG. 2.6(B) MODE 4 (MEMS. 91 & 84 SEVERED)
AT NODES 7,15,25,38,42,49
(VIBRATION FREQUENCY = 5.89 Hz)

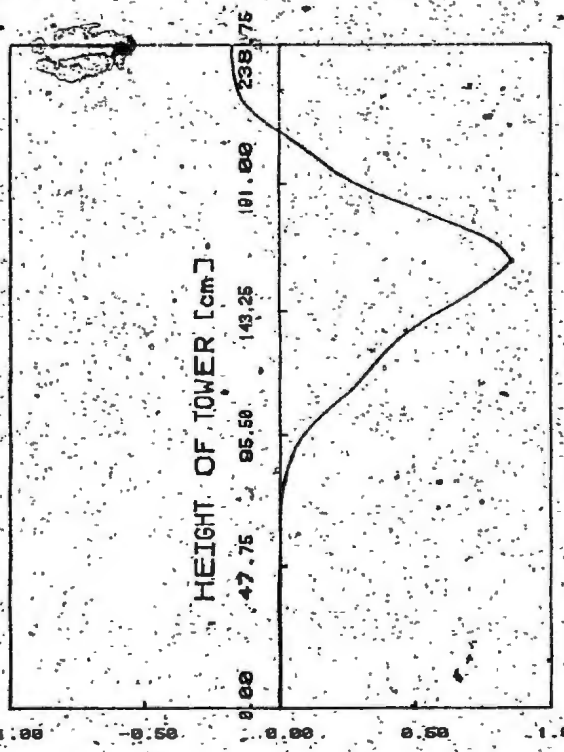

Z AXIS HORIZONTAL DISPLACEMENT

FIG. 2.6(C) MODE 4 (MEMS. 91 & 84 SEVERED)
AT NODES 11,19,33,40,44,57
(VIBRATION FREQUENCY = 5.89 Hz)

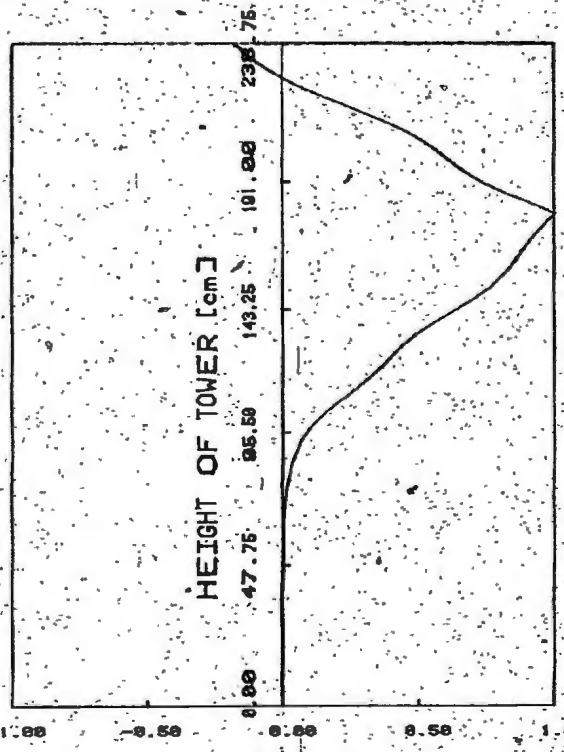

Z AXIS HORIZONTAL DISPLACEMENT

FIG. 2.6(D) MODE 4 (MEMS. 91 & 84 SEVERED)
AT NODES 9,17,29,39,43,53
(VIBRATION FREQUENCY = 5.89 Hz)

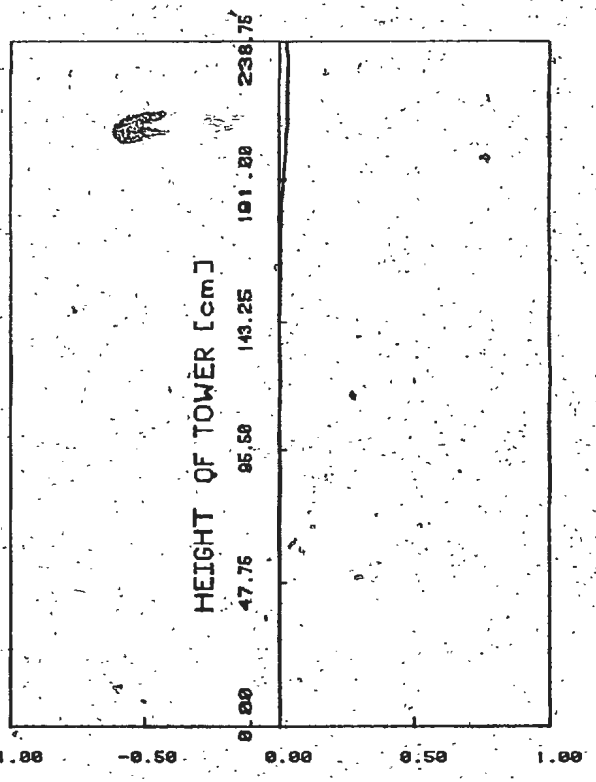

X AXIS HORIZONTAL DISPLACEMENT

FIG. 2.7(A) MODE 4 (MEMS. 91 & 84 SEVERED)
AT NODES 5,13,21,37,41,45
(VIBRATION FREQUENCY = 5.89 Hz)

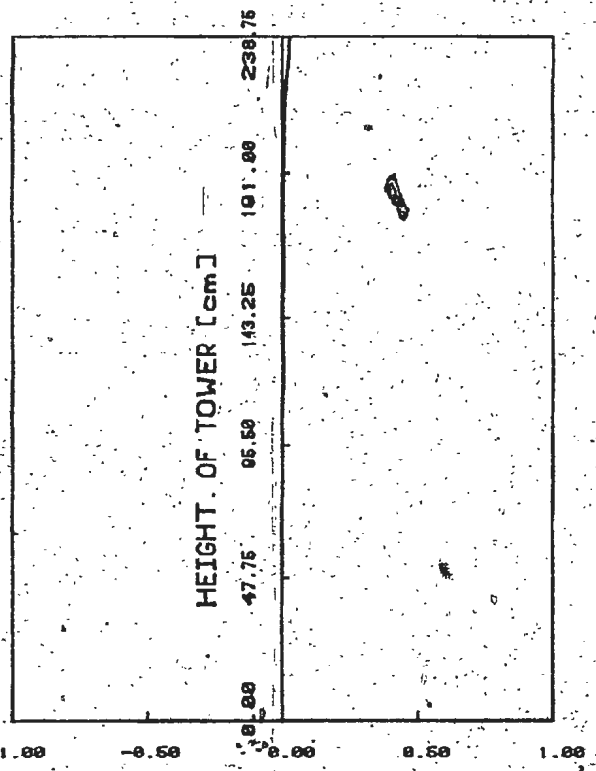

X AXIS HORIZONTAL DISPLACEMENT

FIG. 2.7(B) MODE 4 (MEMS. 91 & 84 SEVERED)
AT NODES 11,19,33,40,44,57
(VIBRATION FREQUENCY = 5.89 Hz)

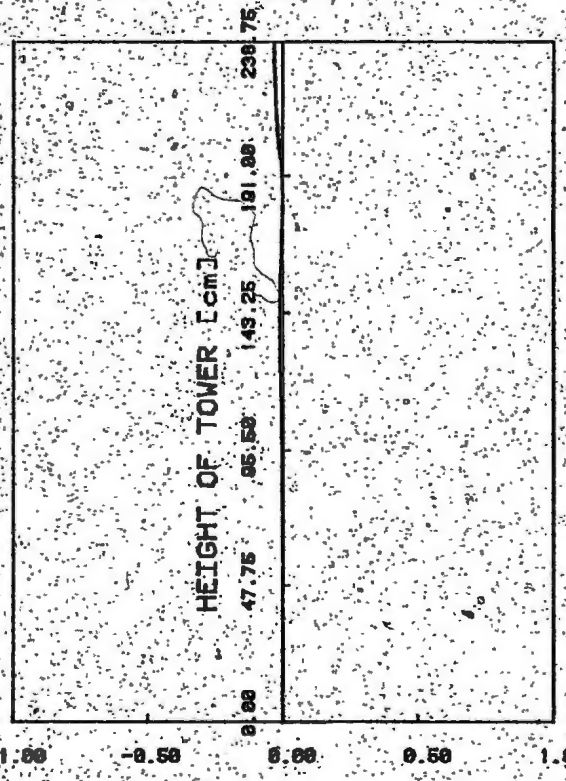

FIG. 2.7(C) MODE 4 (MEMS. 91 & 84 SEVERED)
AT NODES 7,15,25,38,42,49
(VIBRATION FREQUENCY = 5.89 Hz)

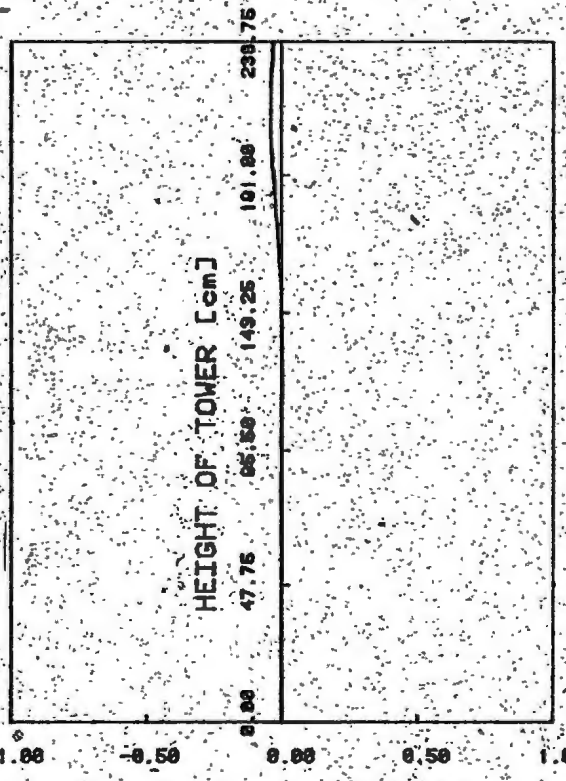

FIG. 2.7(D) MODE 4 (MEMS. 91 & 84 SEVERED)
AT NODES 9,17,29,39,43,53
(VIBRATION FREQUENCY = 5.89 Hz)

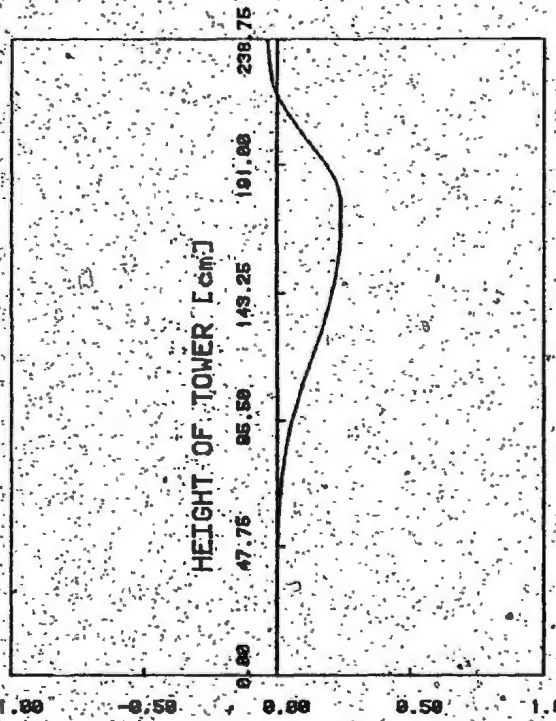

X AXIS HORIZONTAL DISPLACEMENT

FIG. 2.8(A) MODE 4 (MEMBER 84 SEVERED)
AT NODES 5,13,21,37,41,45
(VIBRATION FREQUENCY = 10.01 Hz)

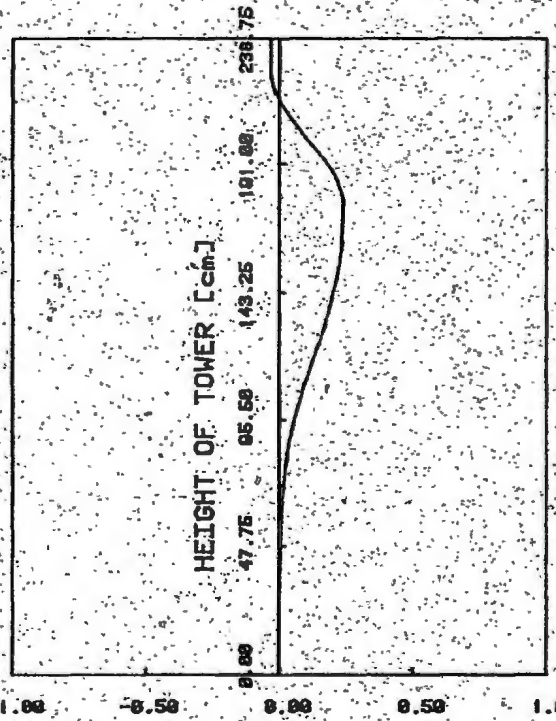

X AXIS HORIZONTAL DISPLACEMENT

FIG. 2.8(B) MODE 4 (MEMBER 84 SEVERED)
AT NODES 11,19,33,40,44,57
(VIBRATION FREQUENCY = 10.01 Hz)

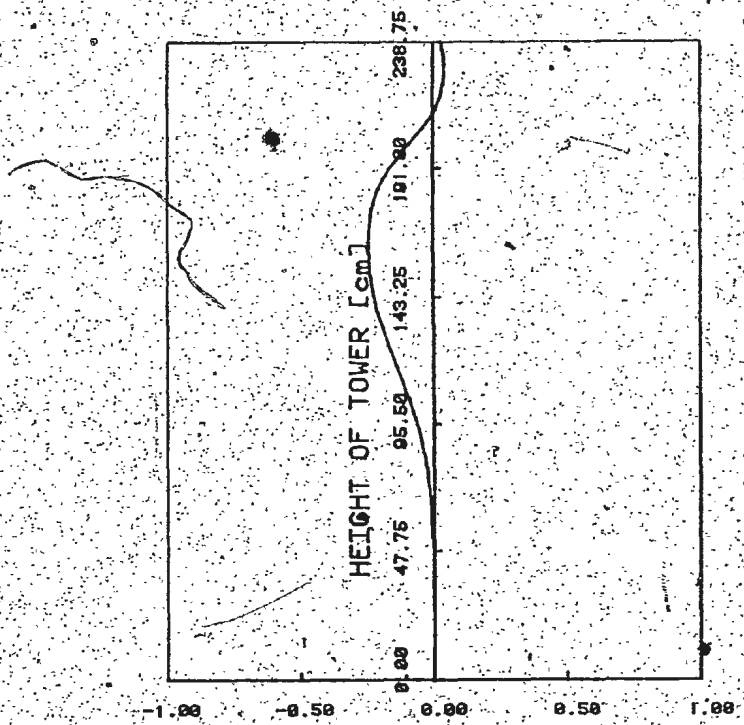

X AXIS HORIZONTAL DISPLACEMENT

FIG. 2.8(C) MODE 4 (MEMBER 84 SEVERED)
AT NODES 7,15,25,38,42,49
(VIBRATION FREQUENCY = 10.01 Hz)

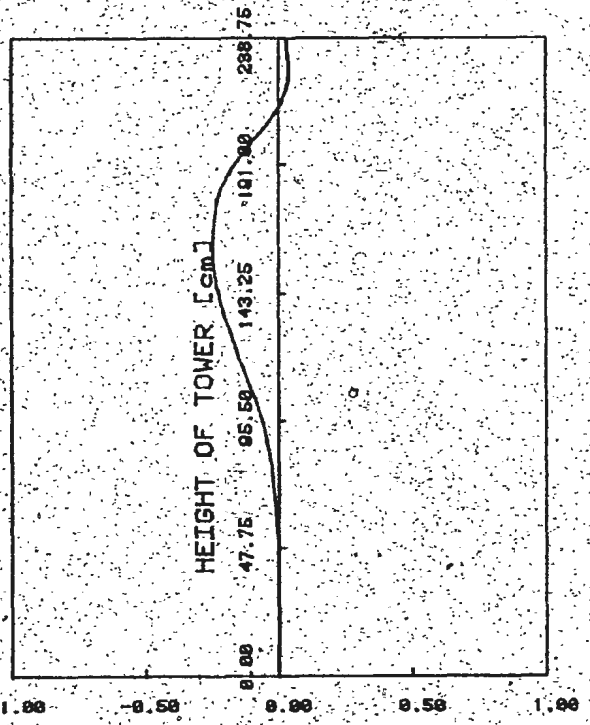

X AXIS HORIZONTAL DISPLACEMENT

FIG. 2.8(D) MODE 4 (MEMBER 84 SEVERED)
AT NODES 9,17,29,39,43,53
(VIBRATION FREQUENCY = 10.01 Hz)

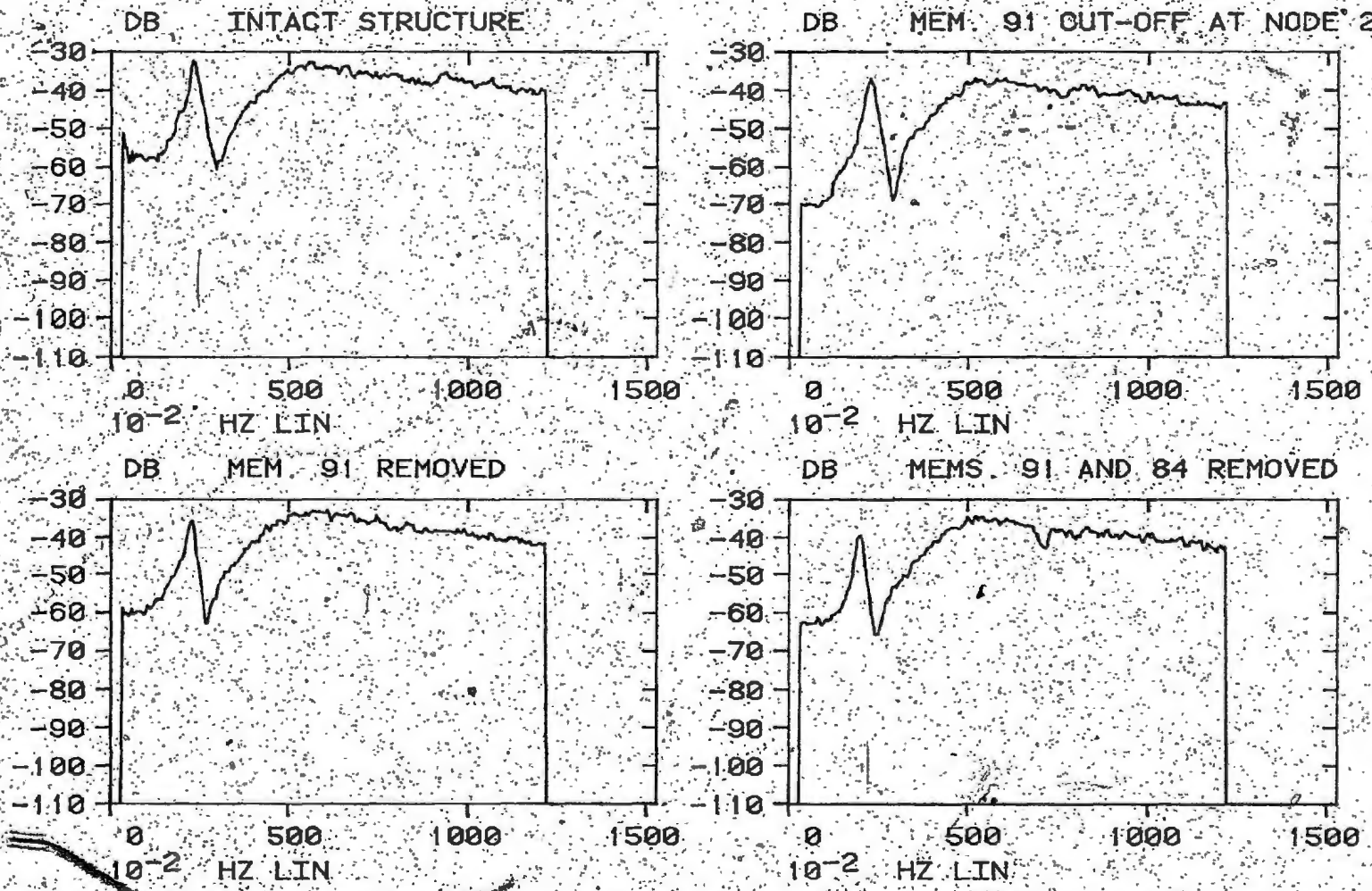

FIG. 3.0 INPUT RANDOM SPECTRA FOR EXPERIMENTS
(LOG. MAGNITUDES)

RESULTS OF RANDOM VIBRATION TESTS ON P.V.C. TOWER IN AIR

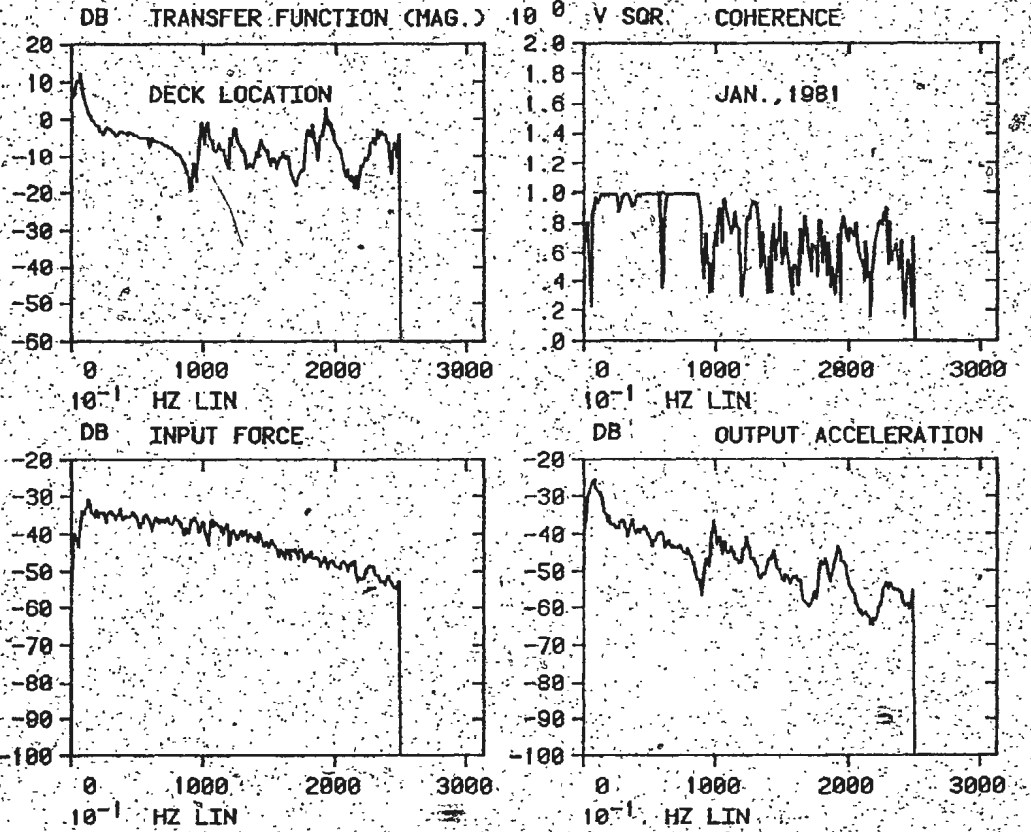

FIG. 3.1 INITIAL TEST RESULTS (NO LUMPED MASSES ADDED)

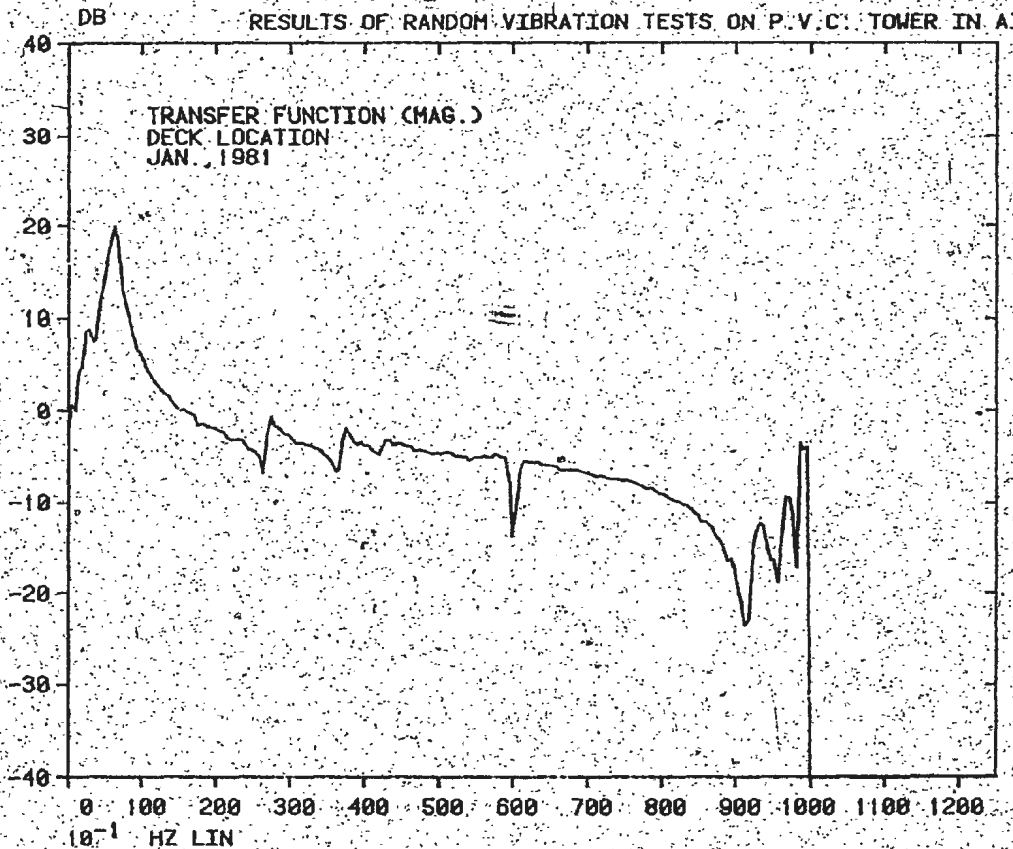

FIG. 3.2 INITIAL TEST RESULTS (NO LUMPED MASSES ADDED)

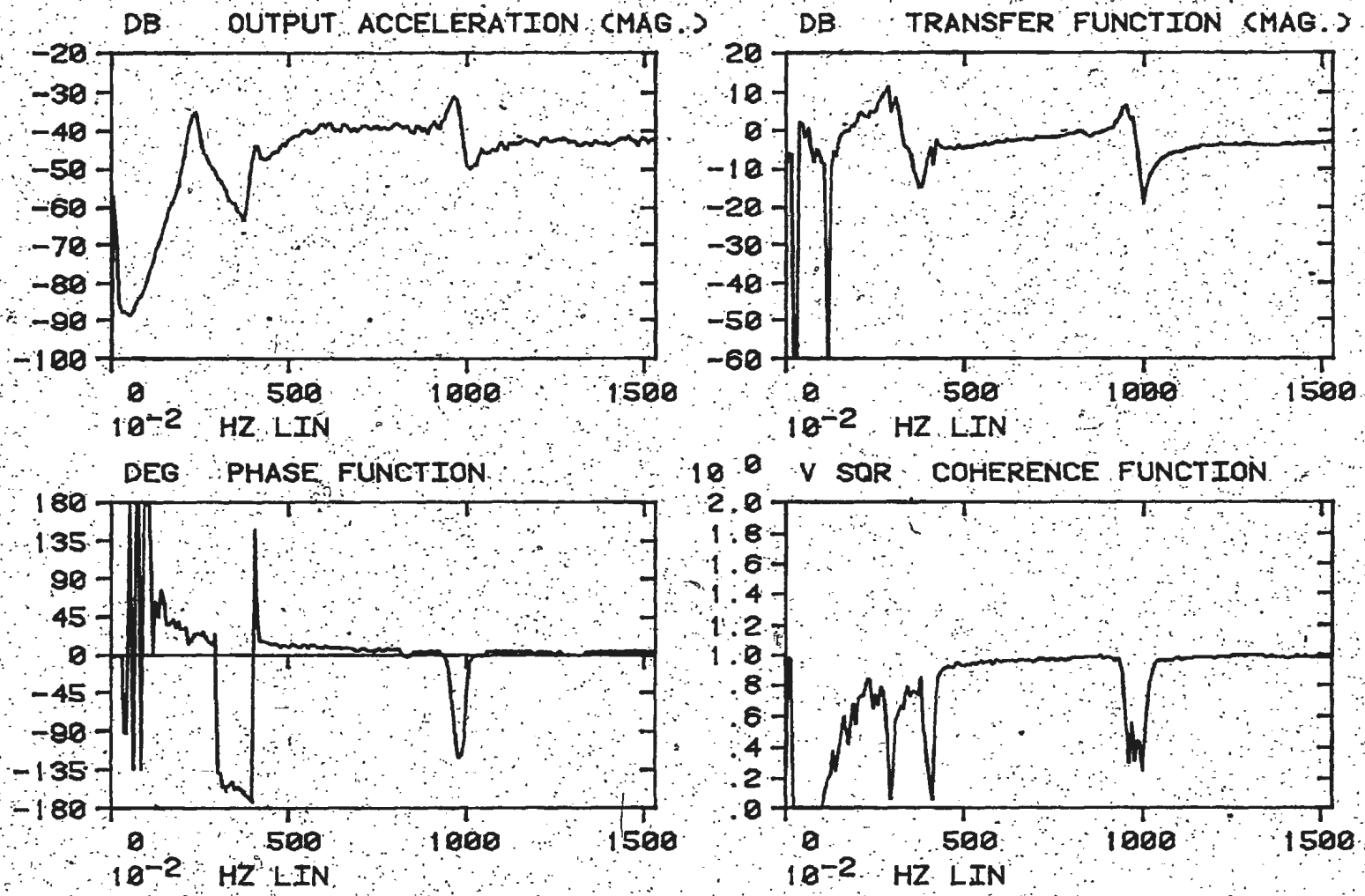

FIG. 3.3 RESULTS OF RANDOM VIBRATION TEST (ACCELERATION)
< INTACT STRUCTURE >

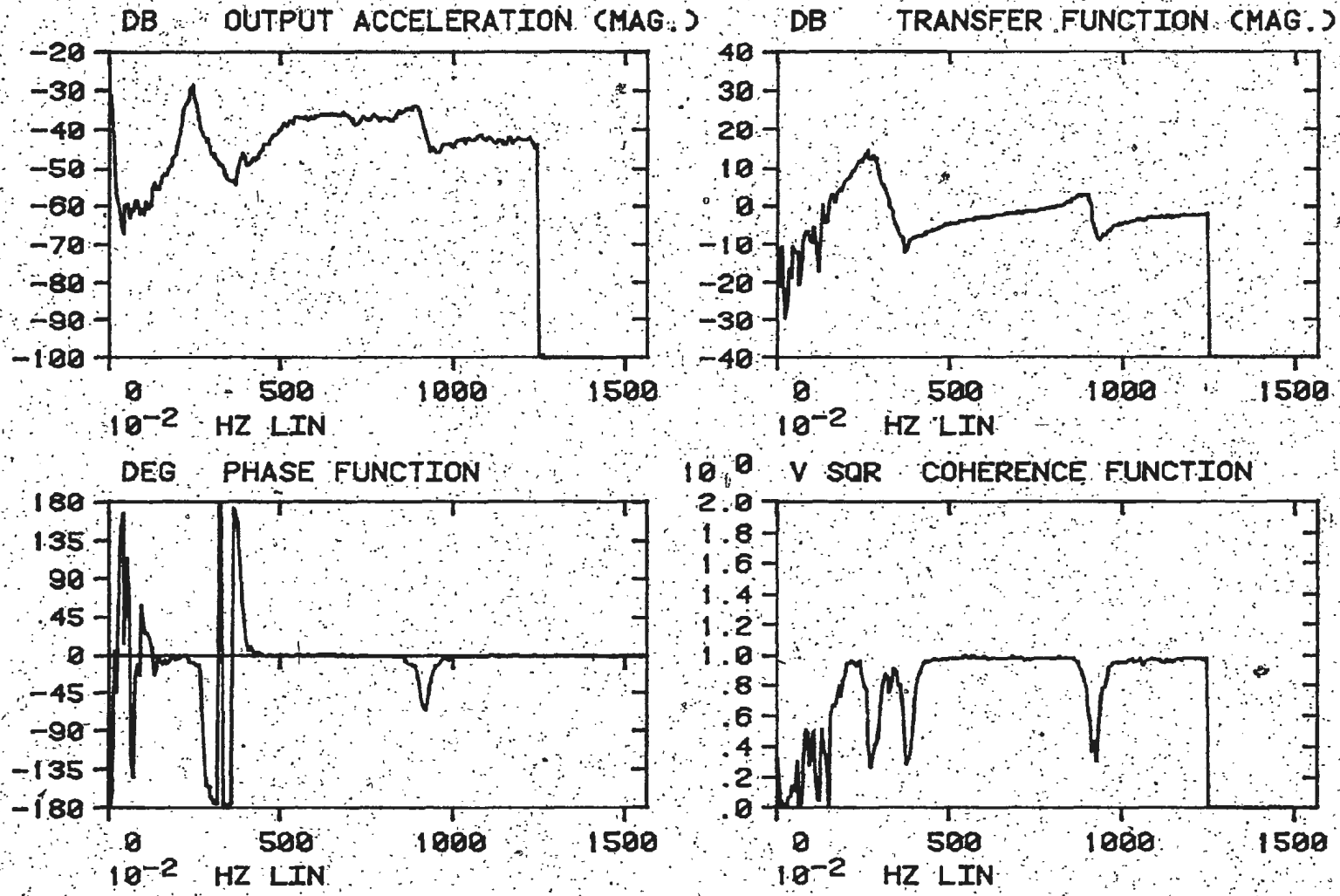

FIG. 3.4 RESULTS OF RANDOM VIBRATION TEST (ACCELERATION)
(MEM. 91 SEVERED HALFWAY AT NODE 23)

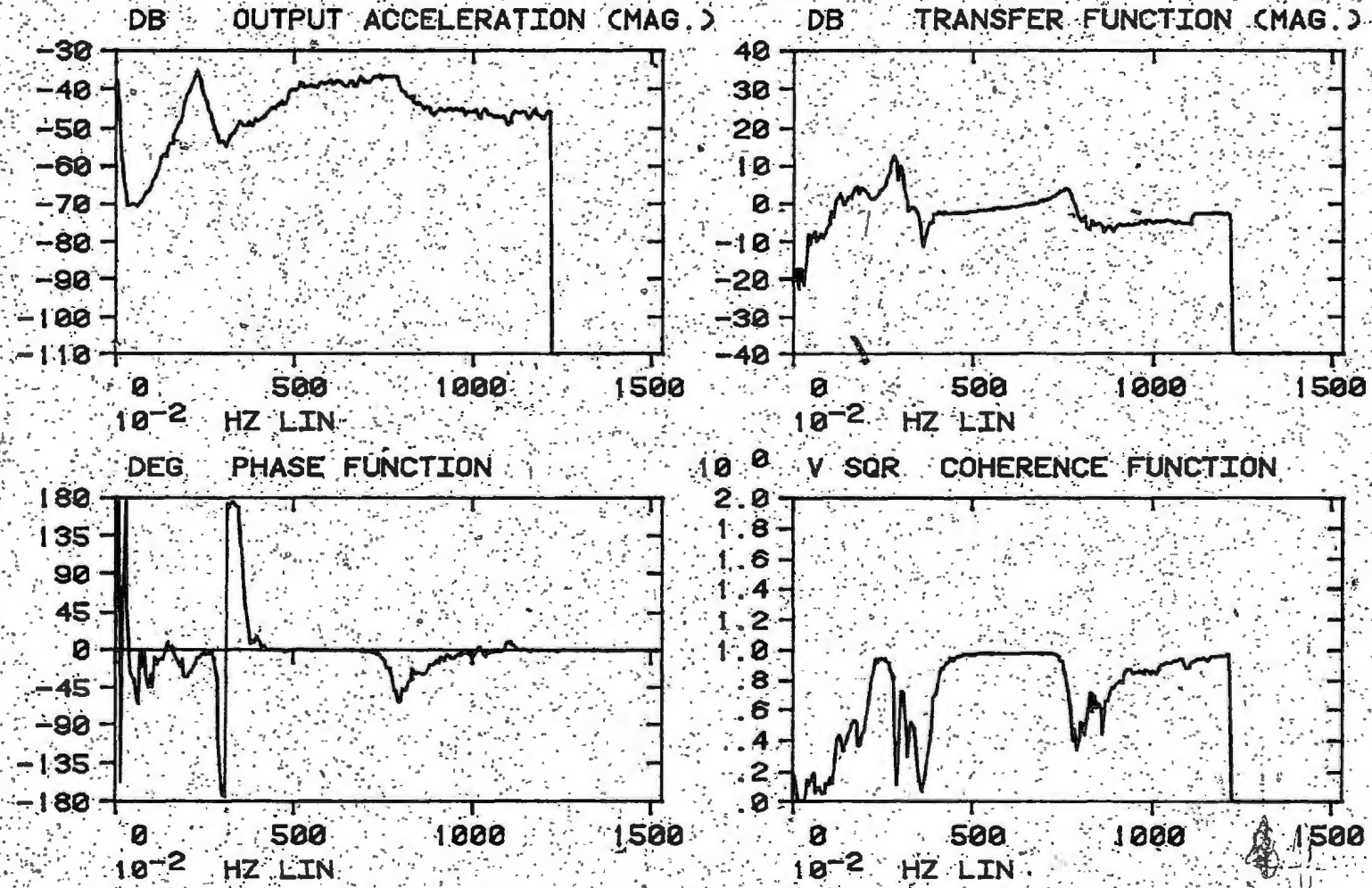

FIG. 3.5 - RESULTS OF RANDOM VIBRATION TEST (ACCELERATION)
(MEM. 91 COMPLETELY SEVERED AT NODE 23)

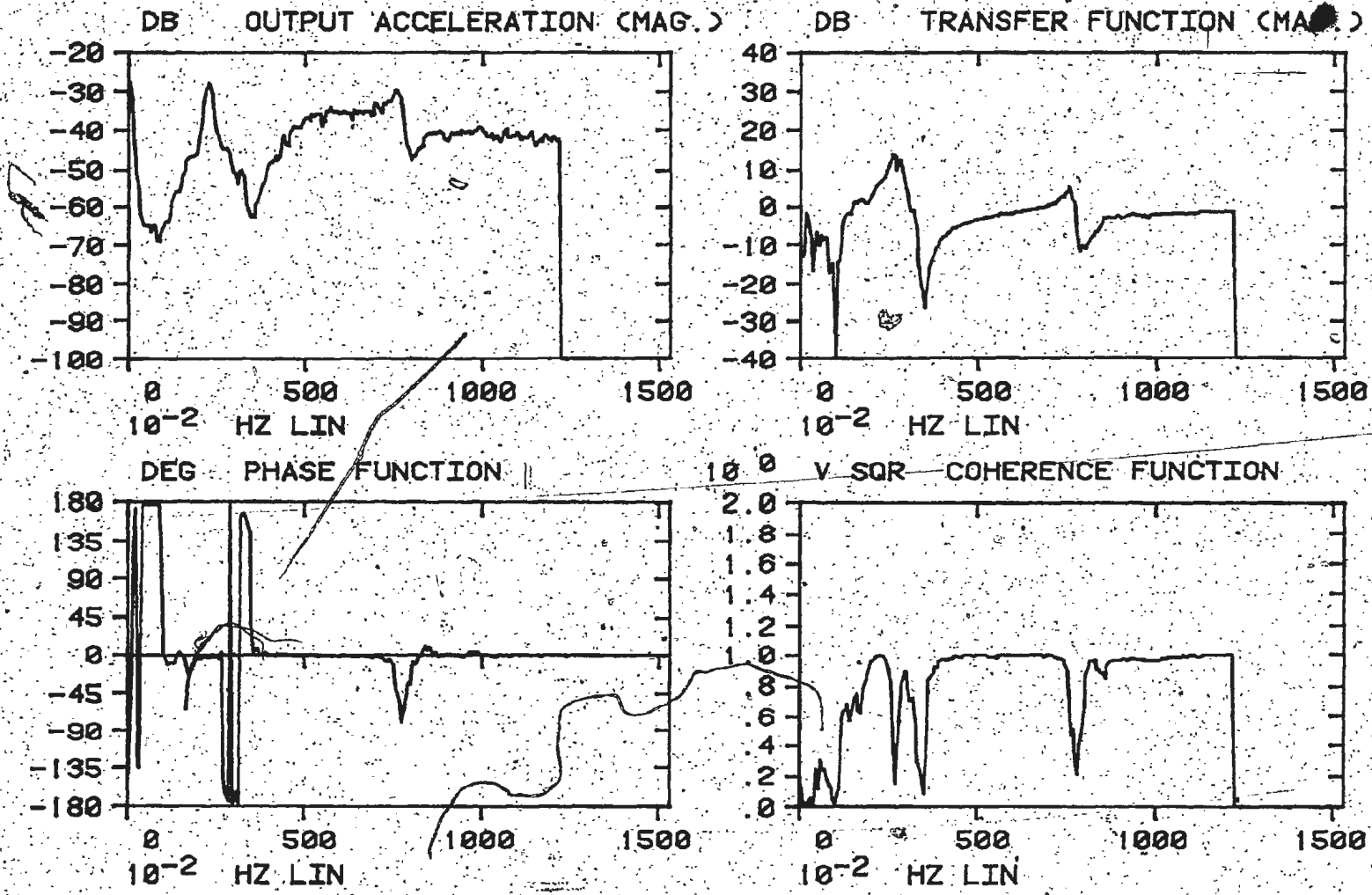

FIG. 3.6 RESULTS OF RANDOM VIBRATION TEST (ACCELERATION)
(MEM. 91 REMOVED)

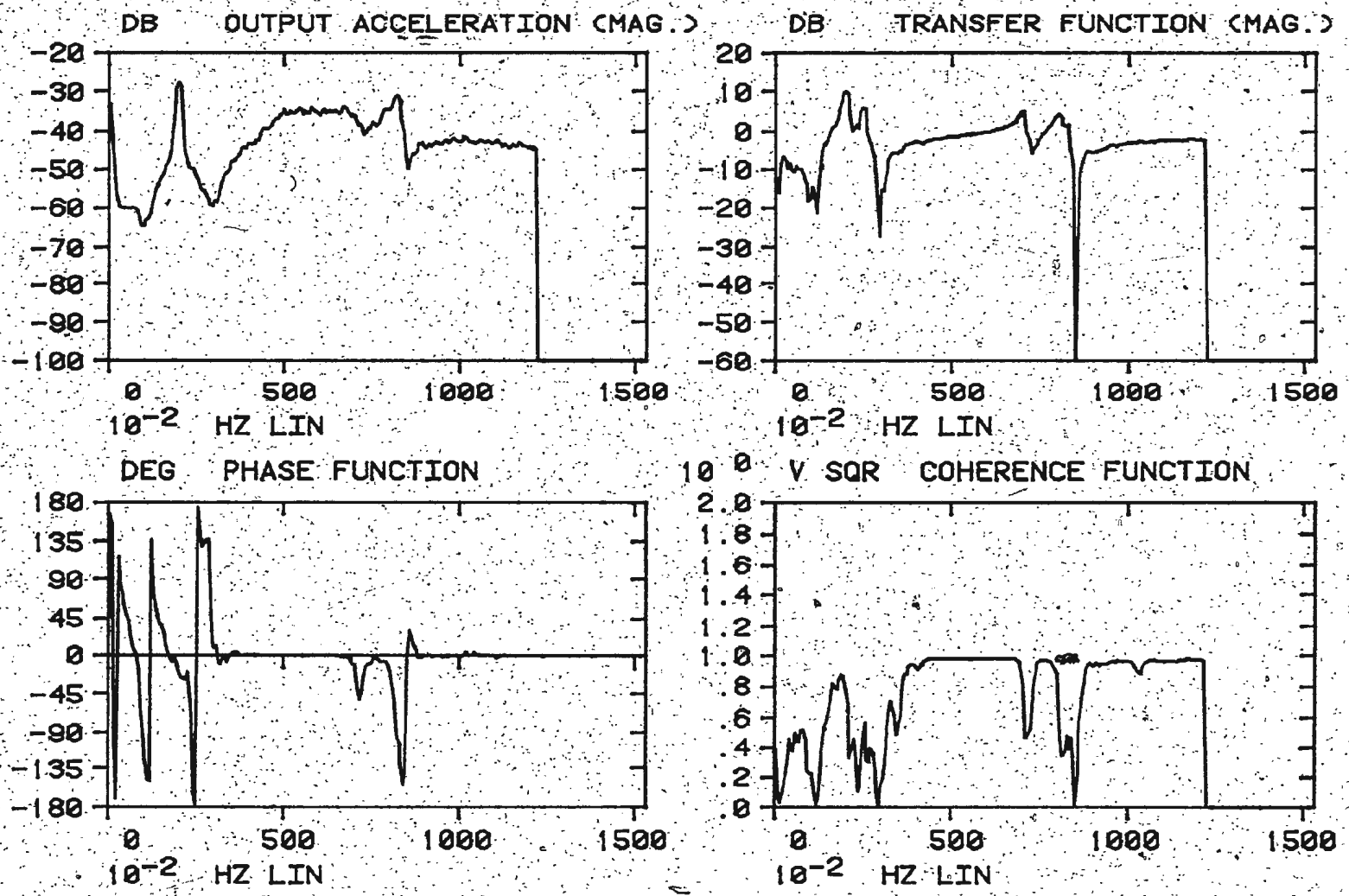

FIG. 3.7 RESULTS OF RANDOM VIBRATION TEST (ACCELERATION)
(MEM. 91 REMOVED AND MEM. 84 CUT-OFF AT NODE 31)

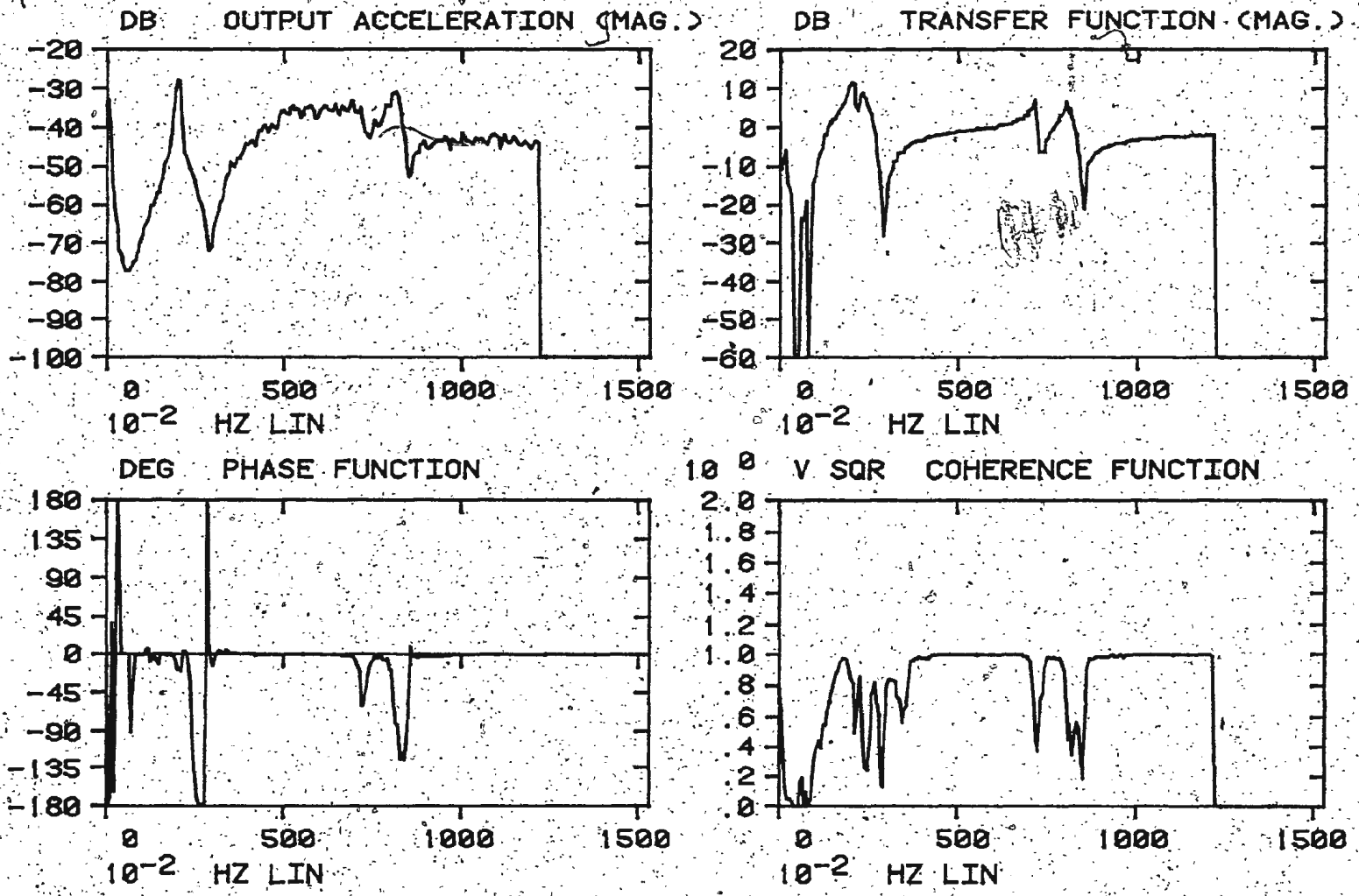

FIG. 3.8 RESULTS OF RANDOM VIBRATION TEST (ACCELERATION)
(MEMS. 91 AND 84 REMOVED)

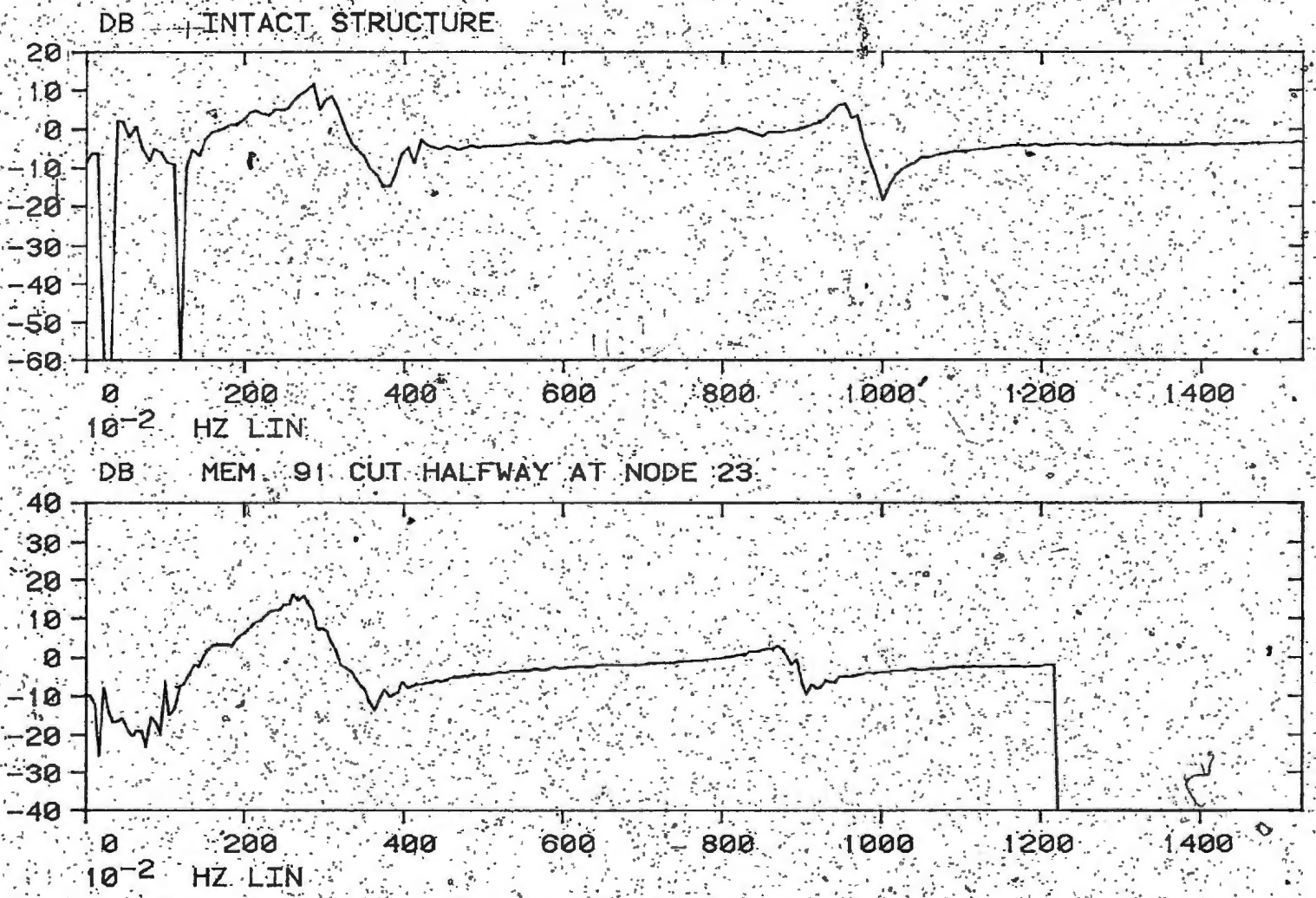

FIG. 3.9 TRANSFER FUNCTIONS (ACCELERATION)

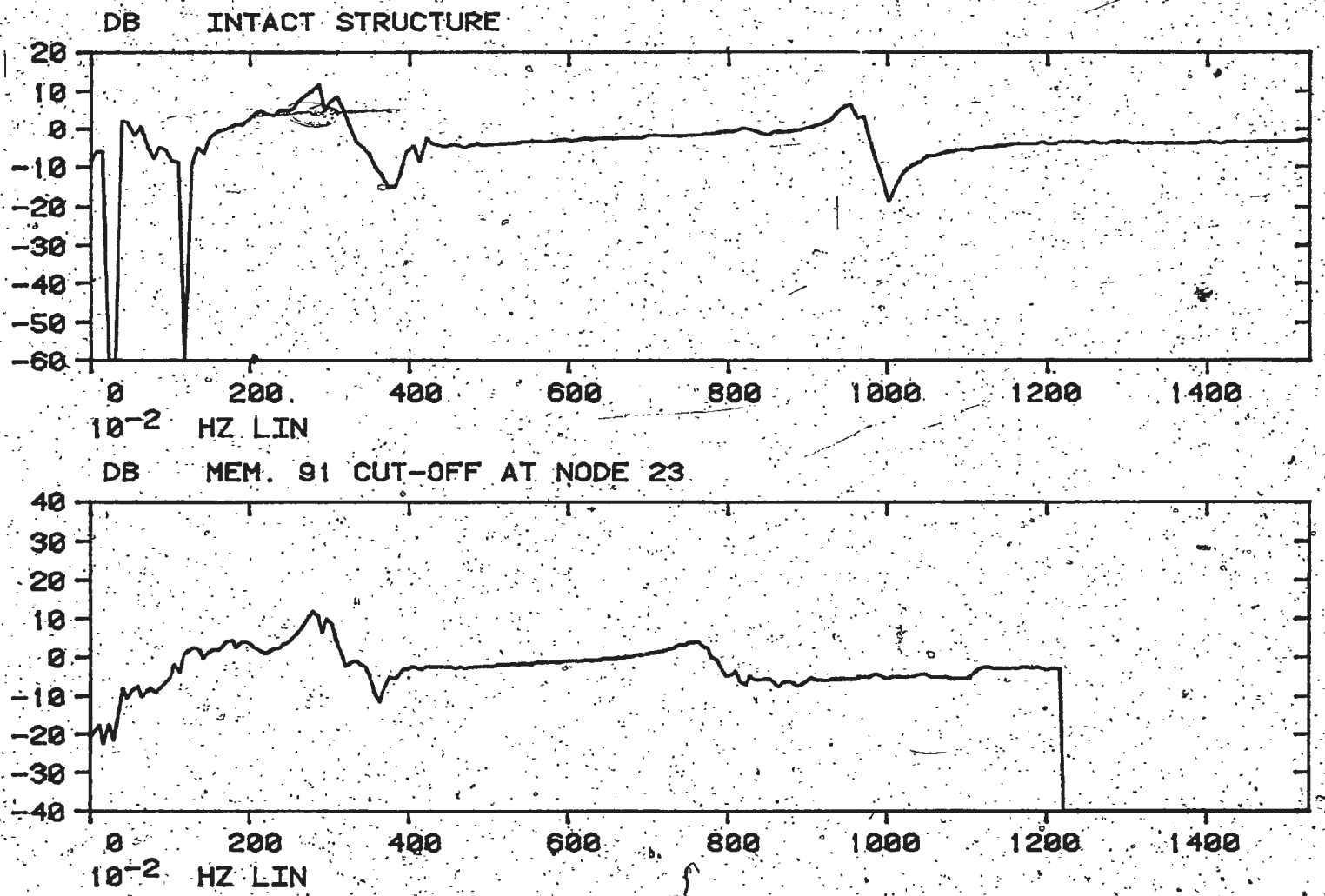

FIG. 3.10 TRANSFER FUNCTIONS (ACCELERATION)

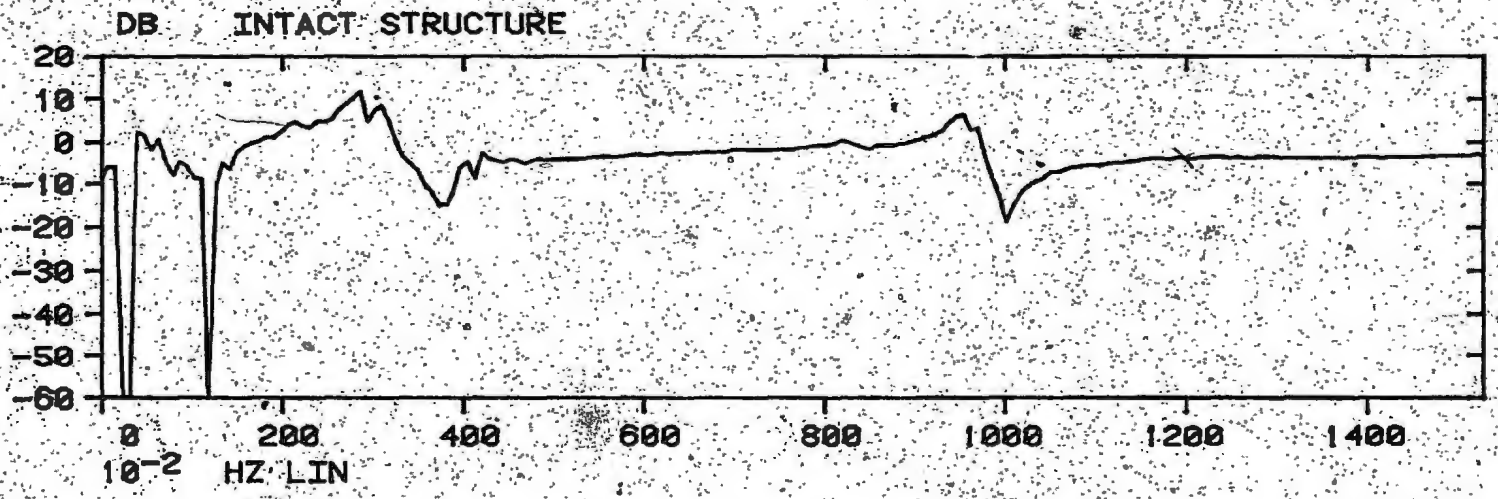

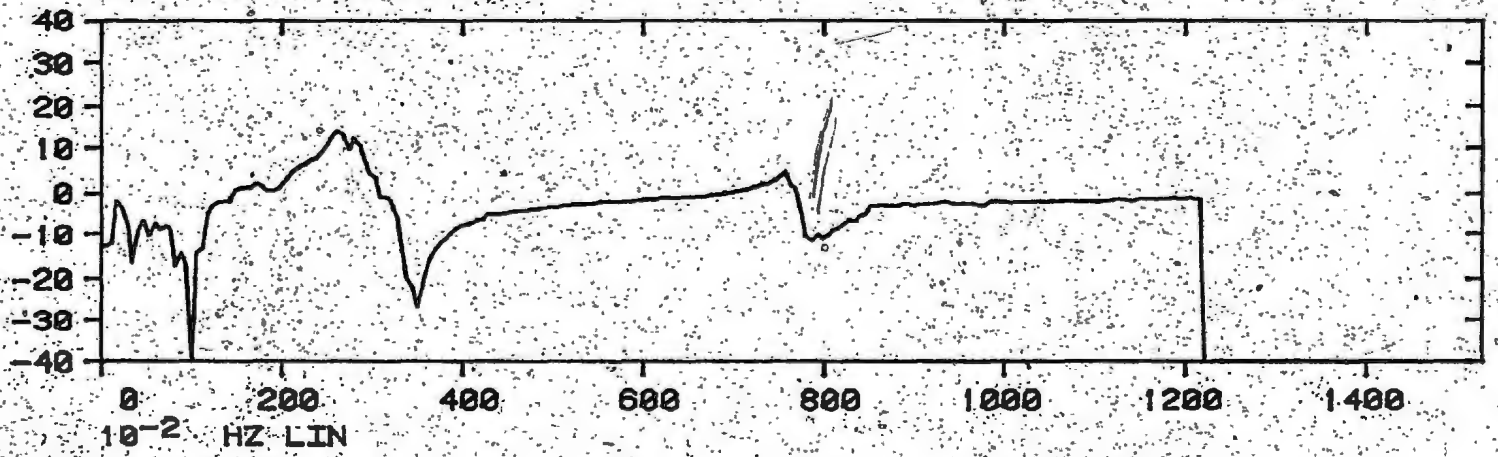

FIG. 3.11 TRANSFER FUNCTIONS (ACCELERATION)

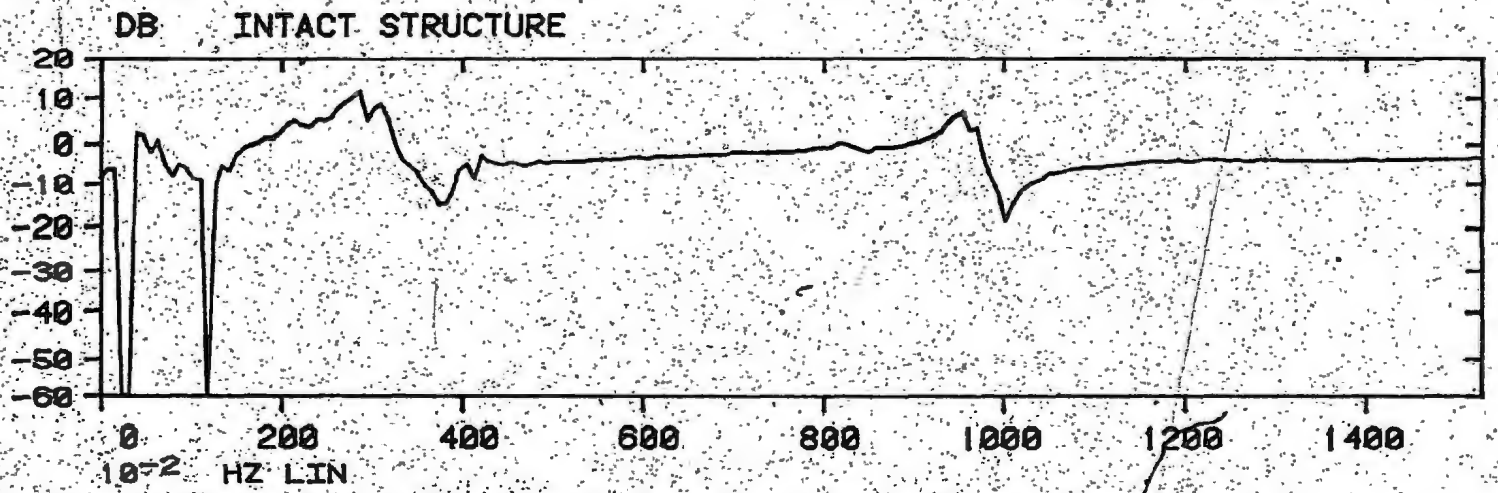

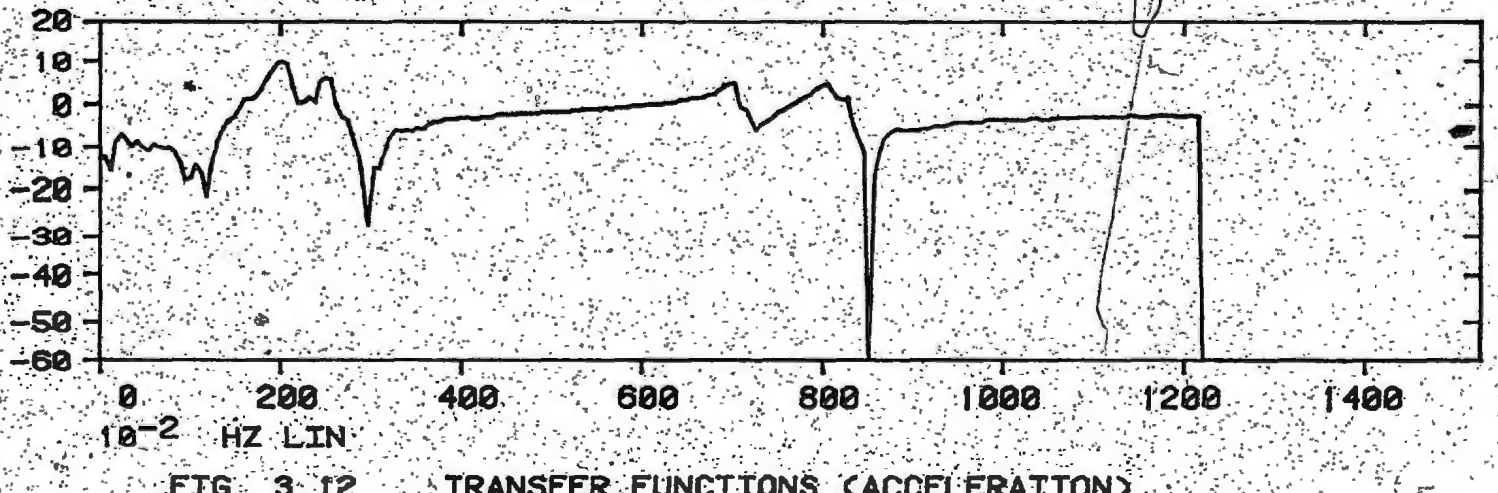

FIG. 3.12 TRANSFER FUNCTIONS (ACCELERATION)

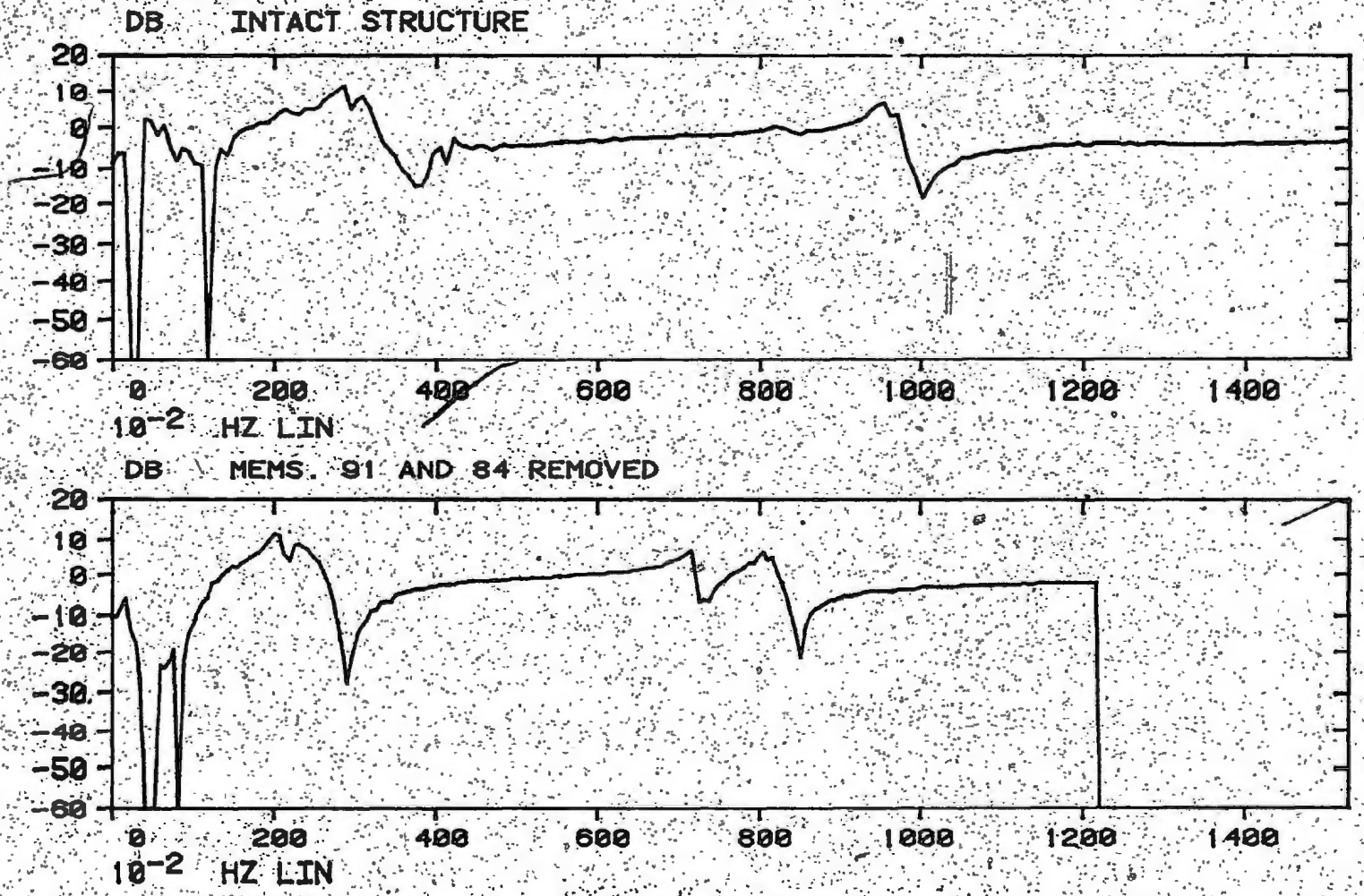

FIG. 3.13 TRANSFER FUNCTIONS (ACCELERATION)

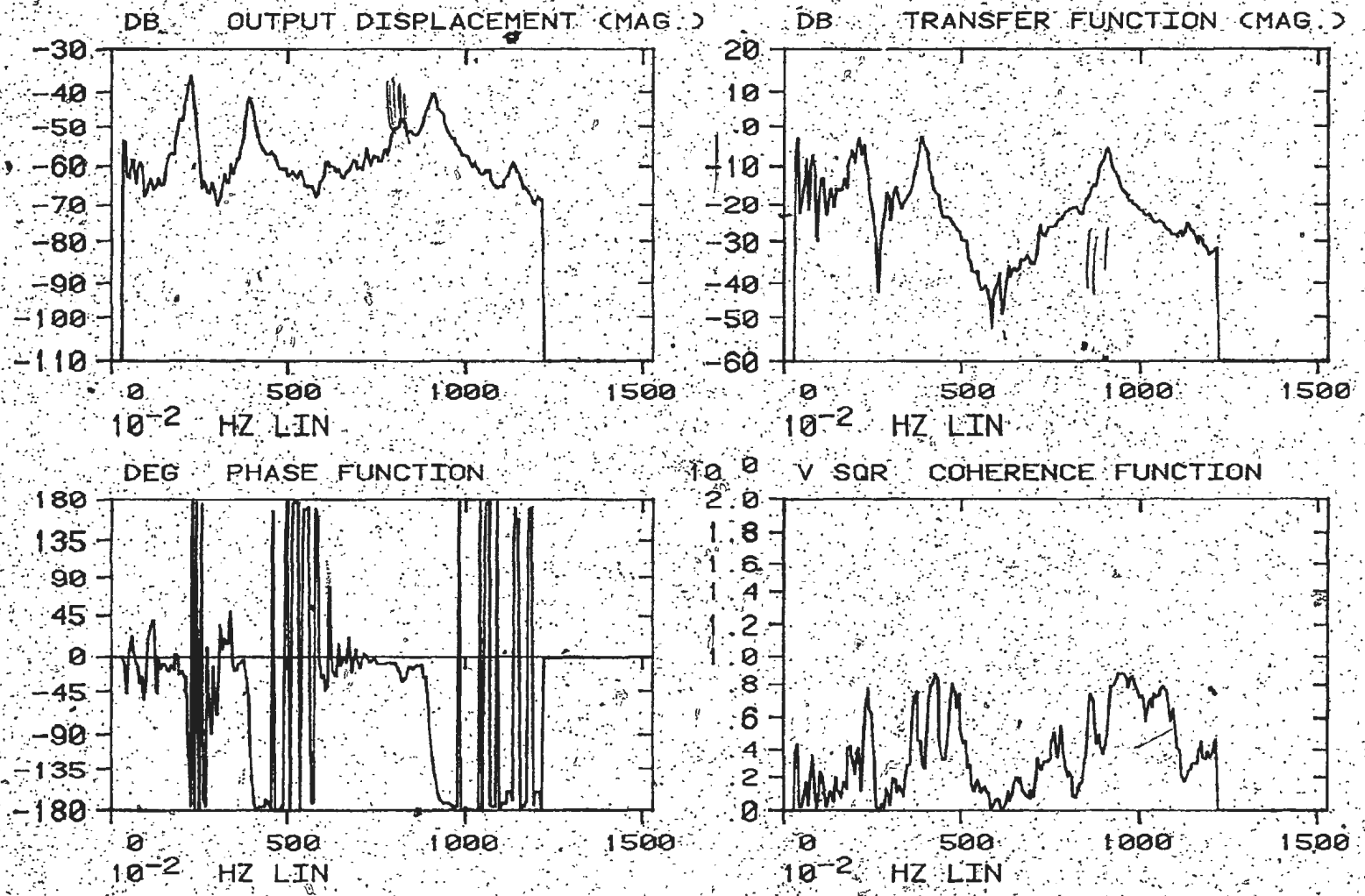

FIG. 4.0 RESULTS OF RANDOM VIBRATION TEST (DISPLACEMENT)
(INTACT STRUCTURE)

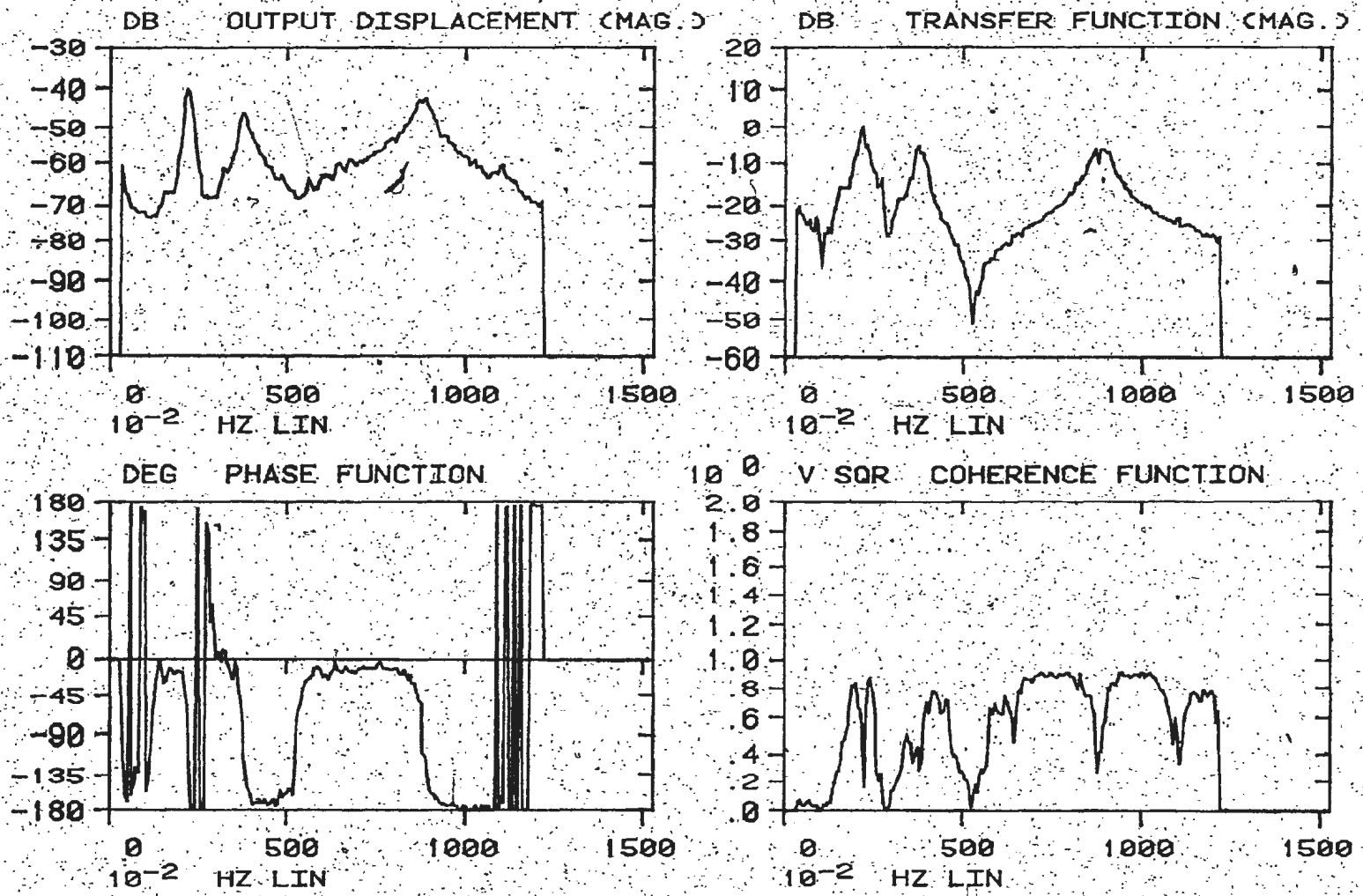

FIG. 4.1 RESULTS OF RANDOM VIBRATION TEST (DISPLACEMENT).
(MEM. 91 SEVERED HALFWAY AT NODE 23)

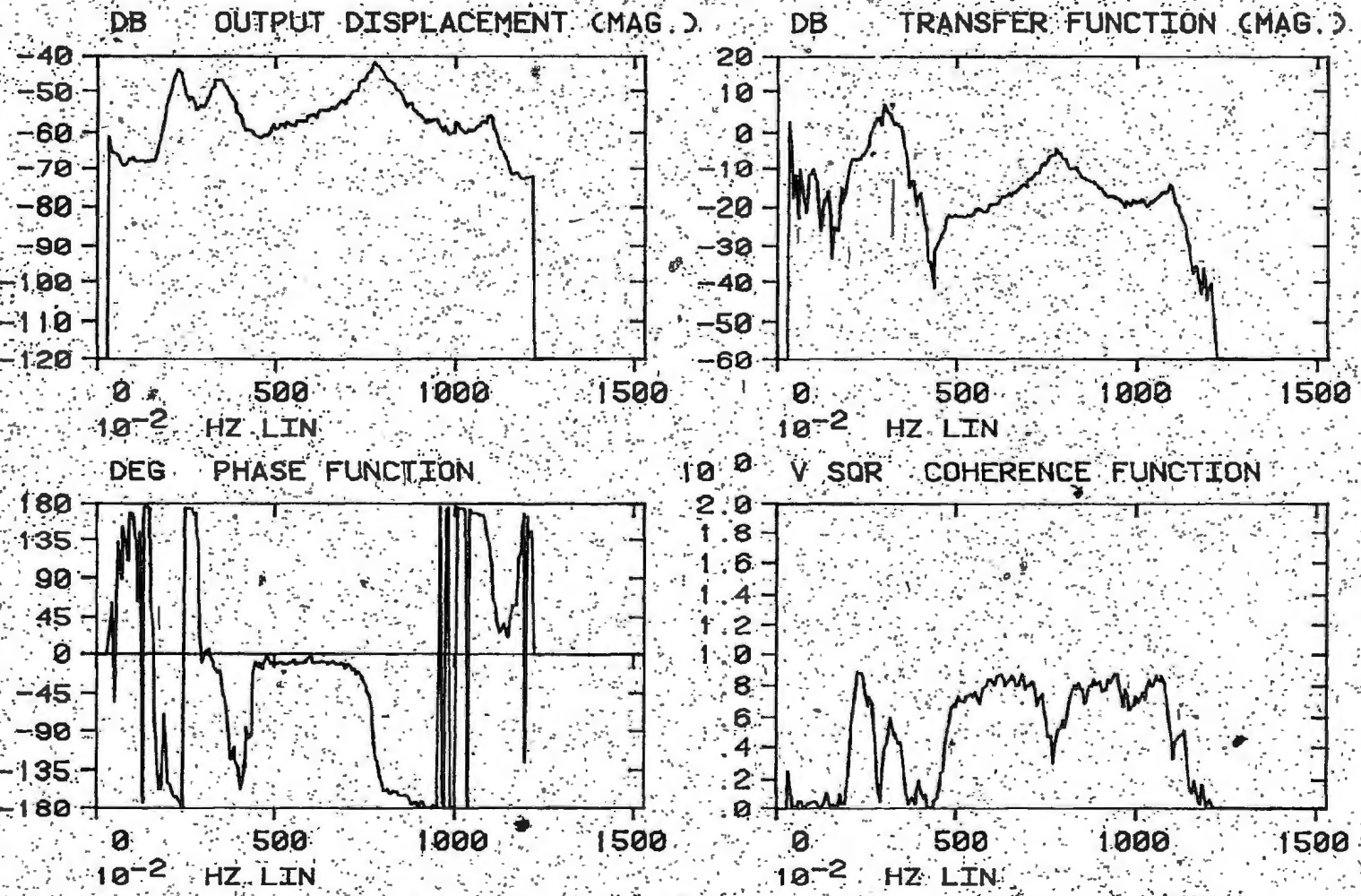

FIG. 4.2 RESULTS OF RANDOM VIBRATION TEST (DISPLACEMENT)
(MEM 91 COMPLETELY SEVERED AT NODE 23)

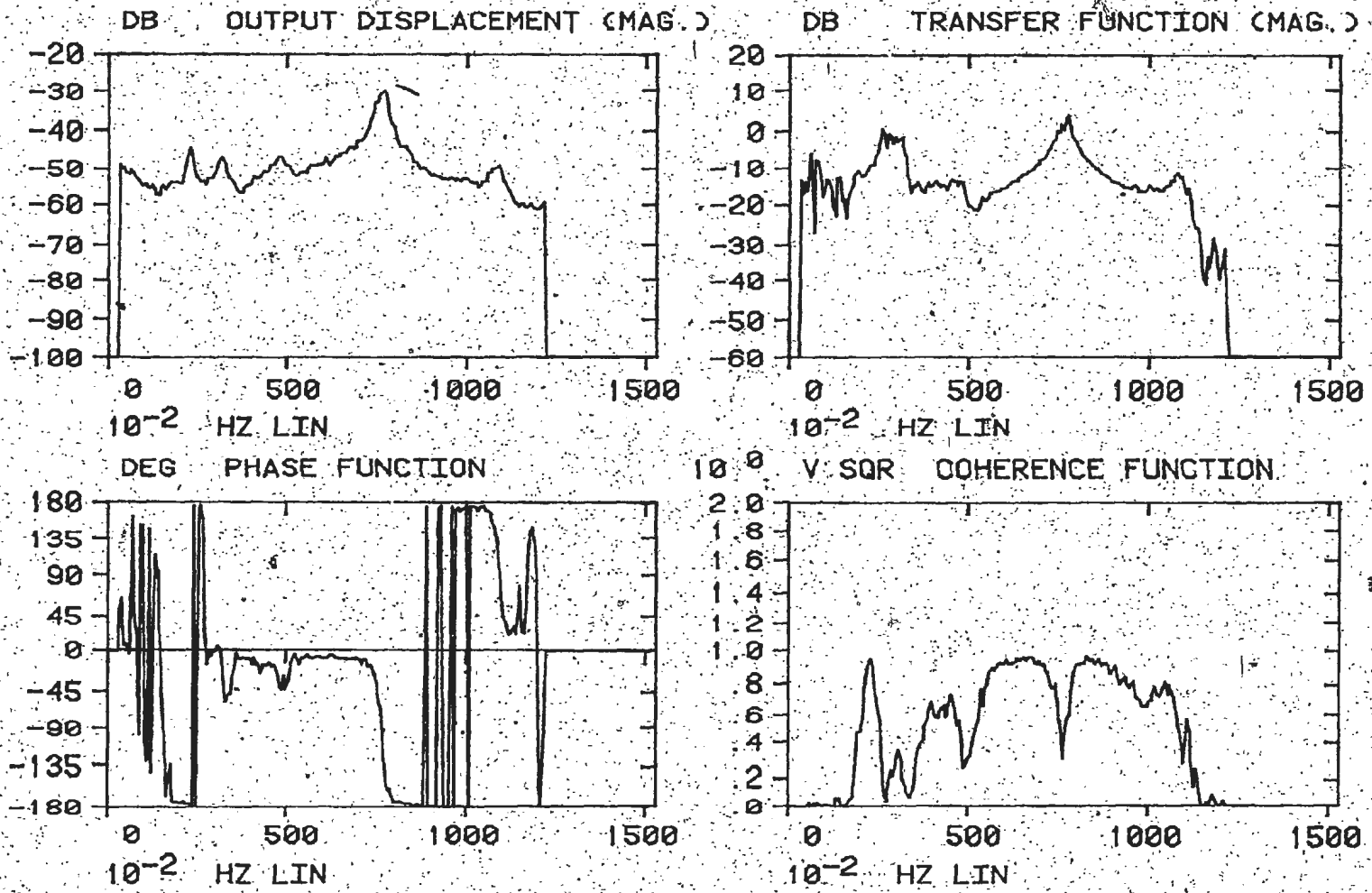

FIG. 4.3 RESULTS OF RANDOM VIBRATION TEST (DISPLACEMENT)
(MEM. 91 REMOVED)

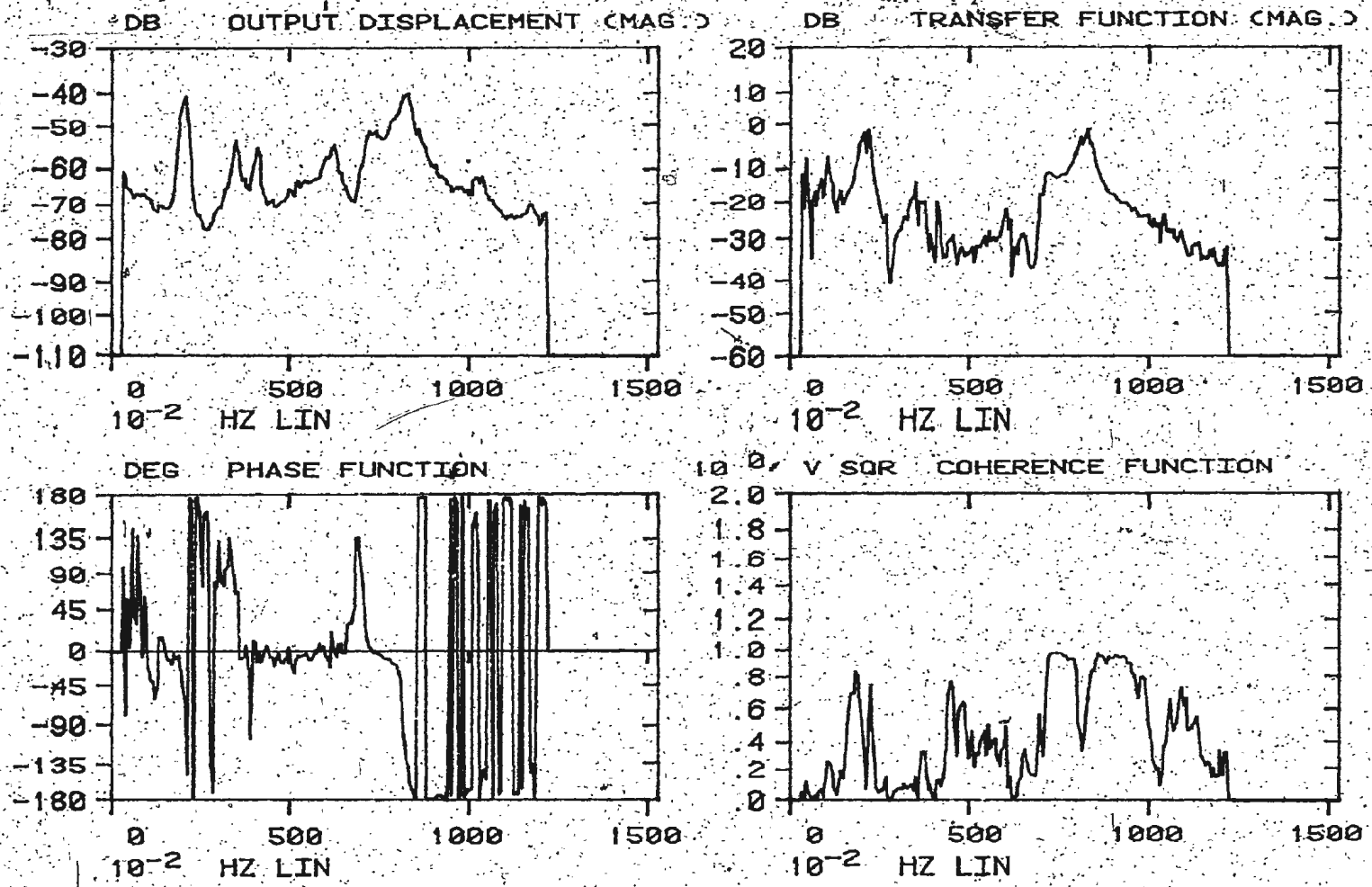

FIG. 4.4 RESULTS OF RANDOM VIBRATION TEST (DISPLACEMENT)
(MEM. 91 REMOVED AND MEM. 84 CUT-OFF AT NODE 31)

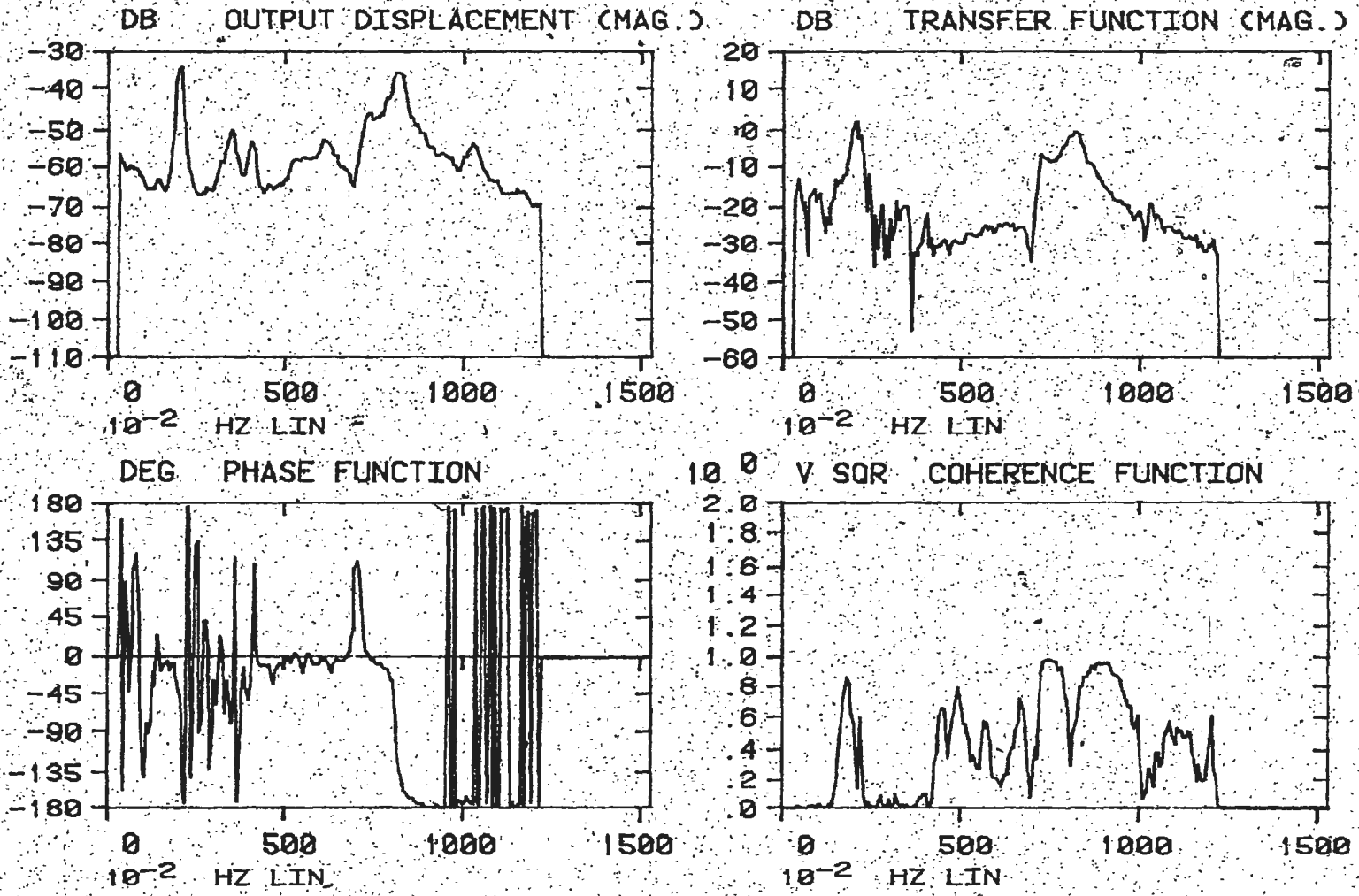

FIG. 4.5 RESULTS OF RANDOM VIBRATION TEST (DISPLACEMENT)
(MEMS. 91 AND 84 REMOVED)

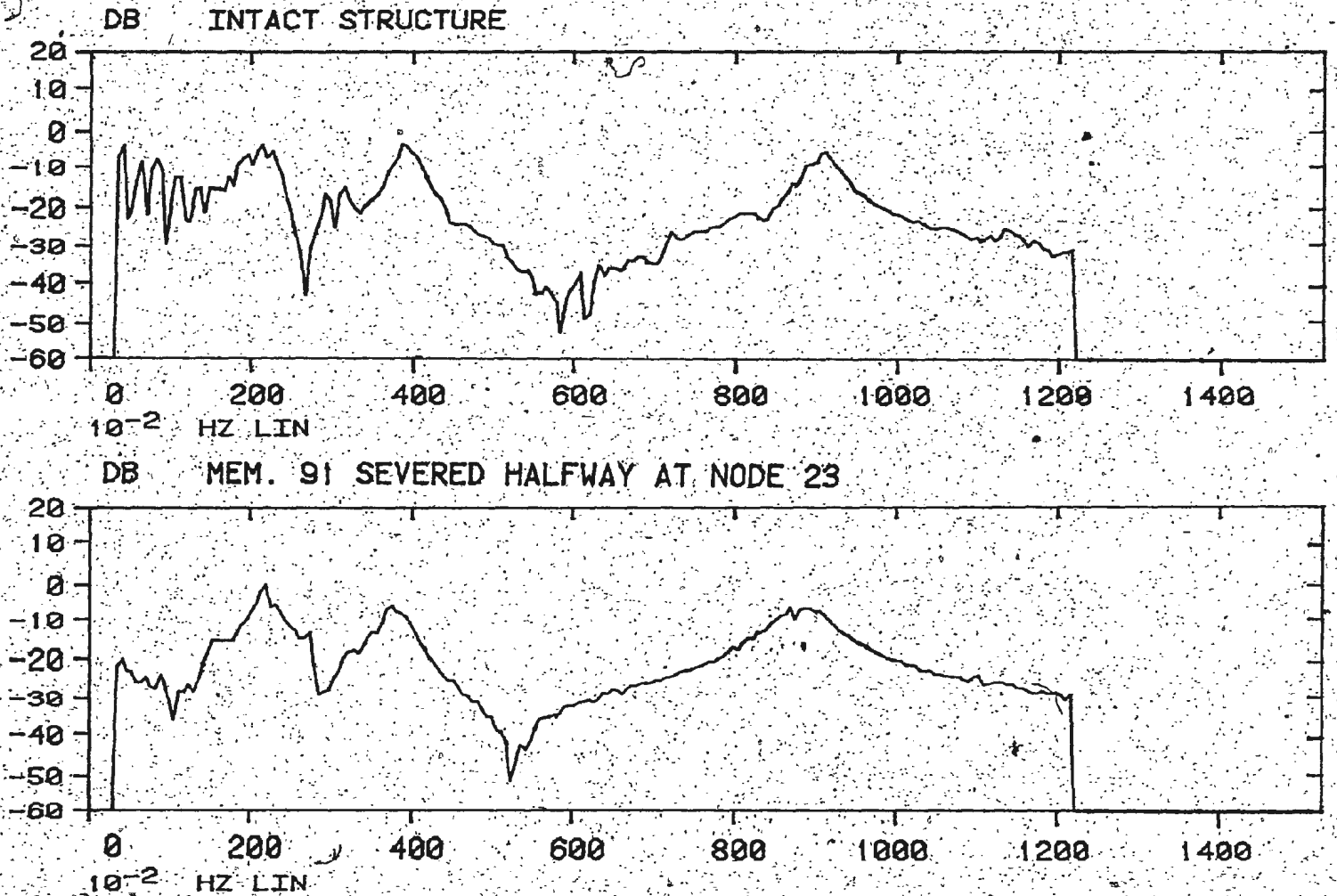

FIG. 4.6 TRANSFER FUNCTIONS (DISPLACEMENT)

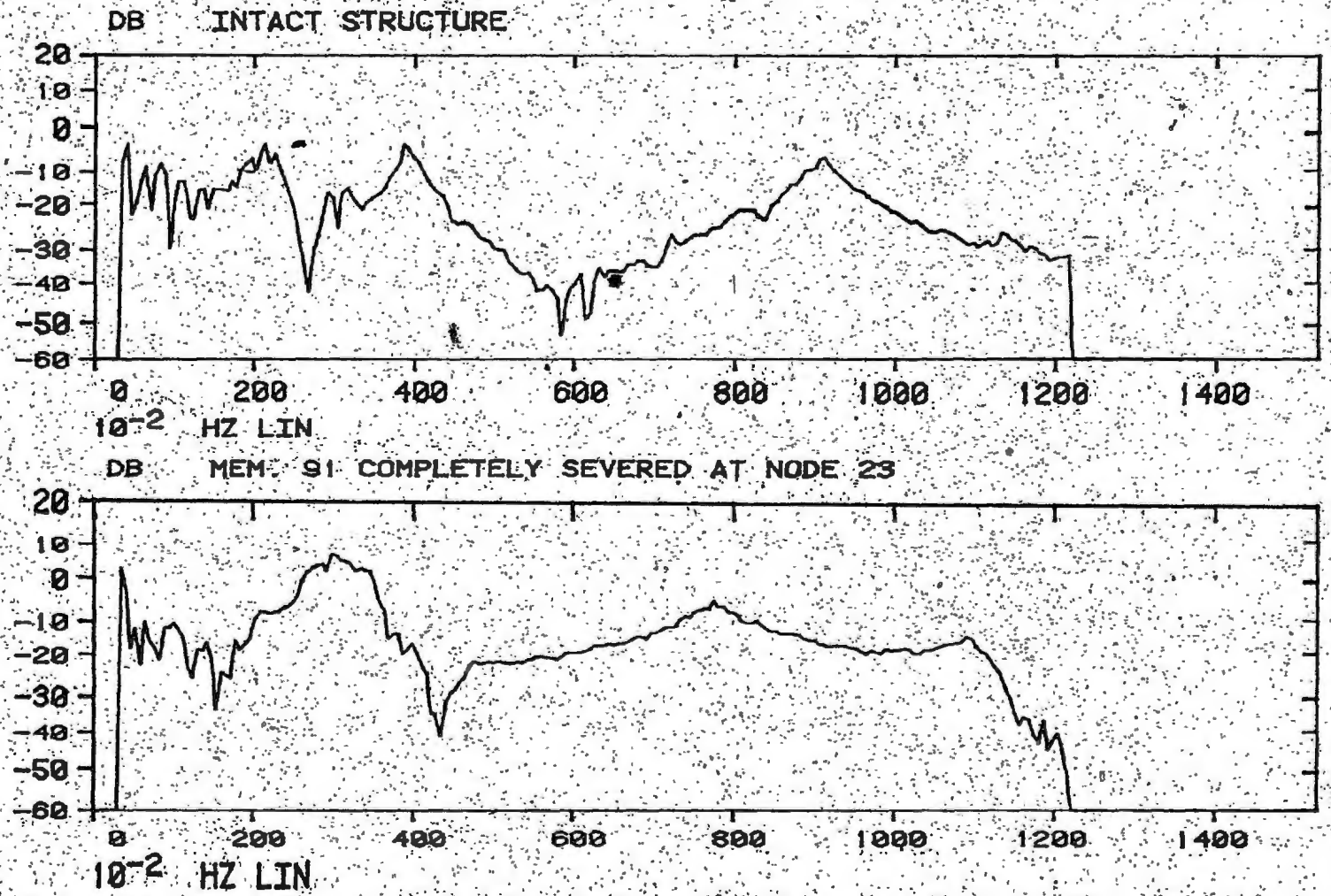

FIG. 4.7 TRANSFER FUNCTIONS (DISPLACEMENT)

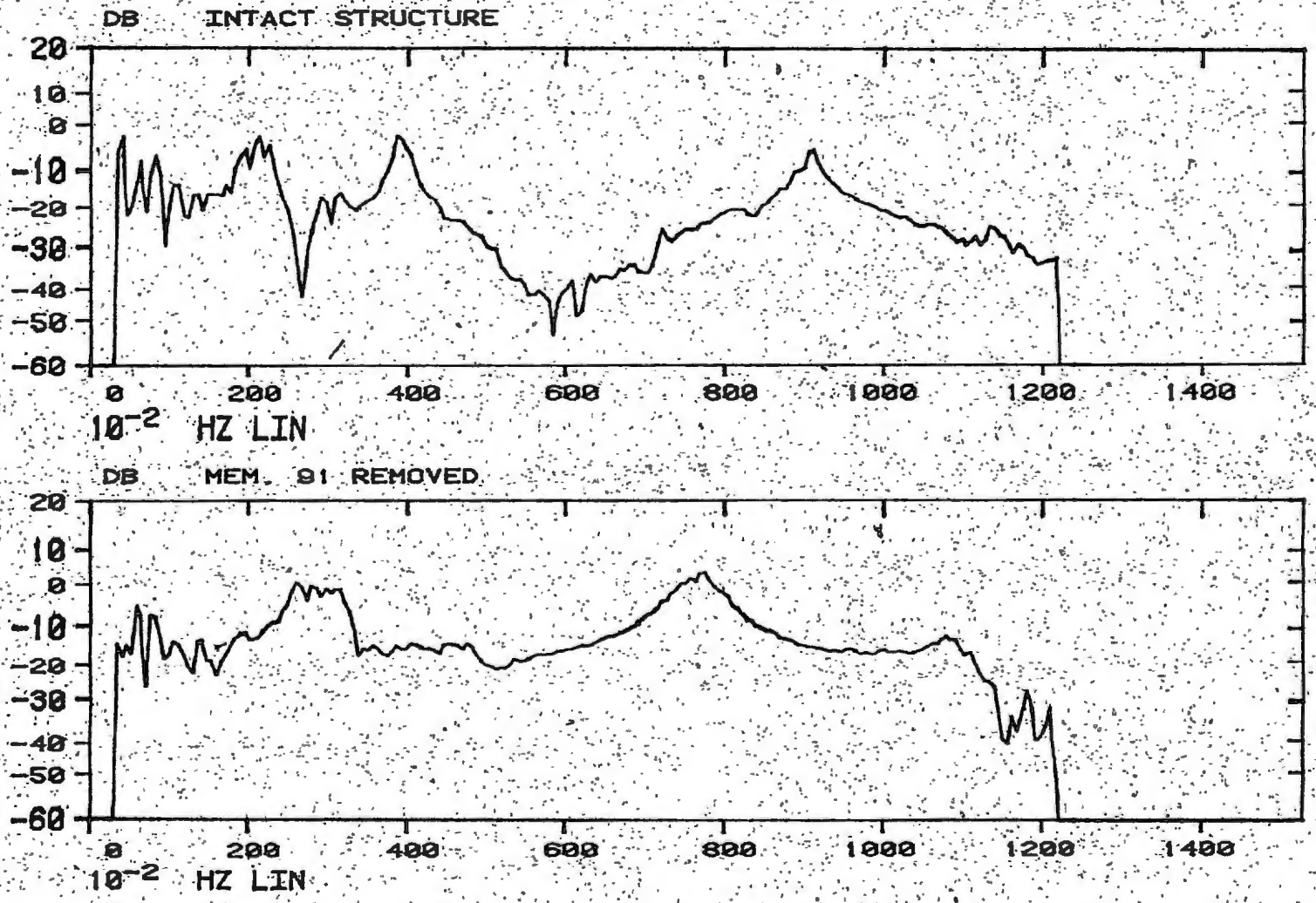

FIG. 4.8 TRANSFER FUNCTIONS (DISPLACEMENT)

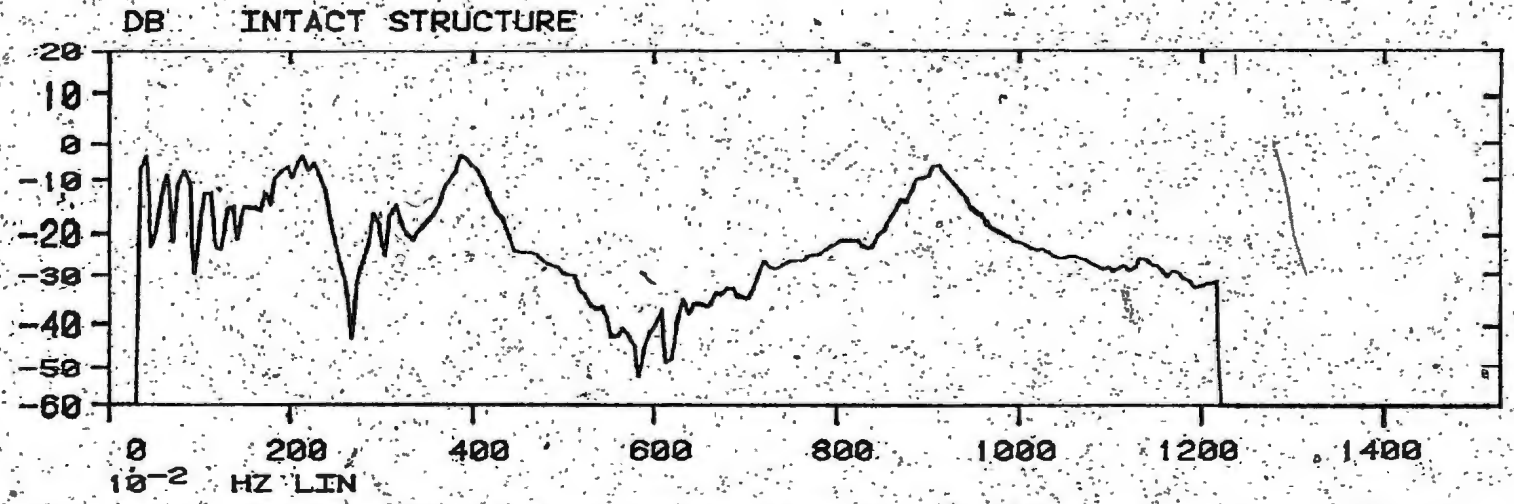

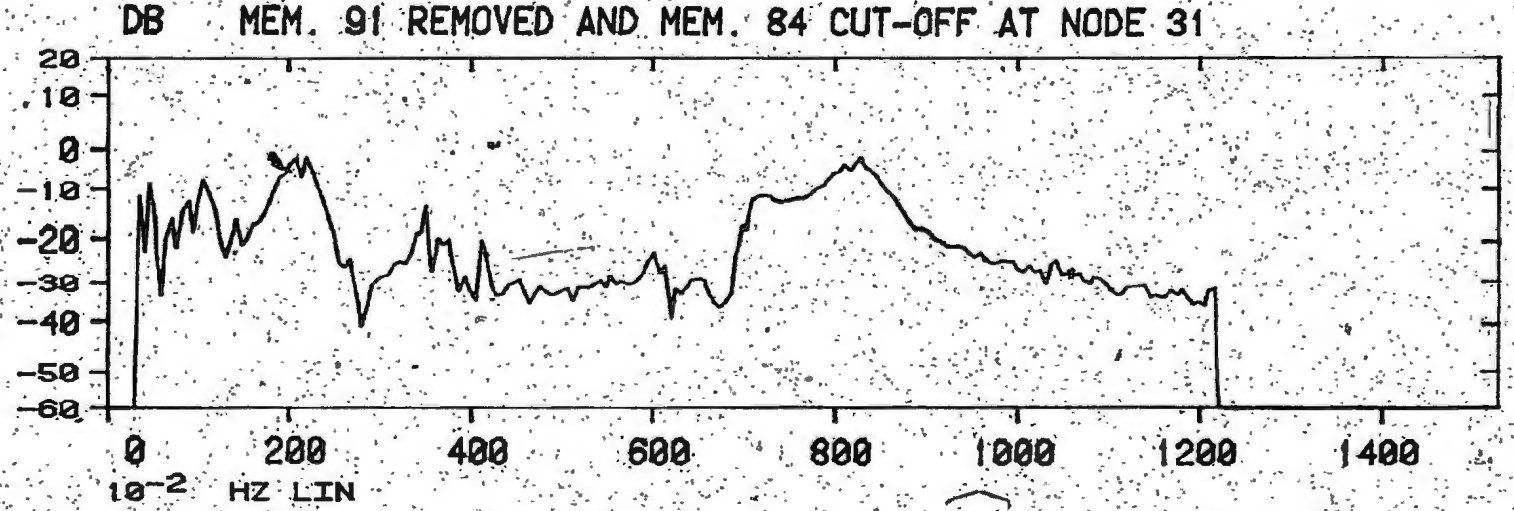

FIG. 4.9 TRANSFER FUNCTIONS (DISPLACEMENT)

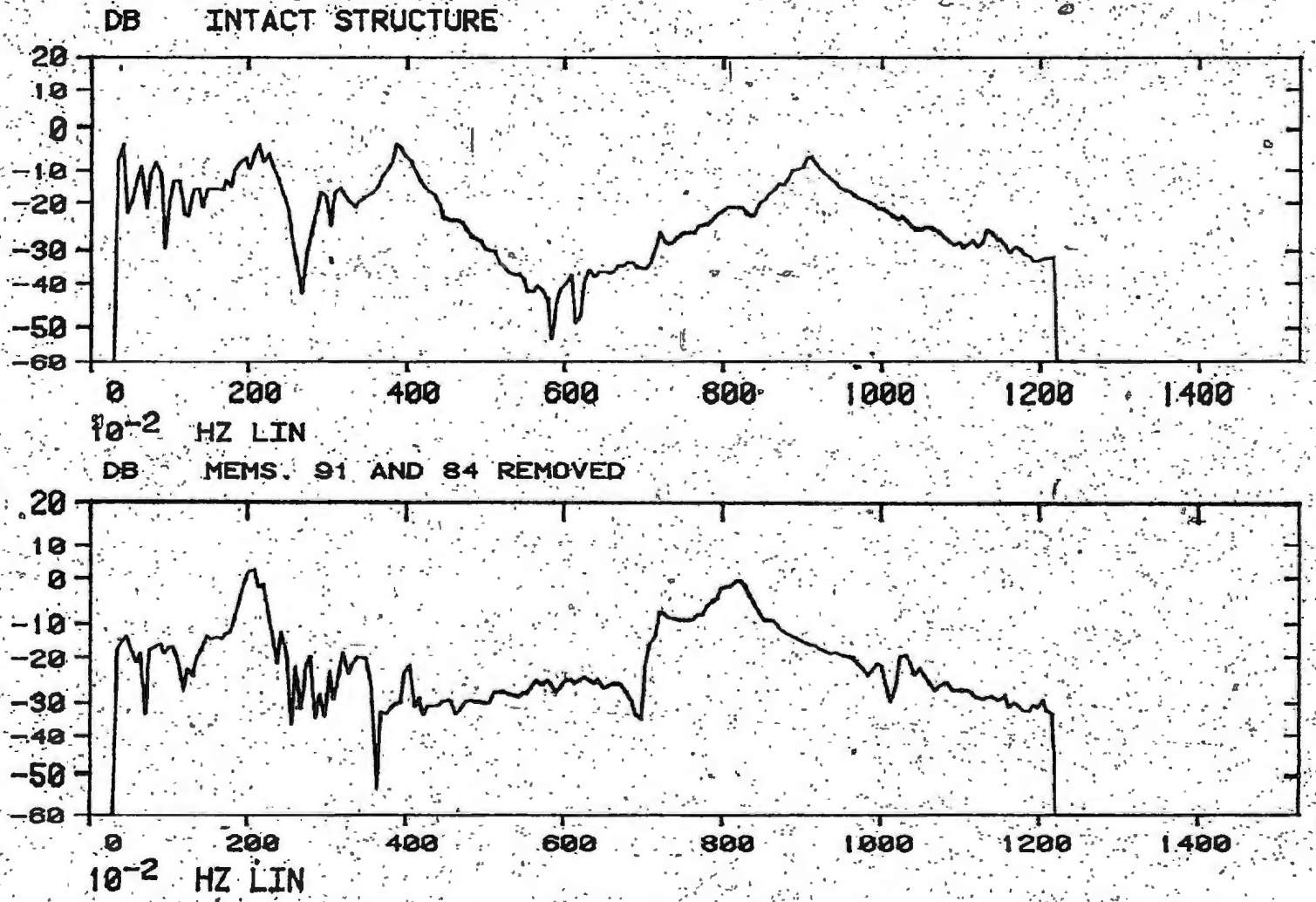

FIG. 4.10 TRANSFER FUNCTIONS (DISPLACEMENT)

APPENDICES

APPENDIX A1

STRUDL computer program for the undamaged structure.

STRUDL computer program for the damaged structure (member 91 is severed)

```
//Y30144GS JOB (3014,4GSC,11,5),'MARSHALL    ',CLASS=C,REGION=704K
//*LOGONID E301441
//*PASSWORD E301441
// EXEC STRUDL2
//SYSIN DD *
STRUDL 'PROJECT' 'FREE VIBRATION IN AIR OF THE P.V.C. OFFSHORE STRUCTURAL MODEL'
$ WITH 1 SLUG MASS DISTRIBUTED AT DECK LEVEL ,AND 1 SLUG MASS DISTRIBUTED AT
$ TWO LEVELS FROM THE DECK ,0.5 SLUG PER LEVEL.
$ UNDAMAGED STRUCTURE , RIGID DECK IS ASSUMED FOR THIS ANALYSIS .
TYPE SPACE FRAME
UNITS IN LB SECOND
JOINT COORDINATES
    1    16.37    0.0     16.37
    2    16.37    0.0    -16.37
    3   -16.37    0.0    -16.37
    4   -16.37    0.0     16.37
    5    16.0     5.98    16.0     S
    6    16.0     5.98    00.0     S
    7    16.0     5.98   -16.0     S
    8     0.0     5.98   -16.0     S
    9   -16.0     5.98   -16.0     S
   10   -16.0     5.98     0.0     S
   11   -16.0     5.98    16.0     S
   12     0.0     5.98    16.0     S
   13    14.0    37.88    14.0
   14    14.0    37.88     0.0
   15    14.0    37.88   -14.0
   16     0.0    37.88   -14.0
   17   -14.0    37.88   -14.0
   18   -14.0    37.88     0.0
   19   -14.0    37.88    14.0
   20     0.0    37.88    14.0
   21    12.0    69.78    12.0
   22    12.0    69.78     7.0
   23    12.0    69.78     0.0
   24    12.0    69.78    -7.0
   25    12.0    69.78   -12.0
   26     7.0    69.78   -12.0
   27     0.0    69.78   -12.0
   28    -7.0    69.78   -12.0
   29   -12.0    69.78   -12.0
   30   -12.0    69.78    -7.0
   31   -12.0    69.78     0.0
   32   -12.0    69.78     7.0
   33   -12.0    69.78    12.0
   34    -7.0    69.78    12.0
   35     0.0    69.78    12.0
   36     7.0    69.78    12.0
   37    12.0    75.78    12.0
   38    12.0    75.78   -12.0
   39   -12.0    75.78   -12.0
   40   -12.0    75.78    12.0
   41    12.0    93.78    12.0
   42    12.0    93.78   -12.0
   43   -12.0    93.78   -12.0
   44   -12.0    93.78    12.0
   45    12.0    99.78    12.0
   46    12.0    99.78     7.0
```

47	12.0	99.78	0.0
48	12.0	99.78	-7.0
49	12.0	99.78	-12.0
50	7.0	99.78	-12.0
51	0.0	99.78	-12.0
52	-07.0	99.78	-12.0
53	-12.0	99.78	-12.0
54	-12.0	99.78	-7.0
55	-12.0	99.78	0.0
56	-12.0	99.78	7.0
57	-12.0	99.78	12.0
58	-7.0	99.78	12.0
59	0.0	99.78	12.0
60	7.0	99.78	12.0

MEMBER INCIDENCES

1	12	5
2	5	6
3	6	7
4	7	8
5	8	9
6	9	10
7	10	11
8	11	12
9	12	6
10	6	8
11	8	10
12	10	12
13	20	13
14	13	14
15	14	15
16	15	16
17	16	17
18	17	18
19	18	19
20	19	20
21	20	14
22	14	16
23	16	18
24	18	20
25	35	36
26	36	21
27	21	22
28	22	23
29	23	24
30	24	25
31	25	26
32	26	27
33	27	28
34	28	29
35	29	30
36	30	31
37	31	32
38	32	33
39	33	34
40	34	35
41	35	23
42	23	27
43	27	31

44	31	35
45	59	60
46	60	45
47	45	46
48	46	47
49	47	48
50	48	49
51	49	50
52	50	51
53	51	52
54	52	53
55	53	54
56	54	55
57	55	56
58	56	57
59	57	58
60	58	59
61	59	47
62	47	51
63	51	55
64	55	59
65	4	11
66	3	9
67	2	7
68	1	5
69	5	20
70	20	11
71	11	19
72	11	18
73	18	9
74	9	17
75	9	16
76	16	7
77	7	15
78	7	14
79	14	5
80	5	13
81	13	35
82	35	19
83	19	33
84	19	31
85	31	17
86	17	29
87	17	27
88	27	15
89	15	25
90	15	23
91	23	13
92	13	21
93	36	37
94	34	40
95	33	40
96	32	40
97	30	39
98	29	39
99	28	39
100	26	38
101	25	38

```
    102  24   38
    103  22   37
    104  21   37
    105  40   44
    106  39   43
    107  38   42
    108  37   41
    109  41   60
    110  44   58
    111  44   57
    112  44   56
    113  44   53
    114  43   53
    115  43   52
    116  42   50
    117  42   49
    118  42   48
    119  41   46
    120  41   45
MEMBERS  1 TO  60 PROPERTIES PRISMATIC AX 0.3369 IY 0.0268 IZ 0.0268 IX 0.04136
MEMBERS 61 TO 84 PROPERTIES PRISMATIC AX 1.0814 IY 0.0881 IZ 0.0881 IX 0.1722
MEMBERS 85 TO 120 PROPERTIES PRISMATIC AX 0.3369 IY 0.0268 IZ 0.0268 IX 0.04136
CONSTANTS
E 3.5E+05 ALL
DENSITY 0.05000 ALL BUT 0.8000 83 86 89 92 1.119 45 TO 60
DAMPING PERCENTAGE 3.0 2
INERTIA OF JOINTS LUMPED
UNITS CYCLES
NORMALIZE EIGENVECTOR
ITERATION VALUE 0.0010 VECTOR 0.010
DYNAMIC ANALYSIS ITERATION EIGENVALUE 8
LIST DYNAMIC EIGENVALUES 8 EIGENVECTORS 8
FINISH
/*
//
```

```
//Y301446S JOB (3014,4GSC,11,5),'MARSHALL    ',CLASS=C,REGION=704K
//*LOGONID E301441
//*PASSWORD E301441
// EXEC STRUDL2
//SYSIN DD *
STRUDL 'PROJECT' 'FREE VIBRATION IN AIR OF THE P.V.C. OFFSHORE STRUCTURAL MODEL'
$ WITH 1 SLUG MASS DISTRIBUTED AT DECK LEVEL ,AND 1 SLUG MASS DISTRIBUTED AT
$ TWO LEVELS FROM THE DECK ,0.5 SLUG  PER LEVEL.
$ DAMAGED STRUCTURE ( RIGID DECK IS ASSUMED ) . MEMBER 91 IS REMOVED FROM THE
$ ANALYSIS TO SIMULATE DAMAGE OF THAT MEMBER .
TYPE SPACE FRAME
UNITS IN  LB  SECOND
JOINT COORDINATES
    1    16.37   0.0     16.37
    2    16.37   0.0    -16.37
    3   -16.37   0.0    -16.37
    4   -16.37   0.0     16.37
    5    16.0    5.98    16.0      S
    6    16.0    5.98    00.0      S
    7    16.0    5.98   -16.0      S
    8     0.0    5.98   -16.0      S
    9   -16.0    5.98   -16.0      S
   10   -16.0    5.98     0.0      S
   11   -16.0    5.98    16.0      S
   12     0.0    5.98    16.0      S
   13    14.0   37.88    14.0
   14    14.0   37.88     0.0
   15    14.0   37.88   -14.0
   16     0.0   37.88   -14.0
   17   -14.0   37.88   -14.0
   18   -14.0   37.88     0.0
   19   -14.0   37.88    14.0
   20     0.0   37.88    14.0
   21    12.0   69.78    12.0
   22    12.0   69.78     7.0
   23    12.0   69.78     0.0
   24    12.0   69.78    -7.0
   25    12.0   69.78   -12.0
   26     7.0   69.78   -12.0
   27     0.0   69.78   -12.0
   28    -7.0   69.78   -12.0
   29   -12.0   69.78   -12.0
   30   -12.0   69.78    -7.0
   31   -12.0   69.78     0.0
   32   -12.0   69.78     7.0
   33   -12.0   69.78    12.0
   34    -7.0   69.78    12.0
   35     0.0   69.78    12.0
   36     7.0   69.78    12.0
   37    12.0   75.78    12.0
   38    12.0   75.78   -12.0
   39   -12.0   75.78   -12.0
   40   -12.0   75.78    12.0
   41    12.0   93.78    12.0
   42    12.0   93.78   -12.0
   43   -12.0   93.78   -12.0
   44   -12.0   93.78    12.0
   45    12.0   99.78    12.0
```

46	12.0	99.78	7.0
47	12.0	99.78	0.0
48	12.0	99.78	-7.0
49	12.0	99.78	-12.0
50	7.0	99.78	-12.0
51	0.0	99.78	-12.0
52	-07.0	99.78	-12.0
53	-12.0	99.78	-12.0
54	-12.0	99.78	-7.0
55	-12.0	99.78	0.0
56	-12.0	99.78	7.0
57	-12.0	99.78	12.0
58	-7.0	99.78	12.0
59	0.0	99.78	12.0
60	7.0	99.78	12.0

MEMBER INCIDENCES

1	12	5
2	5	6
3	6	7
4	7	8
5	8	9
6	9	10
7	10	11
8	11	12
9	12	6
10	6	8
11	8	10
12	10	12
13	20	13
14	13	14
15	14	15
16	15	16
17	16	17
18	17	18
19	18	19
20	19	20
21	20	14
22	14	16
23	16	18
24	18	20
25	35	36
26	36	21
27	21	22
28	22	23
29	23	24
30	24	25
31	25	26
32	26	27
33	27	28
34	28	29
35	29	30
36	30	31
37	31	32
38	32	33
39	33	34
40	34	35
41	35	23
42	23	27

43	27	31
44	31	35
45	59	60
46	60	45
47	45	46
48	46	47
49	47	48
50	48	49
51	49	50
52	50	51
53	51	52
54	52	53
55	53	54
56	54	55
57	55	56
58	56	57
59	57	58
60	58	59
61	59	47
62	47	51
63	51	55
64	55	59
65	4	11
66	3	9
67	2	7
68	1	5
69	5	20
70	20	11
71	11	19
72	11	18
73	18	9
74	9	17
75	9	16
76	16	7
77	7	15
78	7	14
79	14	5
80	5	13
81	13	35
82	35	19
83	19	33
84	19	31
85	31	17
86	17	29
87	17	27
88	27	15
89	15	25
90	15	23
92	13	21
93	36	37
94	34	40
95	33	40
96	32	40
97	30	39
98	29	39
99	28	39
100	26	38
101	25	38

```
    102  24   38
    103  22   37
    104  21   37
    105  40   44
    106  39   43
    107  38   42
    108  37   41
    109  41   60
    110  44   58
    111  44   57
    112  44   56
    113  43   54
    114  43   53
    115  43   52
    116  42   50
    117  42   49
    118  42   48
    119  41   46
    120  41   45
MEMBERS 1 TO 60 PROPERTIES PRISMATIC AX 0.3369 IY 0.0268 IZ 0.0268 IX 0.04136
MEMBERS 61 TO 64 PROPERTIES PRISMATIC AX 1.0814 IY 0.0861 IZ 0.0861 IX 0.1721
MEMBERS 65 TO 90 PROPERTIES PRISMATIC AX 0.3369 IY 0.0268 IZ 0.0268 IX 0.04136
MEMBERS 92 TO 120 PROPERTIES PRISMATIC AX 0.3369 IY 0.0268 IZ 0.0268 IX 0.04136
CONSTANTS
E 3.5E+05 ALL
DENSITY 0.05000 ALL BUT 0.0000 83 86 89 92 1.119 45 TO 60
DAMPING PERCENTAGE 3.0 2
INERTIA OF JOINTS LUMPED
UNITS CYCLES
NORMALIZE EIGENVECTOR
ITERATION VALUE 0.0010 VECTOR 0.010
DYNAMIC ANALYSIS ITERATION EIGENVALUE 8
LIST DYNAMIC EIGENVALUES 8 EIGENVECTORS 8
FINISH
/*
//
```

APPENDIX A2

Instrumentation Settings

Calibration for Proximity Transducer

Instrumentation Settings

Force Preamplifier:

0.1 V/N output

L.L.F. = 0.3 Hz

Direct Output

Acceleration Preamplifier:

1.0 V/g output

L.L.F. = 0.3 Hz

Krohm-Hite Filter (Acceleration and Force):

0.0 dB Gain for both channels

50 Hz and 15 Hz cut off frequency

Rockland Filter (Displacement):

50 Hz and 15 Hz cut off frequency

Low pass band width

Measuring Amplifier (Acceleration):

0.3 x 1

Gain control = 6

Direct output

H.P. Instrumentation Recorder:

Channel 1 -- Force

Calibration 5.0 V peak A.C.

Channel 2 -- Acceleration

Calibration 5.0 V peak A.C.

Channel 4 — Displacement

Calibration 5.0 V peak A.C.

H.P. Noise Generator:

50.0 and 15.0 Hz cut off frequency

Gaussian Noise

Infinite Sequence

NB: The experiments were carried out for both 50.0 Hz and 15.0 Hz independently.

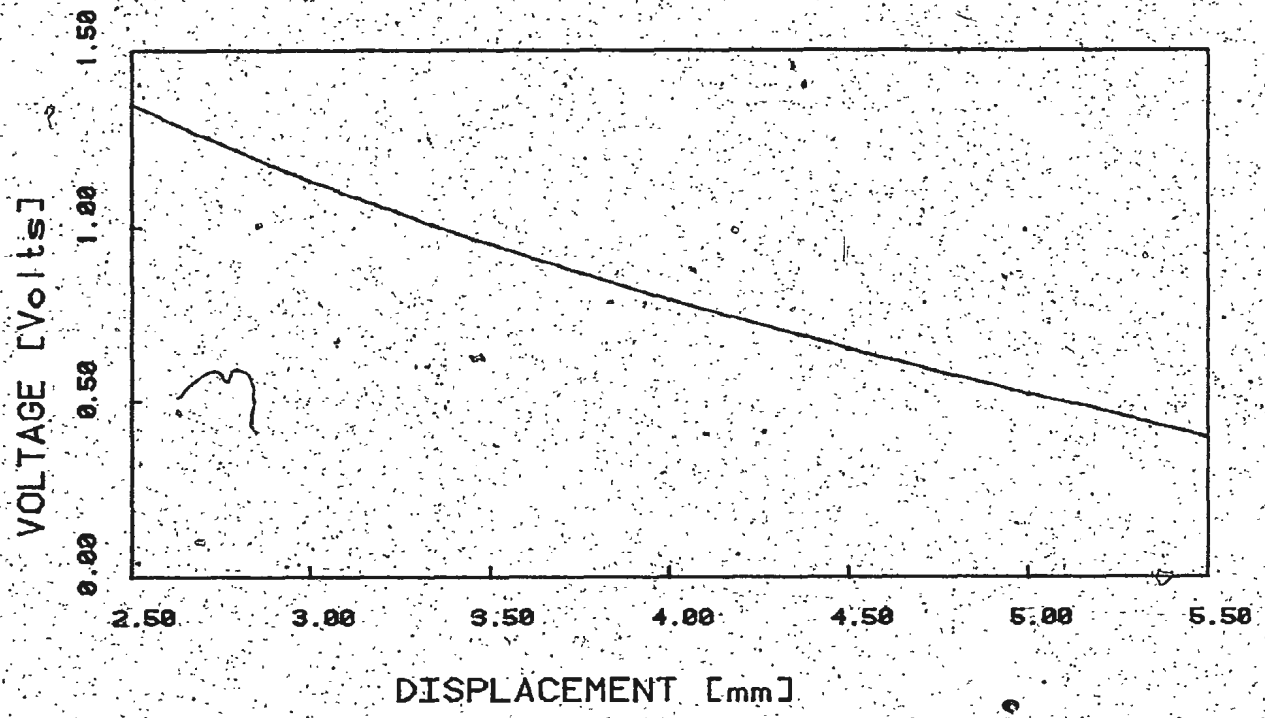

FIG. 5.0 CALIBRATION OF DISA PROXIMITY TRANSDUCER
(NOTE THAT THE RANGE CONSIDERED IS : 3.5 < DISPLACEMENT[mm] < 5.0)